

Sphingomyelin Phosphodiesterase 3, a Critical Regulator of Bone and Tooth

Mineralization

by

Zohreh Khavandgar

Faculty of Dentistry
McGill University, Montreal, Canada

A thesis submitted to McGill University in partial fulfillment of the requirements of the
degree of
Doctor of Philosophy

© Copyright by Zohreh Khavandgar, 2015

TABLE OF CONTENTS

List of Figures and Tables	7
List of Abbreviations Used	9
Abstract	12
Resumé	13
Acknowledgements	15
Contribution of Authors	16
Chapter 1: General Introduction and Literature Review	21
1.1 Bone development	22
1.2 Tooth development	26
1.3 Current understanding of skeletal mineralization	28
1.4. Genetic diseases with ECM mineralization defects	30
<i>1.4.1 Hypophosphatasia</i>	30
<i>1.4.2 Vitamin D-dependent rickets</i>	31
<i>1.4.3 X-linked hypophosphatemia</i>	31
<i>1.4.4 Osteogenesis imperfecta Type VI</i>	32
1.5 Sphingolipid biosynthesis	33
<i>1.5.1 De novo synthesis of sphingolipids</i>	34
<i>1.5.2 Synthesis of sphingolipids by sphingomyelinases</i>	35
1.6 Role of sphingolipids in skeletal cells: <i>In vitro</i> findings	36
<i>1.6.1 Ceramide</i>	36
<i>1.6.2 Sphingosine and its derivatives</i>	39

1.7 Role of sphingolipids in skeletal tissues: <i>In vivo</i> findings	42
1.8 Phosphocholine metabolism and its role in skeletal tissues	43
1.9 The matrix vesicle theory of ECM mineralization.....	44
1.10 Rationale and Aim:.....	45
 Chapter 2: A Cell-Autonomous Role for Neutral Sphingomyelinase 2 in Bone	
Mineralization	47
2.1 Abstract.....	49
2.2 Introduction.....	50
2.3 Results	53
2.3.1 <i>Impaired bone mineralization in fro/fro mice.....</i>	53
2.3.2 <i>The fro mutation abolishes nSMase2 activity but does not affect its membrane localization</i>	54
2.3.3 <i>The fro mutation affects skeletal development</i>	54
2.3.4 <i>Loss of nSMase2 in osteoblasts affects mineralization in vitro</i>	56
2.3.5 <i>Osteoblast-specific expression of Smpd3 in fro/fro mice increases bone nSMase activity</i>	57
2.3.6 <i>Normal bone mineralization in fro/fro; Colla1-Smpd3 mice</i>	59
2.4 Discussion.....	61
2.5 Materials and Methods.....	66
2.5.1 <i>DNA constructs</i>	66
2.5.2 <i>Mice.....</i>	66
2.5.3 <i>Gene expression analysis</i>	67
2.5.4 <i>Skeletal preparation and histologic analysis</i>	67
2.2.5 <i>Immunofluorescence and confocal microscopy</i>	68

2.2.6 Immunoblotting	69
2.5.7 Transient transfection with siRNAs, cell culture, and in vitro mineralization.....	69
2.5.8 Radiography and micro-CT analysis	69
2.5.9 Serum biochemistry.....	70
2.5.10 Sphingomyelinase assays and lipid measurements	70
2.6 Data analysis.....	71
2.7 Acknowledgements	71
Chapter 3: Local Regulation of Tooth Mineralization by Sphingomyelin Phosphodiesterase	
3.....	90
3.1 Abstract.....	92
3.2 Introduction.....	93
3.3 Results	95
3.3.1 Transient tooth mineralization delay in fro/fro mice	95
3.3.2 SMPD3 localization in odontoblasts.....	96
3.3.3 Normal mineral structure and ECM architecture in fro/fro teeth	96
3.3.4 A cell-autonomous requirement of SMPD3 in tooth mineralization.....	97
3.4 Discussion.....	98
3.5 Materials and Methods.....	101
3.5.1 Mice.....	101
3.5.2 Radiography and micro-CT	101
3.5.3 Histology	101
3.5.4 Transmission electron microscopy.....	102
3.5.5 X-ray diffraction.....	102

3.5.6 <i>X-gal staining</i>	103
3.6 Statistical analysis	103
3.7 Acknowledgements	103
Chapter 4: Sphingomyelin Phosphodiesterase 3 and Phosphatase, Orphan 1 Acts in a Relay to Promote Bone Mineralization	112
4.1 Abstract	114
4.2 Introduction	116
4.3 Results	119
4.3.1 <i>Normal bone mineralization in Des1^{-/-} mice</i>	119
4.3.2 <i>Bone and cartilage abnormalities in fro/fro, Phospho1^{-/-} and compound mutant mice</i>	119
4.3.3 <i>Sphingolipids and ceramide measurements in the fro/fro and Phospho1^{-/-} embryos...</i>	120
4.3.4 <i>Osteoblast-specific expression of Smpd3 in Phospho1^{-/-} mice does not rescue the mineralization defect</i>	120
4.3.5 <i>High choline diet corrects the bone mineralization defects in fro/fro mice</i>	121
4.4 Discussion	122
4.5 Materials and Methods	125
4.5.1 <i>Mice</i>	125
4.5.2 <i>Histologic analysis</i>	125
4.5.3 <i>Lipid measurements</i>	126
4.6 Data analysis	126
4.7 Acknowledgements	126
Chapter 5: General Discussion	136
5.1 General Discussion	137

5.2 Future directions	142
5.3 Significance	143
5.4 Conclusion	144
References	145

List of Figures and Tables

Figure 1.1: Endochondral bone formation.....	24
Figure 1.2: Intramembranous bone formation.....	25
Figure 1.3: Tooth development.....	28
Figure 1.4: Chemical structures of sphingosine and its derivatives ceramide and sphingomyelin.	34
Figure 1.5: <i>De novo</i> and sphingomyelinase pathways showing the metabolism of ceramide, sphingomyelin and sphingosine.....	35
Figure 1.6: The major effects of ceramide.....	41
Figure 1.7: Phosphocholine metabolism.....	43
Figure 2.1: Skeletal abnormalities in <i>fro/fro</i> mice.....	74
Figure 2.2: Effects of <i>fro</i> mutation on nSMase2 activity and localization.....	76
Figure 2.3: Effects of <i>fro</i> mutation on the developing skeleton.....	78
Figure 2.4: <i>Smpd3</i> expression and function in osteoblasts.....	80
Figure 2.5: Biochemical analysis of tissue and serum samples from <i>fro/fro; Colla1-Smpd3</i> mice	82
Figure 2.6: Analysis of <i>fro/fro; Colla1-Smpd3</i> bones.....	84
Figure 2.7: A model depicting the local activities of nSMase2 in skeletal tissues.....	85
Figure S1: qRT-PCR analysis of <i>Runx2</i> and <i>Atf4</i> expression in newborn <i>fro/fro</i> bones.....	86
Figure S2: The comparative expression analysis of <i>Enpp1</i> , <i>Ank</i> , <i>Mgp</i> , and <i>Colla1</i> by qRT-PCR in the parietal bones of <i>fro/fro</i> and <i>fro/fro; Colla1-Smpd3</i> mice.....	87
Figure S3: qRT-PCR analysis of <i>Runx2</i> , <i>Colla1</i> , <i>Atf4</i> , and <i>Bglap1</i> expression in the control and <i>Smpd3</i> siRNA-treated MC3T3-E1 cells and <i>Runx2</i> , <i>Atf4</i> , <i>Bglap1</i> , and <i>Smpd3</i> expression in WT and <i>+/fro</i> mice.....	89
Figure 3.1: Effects of the <i>fro</i> mutation on developing teeth.....	105
Figure 3.2: Localization of SMPD3, OSX, DSPP, and AMELX in tooth cells.....	107
Figure 3.3: TEM and X-ray diffraction of 14-day-old molars.....	109

Figure 3.4: Correction of the fro tooth phenotype in <i>fro/fro;Coll1a1-Smpd3</i> transgenic mice ...	111
Figure 4.1: Ceramide biosynthesis by SMPD3 and DES1 and the skeletal analyses of <i>Des1</i> -deficient mice.....	127
Figure 4.2: Bone and cartilage abnormalities in <i>fro/fro</i> , <i>Phospho1^{-/-}</i> and <i>fro/fro;Phospho1^{-/-}</i> compound mutant mice.....	129
Figure 4.3: Phospholipid and ceramide measurements in the E17.5 WT, <i>fro/fro</i> and <i>Phospho1^{-/-}</i> embryos.....	131
Figure 4.4: Analysis of <i>Phospho1^{-/-};Coll1a1-Smpd3</i> bones.	132
Figure 4.5: Effect of a 2%-choline diet on mineralization in <i>fro/fro</i> and <i>Phospho1^{-/-}</i> mice.	134
Figure 4.6: A model depicting ECM mineralization in bone.....	135

List of Abbreviations Used

ALPL:	Tissue-Nonspecific Alkaline Phosphatase
AMELX:	Amelogenin
ANK:	Progressive Ankylosis
ATF4:	Activating Transcription Factor 4
BMPs:	Bone Morphogenetic Protein
BP:	Base Pairs
Br:	Brain
BV/TV	Bone volume
CMV:	Cytomegalovirus
COL1A1:	Type I Collagen
DES1:	dihydroceramide desaturase 1
D-PDM:	D-threo-1-Phenyl-2-Decanoylamino-3-Morpholino-1-Propanol
DSPP:	Dentin Sialophosphoprotein
E:	Embryonic
ECM:	Extracellular Matrix
ENPP1:	Ectophosphodiesterase nucleotide phosphohydrolases
ENU:	N-Ethyl-N-Nitrosourea
ER:	Endoplasmic Reticulum
ERK:	Extracellular Signal-Regulated Kinase
FGFs:	Fibroblast Growth Factors
<i>fro:</i>	<i>fragilitas ossium</i>
<i>Hprt:</i>	Hypoxanthine Guanine Phosphoribosyl Transferase
HSP27:	Heat-Shock Protein 27
IHH:	Indian Hedgehog
IRES:	Internal Ribosome Entry Site
JNK:	c-Jun N-terminal kinase
LPP1-3:	Lipid-Phosphate Phosphatases
MAR	Mineral apposition rate
MCS:	Membrane Contact Sites
MD:	Mineralized Dentin

MGP:	Matrix Gla Protein
micro-CT:	Micro-Computed Tomography
MSC:	Mesenchymal Stem Cells
MVs:	Matrix Vesicles
NF-kappa B:	Nuclear Factor-kappa B
NO:	Nitric Oxide
nSMase:	Neutral Sphingomyelinase
OI:	Osteogenesis Imperfecta
OSX:	Osterix
OV/BV	Osteoid volume/Bone volume
pA:	SV40 Polyadenylation signal
PB:	Parietal Bone
PEDF:	Pigment Epithelium-Derived Factor
PFA:	Paraformaldehyde
PHOSPHO1:	Phosphoethanolamine/Phosphocholine Phosphatase
P_i:	Inorganic Phosphate
PO:	Periosteum
PP_i:	Inorganic Pyrophosphate
PTH:	Parathyroid Hormone
PTHrP:	Parathyroid Hormone-Like Hormone
qRT-PCR:	quantitative Real Time PCR
RANK:	Receptor-Activator of NF-kappa B
RC:	Rib Cartilage
RQ:	Relative Quantification
RUNX2:	Runt-related Transcription Factor 2
S1P:	Sphingosine-1-Phosphate
Sk	Skeletal tissue
SMase:	Sphingomyelinases
<i>Smpd1:</i>	Sphingomyelin Phosphodiesterase 1
<i>Smpd3:</i>	Sphingomyelin Phosphodiesterase 3
Tb.Th	trabecular thickness
TEM:	Transmission Electron Microscopy

<i>TG:</i>	Transgene
TNF-alpha:	Tumor Necrosis Factor-alpha
TUNEL:	Terminal Transferase dUTP Nick End Labelling
UMD:	Unmineralized Dentin
VDDR:	Vitamin D-Dependent Rickets
WT:	Wild-Type
XRD:	X-Ray Diffraction

Abstract

A recessive mutation called *fragilitas ossium* (*fro*) in the sphingomyelin phosphodiesterase 3 (*Smpd3*) gene leads to impaired mineralization of bone and tooth extracellular matrix in *fro/fro* mice. SMPD3 (also known as nSMase2) cleaves sphingomyelin present in the cell membrane to generate ceramide, a bioactive lipid molecule, and phosphocholine, an essential nutrient. We examined endochondral ossification in E15.5 *fro/fro* mouse embryos and observed impaired apoptosis of hypertrophic chondrocytes and severely undermineralized cortical bones in the developing skeleton. To investigate whether SMPD3 plays a cell-autonomous role in these tissues, we examined the *in vitro* mineralization properties of *fro/fro* osteoblast cultures; the *fro/fro* cultures mineralized less than the control osteoblast cultures. We next generated *fro/fro;Colla1-Smpd3* mice, in which expression of *Smpd3* in osteoblasts corrected the bone abnormalities observed in *fro/fro* embryos without correcting the cartilage phenotype. The *Colla1-Smpd3* transgene was also expressed in odontoblast and this expression was sufficient to correct all the tooth mineralization defects in *fro/fro;Colla1-Smpd3* mice. We observed a decrease of ceramide levels in various *fro/fro* tissues. A similar decrease of ceramide levels is also reported upon the inactivation of the *de novo* pathway of ceramide synthesis in *Des1-/-* mice. However, we found that *Des1-/-* mice do not show any bone mineralization defects. This observation raises the possibility that the other SMPD3 metabolite, phosphocholine, might play a role in bone mineralization. The deficiency of phosphatase, orphan 1 (PHOSPHO1), an intracellular enzyme that cleaves phosphocholine to generate free phosphate and choline, has been associated with poor bone mineralization. Our histological analyses of the bones of 4-week-old *fro/fro;Phospho1-/-* compound homozygotes showed that the osteoid amount did not differ from that of control *fro/fro* bones. In addition to the sphingomyelinase pathway, phosphocholine can also be generated by cytosolic choline kinases that can convert dietary choline to phosphocholine. Based on this finding, we fed both *fro/fro* and *Phospho1-/-* mice a 2%-choline diet. This choline-rich diet raised the serum choline levels and decreased the unmineralized bone (osteoid) volume in *fro/fro* mice but not in *phospho1-/-* mice. Taken together, our data suggest that SMPD3 plays a cell-autonomous role in osteoblasts and odontoblasts to regulate bone and tooth mineralization, respectively. Additionally, we show that SMPD3 acts upstream of PHOSPHO1, and choline metabolism may play an important role in hard tissue mineralization.

Resumé

Une mutation récessive appelée fragilitas ossium (retour) dans le gene Sphingomyélinase 3 (*Smpd3*) conduit à une altération de la minéralisation de la matrice extracellulaire des os et des dents chez la souris *fro/fro*. SMPD3 (également connu sous le nom nSMase2) clive la sphingomyéline présente dans la membrane cellulaire pour produire la céramide, une molécule lipidique bioactive, et la phosphocholine, un nutriment essentiel. Nous avons examiné l'ossification endochondrale dans des embryons de souris *fro/fro* à E15.5 et avons observé une altération de l'apoptose des chondrocytes hypertrophiques et un défaut de minéralisation de l'os cortical dans le squelette en développement. Afin de déterminer si SMPD3 joue un rôle cellulaire autonome dans ces tissus, nous avons examiné, *in vitro*, la minéralisation de cultures d'ostéoblastes *fro/fro*; la minéralisation est moindre dans les cultures d'ostéoblastes *fro/fro* que dans les cultures témoins. Nous avons ensuite produit la souris *fro/fro;Col1a1-Smpd3*, dans laquelle l'expression de *Smpd3* dans les ostéoblastes corrige les anomalies osseuses observées dans les embryons *fro/fro* sans toutefois corriger le phénotype du cartilage. Le transgène *COL1A1-Smpd3* est également exprimé dans les odontoblastes et cette expression était suffisante pour corriger tous les défauts de minéralisation des dents de la souris *fro/fro; COL1A1-Smpd3*. Nous avons observé une diminution des niveaux de céramide dans divers tissus de la souris *fro/fro*. Une diminution similaire des niveaux de céramide est également rapporté lors de l'inactivation de la voie de novo de la synthèse des céramides dans la souris *Des1-/-*. Cependant, nous avons constaté que la souris *Des1-/-* ne présente aucun défaut de minéralisation osseuse. Cette observation soulève la possibilité que l'autre métabolite SMPD3, phosphocholine, pourrait jouer un rôle dans la minéralisation osseuse. Un déficit de la phosphatase orpheline 1 (PHOSPHO1), une enzyme intracellulaire qui clive phosphocholine pour générer sans phosphate et de la choline, a été associée à une mauvaise minéralisation osseuse. Notre analyse histologique des os de souris homozygotes composés *fro/fro;Phospho1-/-* âgés de quatre semaines a montré que la quantité d'ostéoïde ne différait pas de celle des os des souris témoins *fro/fro*. En plus de la voie de la sphingomyélinase, phosphocholine peut également être obtenue par des kinases cytosoliques de choline qui peuvent convertir les cholines de l'alimentation en phosphocholine. Partant de ce constat, nous avons nourri les souris *fro/fro* et *Phospho1-/-* avec un régime alimentaire contenant 2 % de cholines. Ce régime riche en colines a permis d'augmenter les niveaux de choline sérique et de diminuer le volume osseux non minéralisée (ostéoïde) chez la

les souris *fro/fro* mais pas chez les *phospho1*^{-/-}. Ensemble, nos données suggèrent que SMPD3 joue un rôle cellulaire autonome dans les ostéoblastes et odontoblastes en régulant, respectivement, la minéralisation des os et des dents. De plus, nous montrons que SMPD3 agit en amont de PHOSPHO1, et que le métabolisme de la choline peut jouer un rôle important dans la minéralisation des tissus solides.

Acknowledgements

I would like to first express my sincere gratitude to my supervisor Dr. Monzur Murshed for his guidance throughout my PhD and to develop myself as a researcher in the field of skeletal biology. Your passion for science is inspiring and your patience with students has been much appreciated over the years. I will surely carry all that I have learned as your student with me throughout my future scientific endeavours.

I would like to thank my supervisory committee members, Dr. René St-Arnaud, Dr. Marc D McKee and Dr. Svetlana Komarova, for their beneficial suggestions and directions over the years. I am extremely fortunate to have had the opportunity to work with a group of dedicated colleagues. My gratitude and appreciation also goes to other past and present members, especially Dr. Jingjing Li, Juliana Marulanda, Sharifa Alebrahim, Garthiga Manickan, Abhinav Parashar, Michelle Berkvens, Shraddha Solanki and Hassem Roman. Appreciation is also expressed to the animal facility technicians Mia Esser, Louise Marineau, and Natalie Girard.

In particular, I thank my parents, Abolfazl and farkhoneh, my sister, Simin, my brother, Mohammad, and my niece and nephew, for always having faith in me and supporting my dreams and ambitions.

Finally I would like to express my gratitude to Canadian Institute Health Research (CIHR) for their financial support.

Contribution of Authors

Chapter 1: **Khavandgar Z** and Murshed M, *Sphingolipid metabolism and its role in the skeletal tissues*. Cell Mol Life Sci. 2015 Mar;72(5):959-69

Khavandgar Z: Contributed to writing of the review paper.

Murshed M: Contributed to writing of the review paper.

Chapter 2: Khavandgar Z, Poirier C, Clarke CJ, Li J, Wang N, McKee MD, Hannun YA and Murshed M., *A Cell-Autonomous Role for Neutral Sphingomyelinase 2 in Bone Mineralization* . Journal of Cell Biology. 2011 Jul 25; 194 (2): 277-289

Khavandgar Z: Participated in the study design, generated and characterized the *Coll1a1-Smpd3* and *fro/fro;Coll1-Smpd3* mice; responsible for the management of mouse colonies and genotyping, performed histology and the static histomorphometry, biomechanical testing, gene expression analysis, plasmid construction, transient transfection with siRNA, mineralization experiments, analyzed the micro-CT data and contributed to manuscript preparation.

Poirier C: Provided *fro/fro* mice and contributed to manuscript preparation.

Clarke CJ: *In vitro* transfection experiments, Western blot, immunofluorescence and confocal microscopy, sphingomyelinase assay and lipid measurements and contributed to manuscript preparation.

Li J: Initial management of mouse colonies and genotyping.

Wang N: Construction of the *Coll1a1-Smpd3* plasmid.

McKee MD: Performed histology and micro-CT of the *fro/fro* mice and contributed to manuscript preparation.

Hannun YA: Provided interpretation of the data obtained by CJC and contributed to manuscript preparation.

Murshed M: Conceptualized, designed and supervised the study, interpreted the data and prepared the manuscript.

Chapter 3: Khavandgar Z, Alebrahim S, Eimar H, Tamimi F, McKee MD and Murshed M, *Local Regulation of Tooth Mineralization by Sphingomyelin Phosphodiesterase 3* . J Dent Res. 2013 Apr; 92(4):358-64.

Khavandgar Z : Generated and characterized the *Colla1-Smpd3* and *fro/fro;Colla1-Smpd3* mice, responsible for the management of mouse colonies and genotyping, performed the radiographic analyses and immunohistochemistry; analyzed the data and contributed to manuscript preparation.

Alebrahim S: Performed the histological analyses and the histomorphometric quantification, contributed to the management of mouse colonies and genotyping; analyzed the data, and contributed to manuscript preparation.

Eimar H: Performed the X-ray diffraction and micro-CT analyses experiments, analyzed the data and contributed to manuscript preparation.

Tamimi F: Provided interpretation of the data obtained by Eimar H and contributed to manuscript preparation.

McKee MD: Performed the electron microscopy, interpretation of the EM data; contributed to manuscript preparation and proof-read the manuscript.

Murshed M: Conceptualized, designed and supervised the study, interpreted the data and prepared the manuscript.

Chapter 4: Khavandgar Z, Clarke CJ, Summers SA, Farquharson C, Millán JL and Murshed M.

Sphingomyelin Phosphodiesterase 3 and Phosphatase, Orphan 1 Acts in a Relay to Promote Bone Mineralization. In preparation.

Khavandgar Z: Generated the *fro/fro;Coll1-Smpd3*, *fro/fro;phospho1-/-* mice, responsible for the management of mouse colonies and genotyping, performed histology and the static histomorphometry, analyzed the data and contributed to manuscript preparation.

Clarke CJ: Performed lipid measurements.

Summers SA: Provided samples from *Des1-/-* mice.

Farquharson C: Contributed to the conceptualization of the study.

Millán JL: Provided *Phospho1-/-* mice, contributed to the conceptualization of the study.

Murshed M: Conceptualized, designed and supervised the study, interpreted the data and prepared the manuscript.

In addition to the publications described above, I have also collaborated in and coauthored the following articles during my doctoral studies:

1. Tabatabaei N ,Rodd C ,Kremer R ,**Khavandgar Z** , Murshed M and Weiler H, *Dietary Vitamin D During Pregnancy has Dose-Dependent Effects on Long Bone Density and Architecture in Guinea Pig Offspring but not The Sows.* **The Journal of Nutrition.** 2014 Dec;144(12):1985-93
2. Li Z, Wu G, Sher RB, **Khavandgar Z**, Hermansson M, Cox GA, Doschak MR, Murshed M, Beier F and Vance DE. *Choline Kinase Beta is required for Normal Endochondral Bone Formation.* **Biochim Biophys Acta.** 2014 Mar 14;1840(7):2112-2122
3. Alebrahim S, **Khavandgar Z**, Marulanda J and Murshed M, *Inducible Transient Expression of Smpd3 Prevents Early Lethality in fro/fro Mice.* **Genesis.** 2014 May;52(5):408-16
4. **Khavandgar Z**, Roman H, Li J, Lee S, Vali H, Brinckmann J, Davis EC and Murshed M, *Elastin Haploinsufficiency Impedes the Progression Of Arterial Calcification in MGP-Deficient Mice.* **J Bone Miner Res.** 2014 Feb; 29(2):327-37
5. Khayat G, Rosenzweig DH, Khavandgar Z, Li J, Murshed M, Quinn TM. *Low-Frequency Mechanical Stimulation Modulates Osteogenic Differentiation of C2C12 Cells.* **ISRN Stem Cells.** 2013; 2013(3698):1-9.

6. Meyers-Needham M, Lewis JA, Gencer S, Sentelle RD, Saddoughi SA, Clarke CJ, Hannun YA, Norell H, Martins da Palma TR, Nishimura MI, Kravetska J, **Khavandgar Z**, Murshed M, Cevik MO and Ogretmen B, *Off-Target Function of the Sonic-Hedgehog Inhibitor Cyclopamine in Mediating Apoptosis via Nitric Oxide-Dependent Neutral Sphingomyelinase 2/Ceramide Induction*. **Mol Cancer Ther.** 2012 Mar 27; 11(5):1092-102.

7. Li J, **Khavandgar Z**, Lin S and Murshed M, *Lithium Chloride Attenuates BMP-2 Signaling and Inhibits Osteogenic Differentiation through a Novel WNT/GSK3- Independent Mechanism*. **Bone.** 2011 Feb 1;48(2):321-31

Chapter 1: General Introduction and Literature Review

Skeletal tissues not only provide structural and biomechanical supports to the vertebrate body, but also maintain the homeostasis of two essential chemical species, inorganic phosphate and calcium ions, which are required for many critical physiological functions. In addition to its role as a mineral reservoir, more recently the skeleton has been recognized as an endocrine organ that secretes hormone(s) to regulate energy metabolism [1, 2]. These myriad roles of the skeleton make it one of the most dynamic tissues in the body that achieves its complex structure and unique cell-extracellular matrix composition through a multistep process during development.

1.1 Bone development

Development of the skeleton in vertebrates involves concerted functions of three major cell types—chondrocytes in cartilage, and osteoclasts and osteoblasts in bone. The spatiotemporal distribution of the precursor stem cells that give rise to these cell types, their proliferation, differentiation and programmed death in the developing skeleton determines the growth, shape and load-bearing capacity of the future skeleton [3-5]. Developmentally, bones can be categorized into two types: endochondral and intramembranous bones. A cartilage ‘precast’ (anlagen) is essential for endochondral bone formation (Fig 1.1), which is not needed for the formation of intramembranous bones. Formation of both bone types however, initiates with the condensation of mesenchymal stem cells (MSC) that first proliferate and differentiate directly into osteoblasts in the case of intramembranous bones (Fig 1.2) or chondrocytes in the case of endochondral bones. Chondrocytes within the core of the developing endochondral bones eventually differentiate to form two distinct growth plates at both ends. Each of these growth plates has four distinct zones: (1) a resting zone of chondrocyte precursors; (2) a proliferative zone with chondrocytes that synthesize extracellular matrix (ECM) proteins

including type II collagen; and (3) prehypertrophic and (4) hypertrophic zones. The hypertrophic zone carries terminally differentiated chondrocytes that go through programmed death after secreting a cartilaginous matrix rich in type X collagen. This matrix becomes mineralized and vascularized, and eventually replaced by a type I collagen-rich bone matrix through the concerted resorptive and formative activities of osteoclasts and osteoblasts, respectively [3-5].

In both endochondral and intramembranous bones, some osteoblasts differentiate and trap themselves in the mineralized matrix. These entrapped cells which are one of the most abundant cell type in bone tissues are called osteocytes [6]. Osteocytes through their lacuna- canalicular network sense the mechanical force as well as changes the levels of in circulating minerals. [6]. Osteocytes also directly regulate bone remodeling by expressing sclerostin [7]. This protein inhibits osteoblast differentiation at sites where the bone experiences reduced mechanical loading. Additionally, osteocytes release RANKL to promote the differentiation of osteoclasts [8].

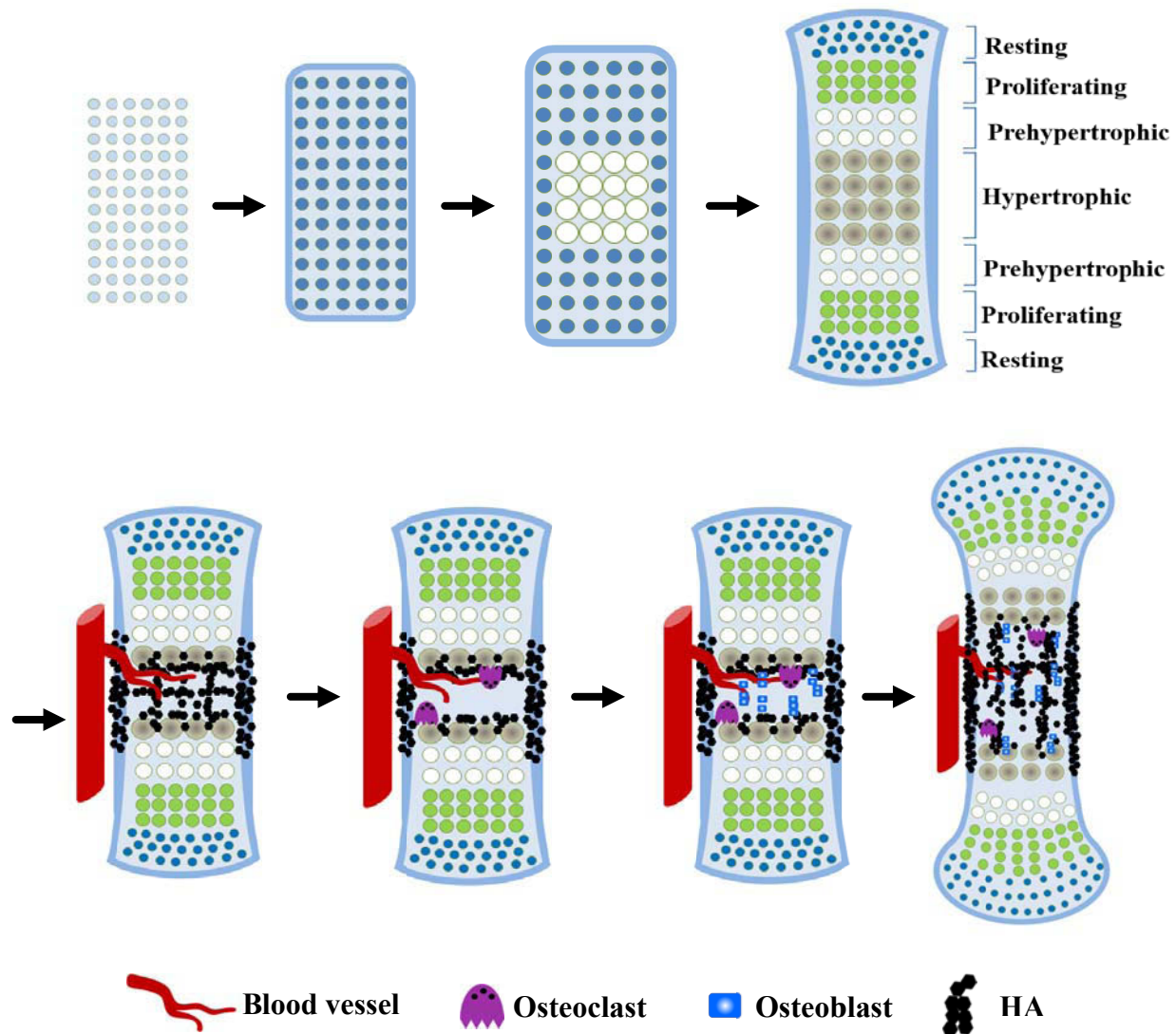


Figure 1.1: Endochondral bone formation.

Endochondral bone formation starts with the condensation of MCs which differentiate to chondrocytes. Then chondrocytes at the centre of the anlagen of the future bone stop proliferating and become hypertrophic chondrocytes. Perichondrial cells differentiate to osteoblast to form the bone collar. In the mid shaft, hypertrophic chondrocytes secrete a type X collagen-rich matrix. This matrix will be mineralized and invasion of the blood vessels bring osteoclast precursors into this area. Mature osteoclasts resorb the mineralized cartilage matrix and osteoblasts migrate to the resorbed matrix to form primary spongiosa. Finally, at the end of the long bones, secondary ossification centres with well-defined growth plates will be formed (Adapted from Dr. Murshed's lecture slides).

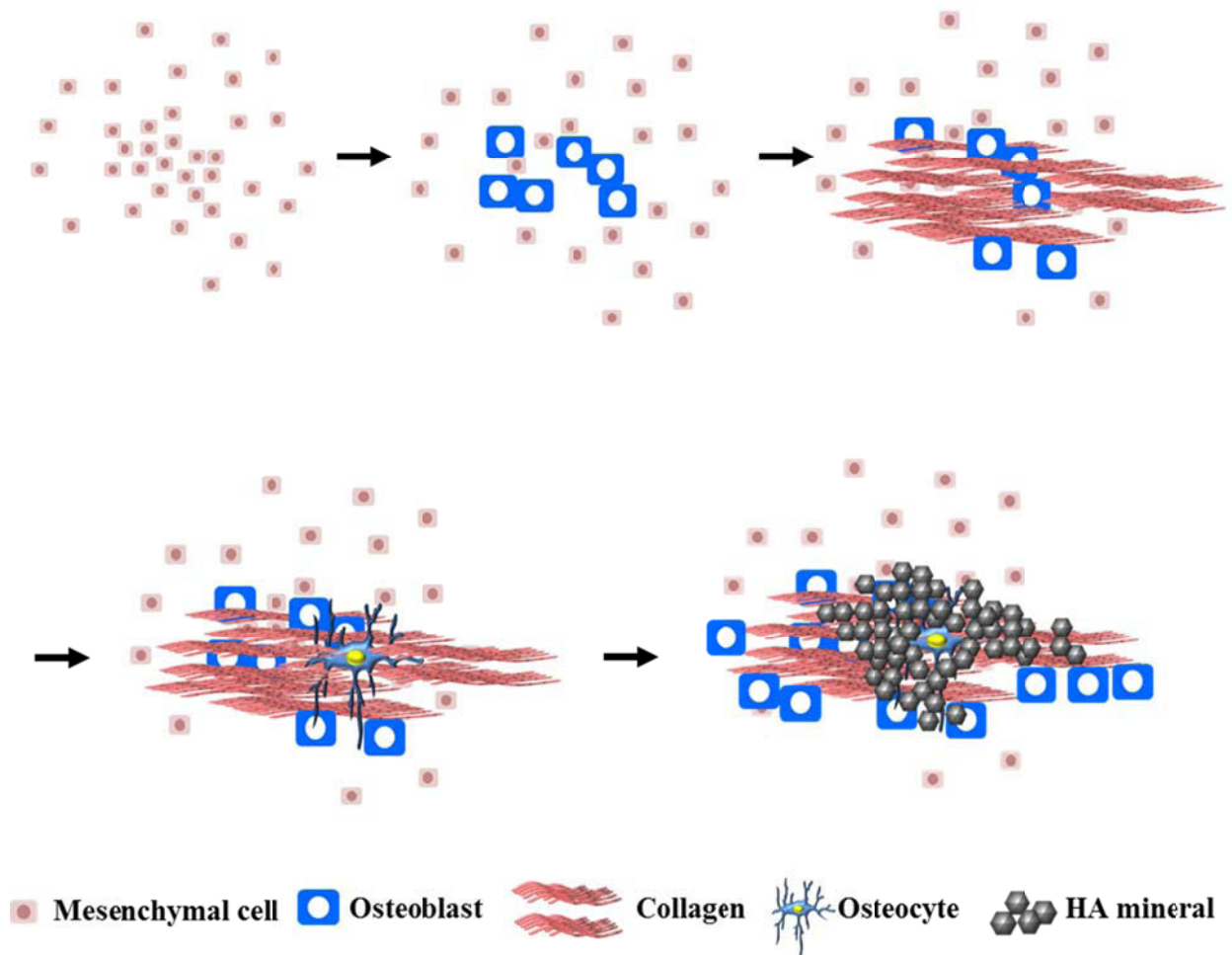


Figure 1.2: Intramembranous bone formation.

To form intramembranous bone, mesenchymal precursors differentiate directly into bone-forming osteoblasts. Then osteoblasts lay down a collagen-rich matrix. This matrix becomes mineralized and entraps some of the osteoblasts. When osteoblasts become trapped in the matrix, they differentiate and become osteocytes (Adapted from Dr. Murshed's lecture slides).

1.2 Tooth development

Teeth in some animals such as fish and reptiles are constantly being formed and replaced many times. However, most mammals like humans have a maximum of two sets of teeth. This is due to the fact that mammals stop growing throughout their life after a certain period of time. On the other hand, some mammals such as rodents have only one set of teeth but their teeth grow constantly. The shape and size of each tooth is determined by their unique position which exposes the precursor cells to a unique environment made up of a cocktail of growth factors and cytokines.

The primary epithelial band in the oral ectoderm plays a critical role in tooth morphogenesis [9]. The cells in the epithelial band proliferate and orient to form two bud-like structures. One of these structures eventually gives rise to vestibular lamina that forms the oral vestibule, the space between the lips and the gingiva. The other structure forms the dental lamina which serves as the bed for future tooth formation [10-12].

Tooth formation begins with the formation of dental organ formation. The initial stage of the dental organ is known as the 'bud stage' which results from the localized proliferation of the epithelial cells in the dental lamina. At this stage an early signaling center directs the underlying mesenchymal cells to start their proliferation and condensation [13].

As the tooth buds grow in size, it drags the surrounding cells of the dental lamina giving it the characteristic shape of a cap sitting on the top of a ball of proliferating cells. This stage of the dental organ is known as the 'cap stage'. At the end of the cap stage, a distinct enamel organ is formed. The enamel organ has four distinct layers: outer enamel (dental) epithelium, inner enamel epithelium, stellate reticulum, and stratum intermedium. Reciprocal signaling between the epithelial and mesenchymal layer promotes the terminal differentiation of both epithelial and underlying mesenchymal cells; the inner epithelial cells become the ameloblasts, while the

mesenchymal cells underneath become the odontoblasts. Both the layers are separated by a basement membrane that is dissolved before the synthesis of dentin and enamel (Fig 1.3) [14-16].

Odontoblasts secrete a collagen-rich predentin that is mineralized in a manner very similar to that of bone [17]. Once the predentin is mineralized, ameloblasts start producing the initial enamel. The differentiation of functional ameloblasts and underlying odontoblasts first start at the cusp of the future tooth and gradually progress towards the cervical region. The formation of new enamel and dentin proceed in opposite directions; enamel is deposited outwards, while dentin is deposited inwards towards the pulp chamber. At this stage the tooth is at its 'bell stage' [13, 18].

Initial mineral crystals in the immature enamel are formed along the long axis spanning the full thickness of the enamel layer [19]. The thickening of the crystals is thought to be inhibited by proteins such as amelogenin [20]. During the maturation phase the inhibitory proteins are degraded allowing the thickening of the enamel crystals. All the ameloblasts die upon completion of the enamel maturation, while odontoblasts continue dentin production throughout life albeit at a slower pace [21].

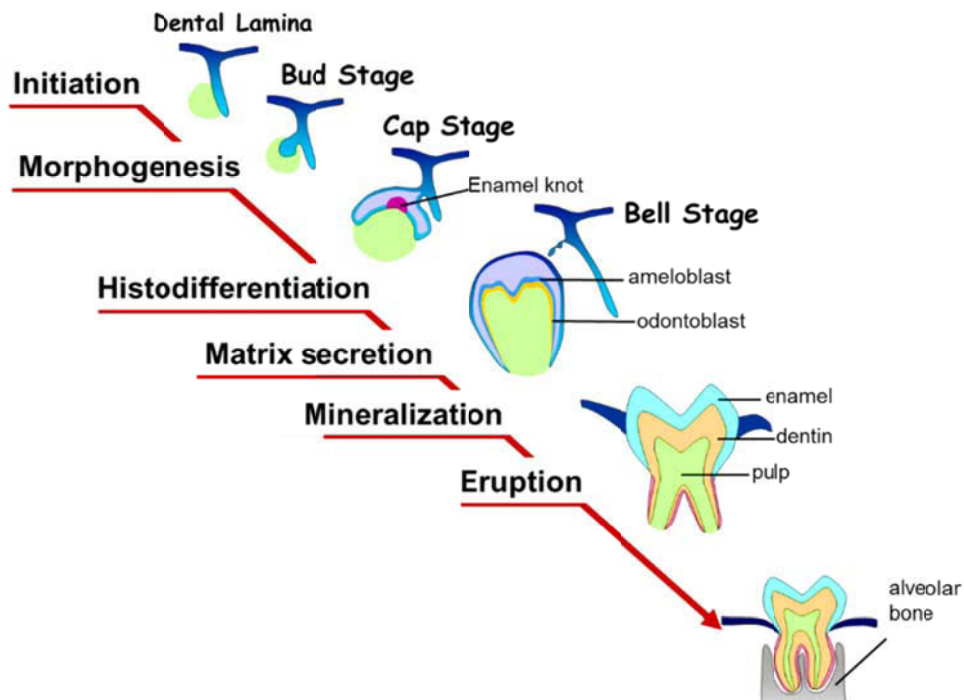


Figure 1.3: Tooth development.

Stages of tooth development are depicted from the thickening to eruption of the tooth. The tooth germ is formed from the oral epithelium. Differentiation of the cells happens in the bell stage setting the stage for enamel and dentin formation.

1.3 Current understanding of skeletal mineralization

The restriction of physiologic apatitic mineralization specifically to bones and teeth in vertebrates can be explained to a large extent by the unique, pro-mineralization environment in these tissues. Two mineral ions – inorganic phosphate (P_i) and calcium – when present at physiologic concentrations, will promote hydroxyapatite (HA) crystal growth within and between newly synthesized collagen fibrils in the skeletal ECM [22-27]. More than forty years ago, it was shown that inorganic pyrophosphate (PP_i), a chemical derivative of P_i , can inhibit the mineralization process [28, 29]. The presence of a scaffolding matrix and a defined extracellular ratio of P_i to PP_i are two critical determinants of ECM mineralization. Paradoxically, ectophosphodiesterase nucleotide phosphohydrolases (*Enpp1*) and *Ank* – two genes important for

the maintenance of extracellular PP_i levels – are abundantly expressed in all skeletal tissues [24, 30, 31]. This observation suggests that a regulatory mechanism must exist to limit the extracellular levels of PP_i in mineralizing tissues. In fact, a cell membrane-bound enzyme known as tissue nonspecific alkaline phosphatase (TNAP/ALPL) is produced by bone and tooth cells, which cleaves PP_i to generate P_i [32]. ALPL enzymatic activity may alter the local P_i to PP_i ratio to favor mineral precipitation [33]. The importance of ALPL during skeletal ECM mineralization was convincingly demonstrated by the identification of a broad spectrum of missense mutations and deletions of *ALPL* in hypophosphatasia patients possessing defects in bone and tooth mineralization [34-37]. The generation and analysis of *Tnap*-deficient mice further confirmed the requirement of this gene for the proper mineralization of these tissues [38, 39]. However, *Alpl* and two genes, *Colla1* and *Colla2*, encoding type I collagen that serves as the ECM substrate for mineralization, are all broadly expressed throughout the body. Such a ubiquitous expression pattern fails to account for the tissue specificity of physiologic mineralization. Interestingly, these genes are uniquely co-expressed in skeletal hard tissues, at sites where mineralization occurs [24]. This observation suggested that the specificity of skeletal mineralization can be explained, in part, by the unique co-expression of these tissue-nonspecific genes. As *in vivo* proof, Murshed *et al.* induced ectopic mineralization when the PP_i cleaving enzyme, ALPL, was over-expressed in the dermis, a fibrillar, collagen-rich soft tissue [24].

Among the dental tissues, enamel mineralization occurs through a unique mechanism. Unlike bone, dentin or cementum enamel mineralization does not require a collagen-rich matrix for mineral scaffolding. Rather, it relies on a protein-regulated process for HA crystal maturation [40, 41]. On the other hand, in dentin and cementum, the mechanism of ECM mineralization is similar to that of bone [17]. This is not surprising as dentin forming odontoblasts and cementum forming cementoblasts are both of mesenchymal origin, just like the bone forming osteoblasts

[42, 43]. The differentiation of these cells is largely regulated by several common signaling molecules and transcription factors such as BMPs, FGFs, RUNX2 and OSX [44-47]. In fact, genetic disorders such as vitamin D-deficient rickets, X-linked hypophosphatemia, hypophosphatasia, cleidocranial dysplasia all affect bone and tooth mineralization and/or the development of these hard tissues. A brief account of some of these mineralization disorders have been given below.

1.4. Genetic diseases with ECM mineralization defects

1.4.1 Hypophosphatasia. Hypophosphatasia is an autosomal recessive genetic disorder caused by mutation in *ALPL* gene [48]. The patients show poor bone and tooth mineralization and the severity of the disease vary with the type of mutation [49]. Some forms of the disease can be embryonically lethal, while some other forms show mild manifestation of the disease e.g. dentition problems during the adulthood [34]. The clinical features include reduced serum alkaline phosphatase levels, increase of unmineralized bone and tooth matrix, bone deformities and fracture and premature tooth loss. Additionally, growth retardation and osteopenia is common in these patients [34, 48]. There are two gene targeted mouse models for alkaline phosphatase deficiency reported. Interestingly, although serum alkaline phosphatase levels are undetectable in these mice the bone mineralization defects appear to be normal at birth and progressively increases with time [38, 50]. The mice suffer from seizure and die before weaning due to impaired vitamin B metabolism. Injection of pyridoxal prevents early death but does not correct the bone mineralization defects [50]. Bone mineralization defects are thought to be caused by an imbalance in P_i to PP_i ratio. More recently, enzyme replacement therapy has been successfully used to prevent the progression of bone and tooth mineralization defects in both animal models and humans [51-53].

1.4.2 Vitamin D-dependent rickets. Vitamin D-dependent rickets (VDDR) can be caused by mutations in the enzymes that are essential to synthesize the active form of vitamin D (1,25 dihydroxy vitamin D₃) or vitamin D receptor or its effector protein [26, 54]. The poor bone and tooth mineralization defects are primarily caused by markedly reduced serum P_i and ionic calcium levels. VDDR Type IA is caused by 25-Hydroxyvitamin D₃ 1-alpha-hydroxylase (CYP27B1) gene, while Type 1B is caused by Vitamin D 25-hydroxylase (CYP2R1) gene [55, 56]. Type 2A and 2B VDDR are caused by mutations in vitamin D receptor nuclear protein affecting the functions of vitamin D receptor, respectively. These mutations in turn lead to end organ unresponsiveness to active vitamin D [57]. Currently, there are two different mouse models available in which the gene encoding vitamin D receptor has been ablated. Both of these mice show low serum P_i and ionic calcium levels, severe osteomalacia and rickets mimicking the human disease conditions [58-61]. A mineral-rich diet has been shown to correct the osteomalacia and skeletal abnormalities [62, 63].

1.4.3 X-linked hypophosphatemia. X-linked hypophosphatemia is caused by mutations in PHEX gene [64]. *PHEX* is expressed in osteoblasts and osteocytes and its mutation affects circulating P_i levels and the metabolism of vitamin D, without any significant alterations in ionic calcium and PTH levels. As the patients do not respond to vitamin D treatments, the disease is also known as vitamin D-resistant rickets. In the absence of functional PHEX, the serum levels of FGF23, an osteoblast-/osteocyte-derived hormone, increases, which acts on the cells of kidney proximal tubule decreasing the expression of sodium-phosphate cotransporter type II (NPT2 encoded by *NaPi2a*) [65-69]. The reduction of sodium-phosphate cotransporter in turn results in impaired reabsorption of P_i by proximal tubule cells decreasing the blood P_i levels. Hypophosphatemia appears to be the primary cause of bone and tooth mineralization defects in this disease. However, recent works suggest that PHEX and FGF23 may affect bone independent of serum

phosphate levels. This conclusion was drawn from the observation that the skeletal phenotype of *Fgf-23-/-/NaPi2a-/-* mice resembles the one of *Fgf23-/-* mice despite the complete reversal of serum phosphate levels [69]. Unexpectedly, FGF23-deficient mice show osteomalacia, although serum phosphate levels are increased in these mice [25]. P_i-induced upregulation of osteopontin, a mineralization inhibitor may contribute to the osteomalacia phenotype in FGF23-deficient mice [70]. More recently, osteopontin has been shown as a substrate for PHEX in an *in vitro* experiment [71].

Several mouse models have been generated to study X-linked hypophosphatemia, of which *Hyp* mice carrying a deletion mutation in *PheX* gene has been widely used [64, 72, 73]. A second model Gy and a third model generated by N-ethyl-N-nitrosourea (ENU) mutagenesis are also available [74, 75]. All these mice demonstrate hypophosphatemia and rickets as seen in human patients. Apart from these gene targeted models for FGF23 and NPT2 and multiple transgenic mice expressing FGF23 and PHEX have been proven to be useful to fully understand the pathophysiology of X-linked hypophosphatemia [76, 77].

1.4.4 Osteogenesis imperfecta Type VI . The most common forms of osteogenesis imperfecta (OI) in humans are caused by mutations in Type I collagen genes (*Colla1* and *Colla2*) and the bones of these patients do not show any signs of osteomalacia [78, 79]. In Type VI OI patients however, osteomalacia and decreased mineral apposition rates are common features [80]. More recently, it has been shown that OI Type VI is caused by a premature nonsense mutation in SERPINF1 gene, and unlike other type of OI, collagen folding, posttranslational modification, or collagen secretion are not affected [81]. SERPINF1 encodes pigment epithelium-derived factor (PEDF), a secreted glycoprotein of the serpin superfamily. It has been suggested PEDF, an inhibitors of angiogenesis, has a role in bone homeostasis [82]. At present no genetically-modified mouse model is available to study the role of SERPINF1 in the skeletal tissues.

The focus of this thesis is primarily on bone and dentin mineralization. The original hypothesis, suggesting the reliance of ECM mineralization on the extracellular levels of calcium and P_i , the metabolism of mineralization inhibitors and the presence of a collagen-rich matrix does not rule out the existence of auxiliary mechanisms working in concert to mineralize the skeletal ECM. The possibility of additional mechanism(s) is supported by the fact that, in *Alpl*-deficient mice, skeletal tissues are mineralized normally at birth [38]. A recently identified mutation in a mouse model, which displays altered sphingolipid metabolism and severe bone and tooth mineralization defects, further enforces the likelihood that multiple mechanisms are involved in skeletal mineralization [83]. The segments 1.5-1.7 will provide a literature review on the key sphingolipids and their effects on major skeletal cell types and tissues.

1.5 Sphingolipid biosynthesis

Sphingolipids carry long-chain aliphatic-amine backbones containing two or three hydroxyl groups which are known as sphingoid bases [84-86]. The most abundant sphingoid base in animal tissues is sphingosine. Additionally, tissues contain a saturated analog of sphingosine known as dihydrosphingosine or sphinganine. Enzymatic modifications of these simple sphingoid bases generate a wide array of sphingolipids with diverse structural and functional properties (Fig. 1.4). The most common functional sphingolipids involve more than hundred species of ceramide, phosphorylated ceramides, sphingoid bases and sphingoid base phosphates among others [84-86].

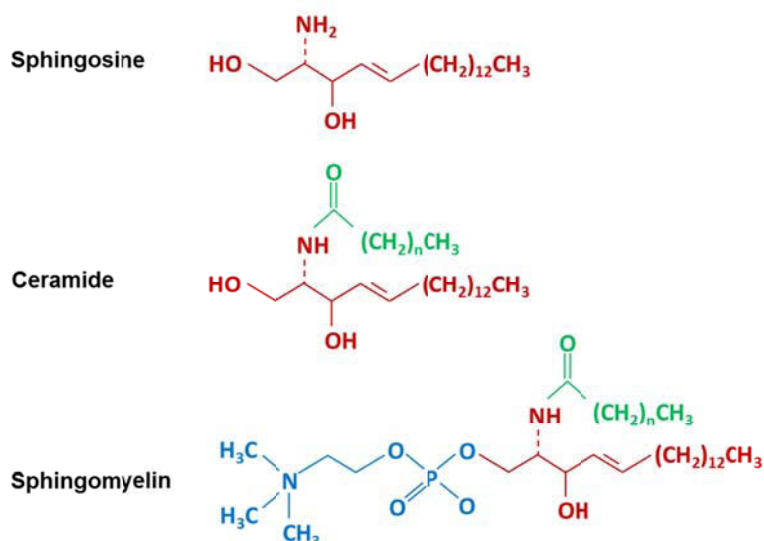


Figure 1.4: Chemical structures of sphingosine and its derivatives ceramide and sphingomyelin.

1.5.1 De novo synthesis of sphingolipids

Sphingolipids are primarily synthesized in the endoplasmic reticulum (ER), but are transported to the plasma membrane and endosomes, where they perform many of their functions [87-89]. In the ER, sphingolipids can be synthesized *de novo* using simple precursors, such as serine and palmitoyl CoA. In a condensation reaction catalyzed by a ubiquitous enzyme called *serine palmitoyltransferase* these two substrates first generate 3-ketosphinganine, which is converted to sphinganine by *ketosphinganine reductase* [87-89]. A *dihydroxyceramide synthase* then acetylates sphinganine to generate dihydroxyceramide. Finally, a *desaturase*-catalyzed reaction converts an inactive dihydroxyceramide to ceramide, an important lipid second messenger that regulates a variety of cellular activities (Fig. 1.5). Ceramide serves as a substrate for one of three enzymes that produce sphingolipids, such as glucosyl ceramide, galactosyl ceramide and sphingomyelin. Ceramide can also be phosphorylated by a family of ceramide bioactive lipid with signaling properties. S1P can also be dephosphorylated by a class of lipid-phosphate phosphatases (LPP1-3). These transmembrane enzymes with extracellular catalytic sites play an important regulatory role in S1P-mediated signaling events.

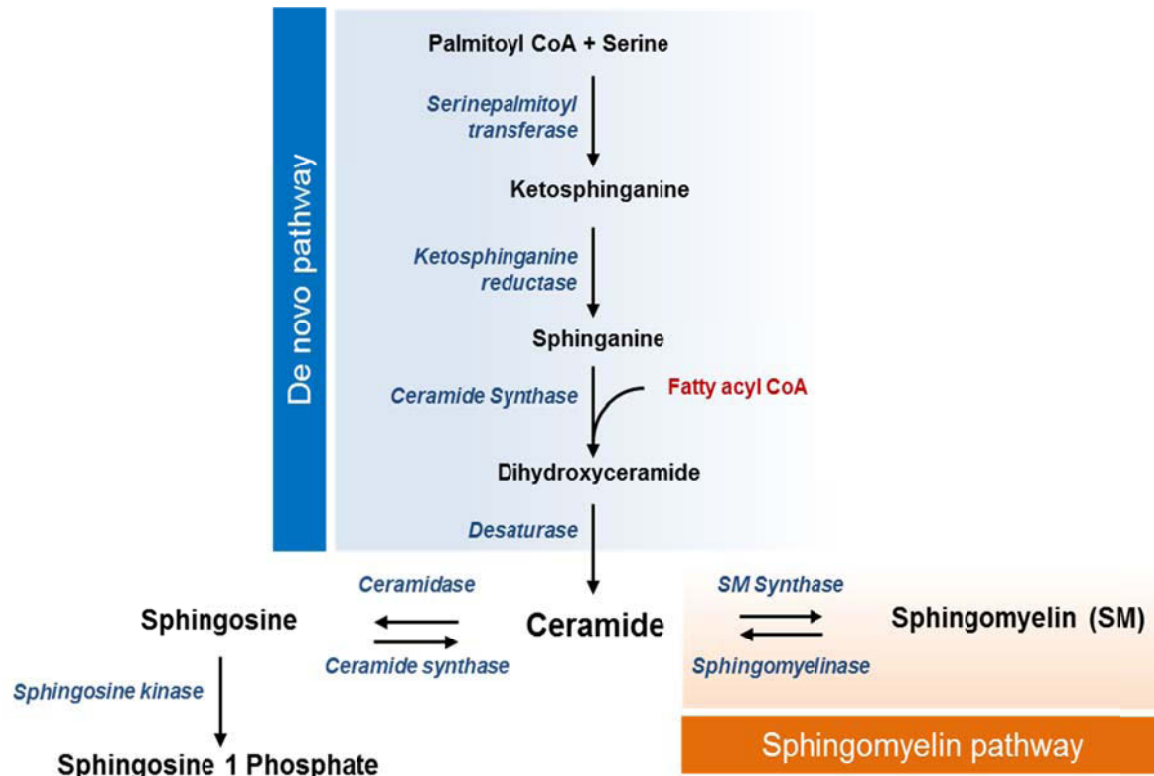


Figure 1.5: *De novo* and sphingomyelinase pathways showing the metabolism of ceramide, sphingomyelin and sphingosine

1.5.2 Synthesis of sphingolipids by sphingomyelinases

In addition to the *de novo* pathway described above, various sphingomyelinases (SMase) play a critical role in sphingolipid biosynthesis (Fig. 1.2). Sphingomyelinases belong to a class of enzymes, which cleave sphingomyelin to generate ceramide and phosphocholine. Depending on their pH optima, these enzymes have been classified into three categories—acidic, alkaline and neutral sphingomyelinases [90, 91].

Acidic sphingomyelinases are the most extensively studied enzymes among the three subclasses. Mutations in acidic sphingomyelin phosphodiesterase 1 gene (*Smpd1*) cause Niemann-Pick disease, which is characterized by abnormal lipid accumulation in the spleen, liver, lung, bone marrow and brain [91]. Recently, this enzyme has been implicated in ceramide-mediated signaling events [92].

Alkaline sphingomyelinase hydrolyzes dietary sphingomyelin and generates sphingolipid metabolites in the gut [93]. Impaired sphingomyelin metabolism in the intestine might have implications in colon cancer development as dietary supplementation with sphingomyelin and ceramide analogs was found to inhibit the development of chemically-induced colon cancer in animal models [94].

Neutral sphingomyelinases are the key enzymes involved in ceramide-mediated signaling events. So far, three sphingomyelin phosphodiesterases (SMPD2, 3 and 4) have been identified that belong to this subclass [91]. Although all these isoforms are present as membrane-bound forms, they differ in their tissue distribution. SMPD2 and 4 are ubiquitously expressed, while SMPD3 expression is largely restricted to the bone, brain and cartilage [95].

1.6 Role of sphingolipids in skeletal cells: *In vitro* findings

The functions of two major sphingolipids, ceramide and S1P, in skeletal cells have been discussed below

1.6.1 Ceramide

Obeid *et al.* used synthetic C2-ceramide first to demonstrate the role of sphingolipids in apoptosis [96]. This study showed that this ceramide analog promotes DNA fragmentation and apoptosis in U937 monoblast leukemia cells via upregulation of Tumor Necrosis Factor-alpha (TNF-alpha). Since then numerous studies have reported the pro-apoptotic role of ceramide in many different cell types. These studies described multiple signaling intermediates/pathways including ceramide-activated protein kinase and the activation of mitogen-activated protein kinase to induce cellular apoptosis. For example, ceramide-induced apoptosis may involve the

activation protein kinase C-zeta to promote c-Jun N-terminal kinase (JNK) activation and the nuclear translocation of transcription factor nuclear factor-kappa B (NF-kappa B) [96].

It has been suggested that the membrane contact sites (MCS) between ER and mitochondria facilitate ceramide-induced apoptosis. Ceramide produced by SMPD3 in the ER membrane may translocate to the outer mitochondrial membrane to form ceramide channels, which may in turn release pro-apoptotic molecule cytochrome C [97]. A recent study proposed that ceramide serves as a precursor for S1P and hexadecenal which in turn regulates apoptosis. These molecules activate apoptotic regulators Bak and Bax, promoting the release of cytochrome C from the mitochondria, which then activates caspases, enzymes essential for apoptotic cell death [98].

So far, only a handful of studies have been performed to examine the effects of ceramide on the apoptosis of bone cells *in vitro*. Treatment of MC3T3-E1 preosteoblasts with the nitric oxide (NO) donor sodium nitroprusside causes apoptosis [99]. This study reports an increase of long-chain intracellular ceramides, C22 and C24, upon this treatment. Interestingly, NO has been recently shown to promote the release of cytochrome C from the mitochondria [100]. It is therefore likely that NO increases the release of long-chain ceramides, which in turn results in the release of cytochrome C from the mitochondria turning on the intrinsic apoptotic pathways in cultured osteoblasts.

In another cell-culture study, murine MC3T3-E1 preosteoblasts were treated with TNF-alpha to induce apoptosis. Within 3 min of TNF-alpha treatment, detectable increase of endogenous ceramide levels was apparent, which reached to its peak by 30 min. TNF-alpha treatment of MC3T3-E1 cells also promoted the nuclear translocation and activation of NF-kappa B. Interestingly, treatment of the preosteoblasts with a ceramide analog alone was sufficient to affect the nuclear translocation/activation of NF-kappa B in a similar fashion. This

observation lead to the conclusion that in osteoblasts, TNF-alpha modulates NF-kappa B localization and function through the upregulation of ceramide synthesis [101]. A separate study showed that the treatment of MC3T3-E1 cells with dexamethasone, a known immunosuppressant, reduces TNF-alpha-induced ceramide production and dampens not only the activation of NF-kappa B, but also the activities of two pro-apoptotic enzymes, JNK and caspase-3-like extracellular protease. Additionally, there was a redistribution of cytochrome C in these cells [102]. This later observation further confirms that mitochondrial pathways might be relevant in the apoptosis of bone cells. Collectively, these findings indicate that inflammation-induced ceramide production in osteoblasts, may result in apoptosis through multiple mechanisms.

A more recent study reported that although high-dose treatment (2×10^{-6} M) of mouse primary osteoblasts with C2-ceramide-induced apoptosis, the low-dose treatment (10^{-7} M) actually resulted in increased cell survival through the protein kinase C activity. It is possible that there might be separate pathways that promote ceramide-mediated pro-apoptotic and pro-survival signaling events [103].

As is the case with the cultured osteoblasts, a high dose (3×10^{-5} to 10^{-4} M) of C2-ceramide treatment induced apoptosis of chondrocytes in rabbit articular cartilage explants. Also, C2-ceramide treatment increased matrix metalloproteinase activity in these explants. These data provide evidence that chronic inflammatory responses that increase matrix remodeling in osteoarthritis might be caused by an upregulation of ceramide synthesis [104]. C2-ceramide induced apoptosis in murine chondrogenic ATDC5 cells without affecting the expression of chondrogenic markers *Sox9*, *Col2a1* and *Coll10a1* [105].

Although C2-ceramide treatments lead to increased apoptosis in both osteoblasts and chondrocytes, there was no effect of this cell-permeable synthetic ceramide on the apoptosis of

rabbit mature osteoclasts [106]. However, treatment with ceramide inhibited F-actin ring formation within the sealing zone of osteoclasts and impaired their resorption capacities. A similar effect was observed when these cells were treated with exogenous sphingomyelinase [106]. Interestingly, TNF- α treatment that promotes apoptosis in osteoblasts by upregulating ceramide synthesis, actually favors the survival of cultured murine osteoclasts [107]. As shown by this study, TNF- α treatment activates pro-survival pathways in osteoclasts by engaging phosphatidylinositol 3-kinase, Akt and MEK/ERK signaling.

Several studies suggest that ceramide and its derivatives play an important role in osteoclastogenesis. Lactosylceramide, a derivative of ceramide, has been shown to induce the expression of the receptor-activator of NF- κ B (RANK) in bone marrow-derived osteoclasts [108]. Moreover, this study showed that the inhibition of glucosylceramide synthase by d-threo-1-phenyl-2-decanoylamino-3-morpholino-1-propanol (d-PDM) prevented granulocyte-macrophage colony-stimulating factor and RANK ligand-mediated osteoclastogenesis. In a subsequent study, it was shown that the d-PDM-mediated inhibition of osteoclastogenesis could be rescued by treating the osteoclasts with lactosylceramide [109].

1.6.2 Sphingosine and its derivatives

Sphingosine and its derivatives have been implicated in a variety of cell functions in osteoblasts. In MC3T3-E1 preosteoblast cultures, S1P induces the synthesis of heat-shock protein 27 (HSP27), a molecular chaperon that acts as a stress-response protein; HSP27 in turn negatively regulates the synthesis of osteocalcin, a marker expressed by functional osteoblasts [110, 111]. Interestingly, treatment of myogenic C2C12 cells with bone morphogenetic protein-2 (BMP-2) in combination with S1P or FTY720 (an agonist of S1P receptor) significantly increased the expression of osteocalcin and several other osteogenic markers [112]. Although the latter study did not report osteocalcin protein levels, this apparent discrepancy in osteocalcin

expression might be caused by the differences in the differentiation stages and cell types used for these two studies. Exposure of MC3T3-E1 cells to sphingosine, S1P and sphingosylphosphorylcholine promoted intracellular calcium release increasing cytosolic calcium levels [113, 114]. Also, S1P treatments of rat calvarial osteoblasts and human SaOS-2 osteosarcoma cells have been shown to prevent apoptosis of these cells that was initiated by serum deprivation [115].

S1P signaling has been implicated in osteoblast migration; S1P acts as a chemorepellent for the undifferentiated preosteoblasts [116]. As opposed to S1P function, it was shown that platelet-derived growth factor (PDGF) that plays a role in bone remodeling and fracture healing, acts as a chemoattractant for preosteoblasts. Upon treatment with BMP-2, these cells differentiate to mature osteoblasts retaining their abilities to respond to PDGF but not to S1P. Roelofsen *et al* . suggested that migration of osteoblasts is controlled by the balance between PDGF and S1P allowing only differentiated osteoblasts to travel to the site of bone formation. Although interesting, this notion has been challenged by a more recent study identifying S1P as a chemoattractant for MSCs that give rise to cells of the osteoblast lineage. According to this study, bone-resorbing osteoclasts release S1P to induce the migration of MSCs and thereby promote the recruitment of the osteoblast precursors at the sites undergoing bone remodeling. It is, however, possible that osteoblasts at different stages of differentiation may respond differently to S1P [117].

S1P has been shown to promote the proliferation of rat primary chondrocytes [118]. S1P treatment induced phospholipase C-mediated cytosolic calcium release in these cells. Also, extracellular signal-regulated kinase (ERK) and p38 mitogen-activated kinases were induced. When treated with ERK inhibitor PD98059 the cell proliferation was almost completely blocked, while p38 kinase inhibitor SB203580 did not have any effect. These data suggest a

cardinal role for ERK in S1P-mediated chondrocyte proliferation. In articular chondrocytes, S1P signaling has been implicated in cartilage matrix degradation, upregulation of vascular endothelial growth factor and the progression of arthritis [119, 120].

S1P signaling has also been shown to regulate the migration of osteoclast precursors. Two S1P receptors, S1PR1 and S1PR2, play a critical role in this process. S1PR1 promotes the chemotaxis towards S1P in bone marrow where S1P level is normally low, while S1PR2 mediates the S1P chemorepellant properties in circulation where S1P level is high. This mechanism may facilitate the infiltration of osteoclast precursors from the circulation to the bone marrow [121]. The major effects of ceramide and S1P on the three major cell types in the skeleton have been depicted in Fig. 1.6.

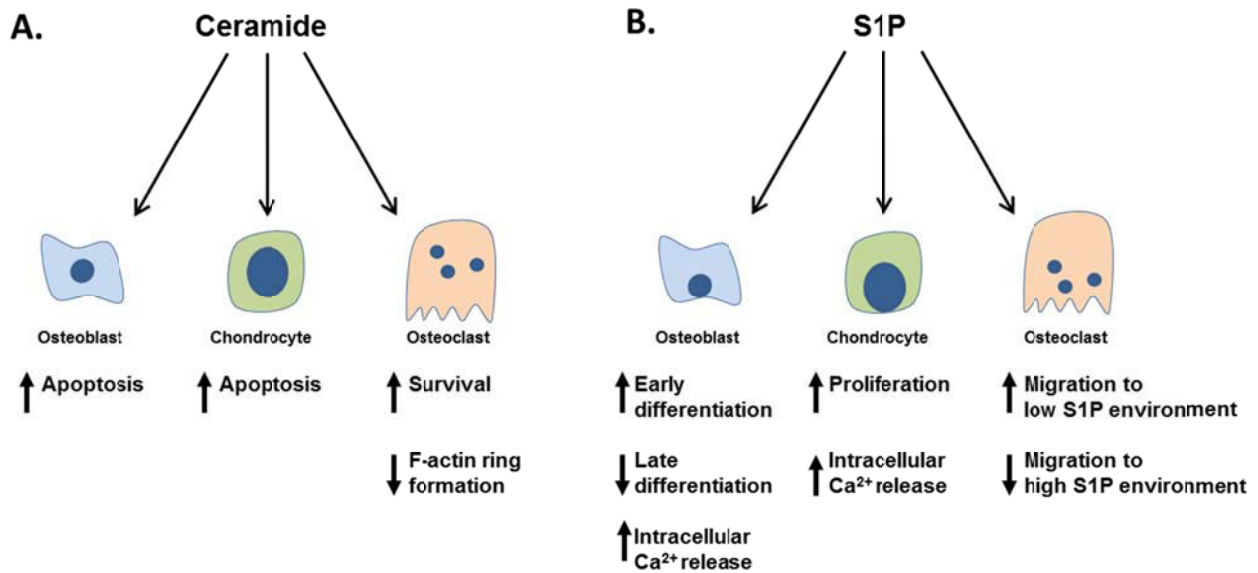


Figure 1.6: The major effects of ceramide.

(A) and Sphingosine 1 phosphate (S1P) (B) on osteoblasts, chondrocytes and osteoclasts. The ↑ thick arrows indicate activation and the ↓ thick arrows indicate inhibition.

1.7 Role of sphingolipids in skeletal tissues: *In vivo* findings

The role of osteoclast-derived S1P on bone remodeling has been elaborated in an *in vivo* study by Lotinun *et al.* [122]. In this study, osteoclast-specific inactivation of cathepsin K, an extracellular matrix degrading enzyme, resulted in an increase of S1P secretion by these cells. Secreted S1P promoted increased bone formation by osteoblasts primarily by enhancing the differentiation of osteoblast precursors to functional osteoblasts. As described by Quint *et al.* [117], osteoclasts through S1P release may also promote the recruitment of MSCs that give rise to osteoblast precursors and thereby contribute to the observed high bone mass phenotype. A recently published study showed that calcitonin, a thyroid-derived hormone, affects bone formation by regulating the release of S1P by osteoclasts [123].

Emerging data from the analysis of genetically altered mouse models suggest that sphingolipid metabolism during embryonic development plays a critical role in normal skeletogenesis. This insight originally came from two different mouse models lacking a neutral sphingomyelinase, nSMase2, also known as sphingomyelin phosphodiesterase 3 (SMPD3). Currently, there are two SMPD3-deficient mouse models available; one carries a chemically induced deletion of 1,758 base pairs encompassing part of intron 8 and most of exon 9 (*fro*) in the *Smpd3* locus (*fro/fro* model) and the other was generated by gene targeting (*Smpd3*^{-/-} model) [83, 124, 125]. So far no skeletal abnormalities in mice lacking SMPD1 and SMPD2 activity have been reported.

Both *fro/fro* and the gene targeted *Smpd3*^{-/-} mice share similar gross skeletal abnormalities, i.e. short-limb dwarfism, deformation of long bones and abnormally formed rib cages. However, Stoffel *et al.* [126] did not observe the bone and tooth mineralization abnormalities documented in *fro/fro* mice in their gene targeted model. The phenotypic variations in *fro/fro* and *Smpd3*^{-/-} mice cannot be attributable to the presence of any additional

genetic alterations in the former strain as such mutation(s), if not closely associated, would have been fully segregated during the propagation of *fro/fro* mice in multiple laboratories over the past four decades. This inference, together with the observation that the fully penetrant *fro/fro* phenotype including the severe hypomineralization defect, is always associated with the *Smpd3* deletion mutation identified by Aubin *et al.* strongly suggests that the loss of SMPD3 function is indeed the cause of the *fro/fro* phenotype [83].

1.8 Phosphocholine metabolism and its role in skeletal tissues

SMPD3 and other sphingomyelinases, cleave sphingomyelin to generate ceramide and phosphocholine [87, 89, 127]. Apart from the sphingomyelinase pathway, phosphocholine can also be generated from exogenous choline taken up by the cells and phosphorylated by cytosolic choline kinases [128]. Increased activity of choline kinase in colon cancer and adenoma patients also resulted in an elevation of phosphocholine. It has been suggested that choline kinase activity in these patients might causes tumor growth [129]. In an animal study a choline-rich diet has been shown to increase tissue phosphocholine levels [130, 131].

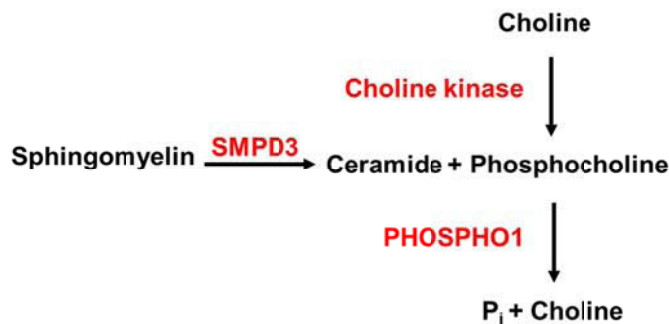


Figure 1.7: Phosphocholine metabolism.

SMPD3 cleaves sphingomyelin to generate ceramide and phosphocholine. Cytosolic choline kinases can also generate phosphocholine from free choline. Phosphocholine can be hydrolysed to produce inorganic phosphate and choline.

Phosphocholine can be converted to phosphatidylcholine, an important metabolic mediator or alternatively, it can be hydrolyzed by phosphoethanolamine/phosphocholine phosphatase (Phosphatase, orphan 1 or PHOSPHO1) into choline and phosphate (Fig. 1.7) [132-134]. It has been reported that inhibition of PHOSPHO1 activity in chicken embryos causes impaired skeletal mineralization during limb development [135]. These abnormalities are also seen in *Phospho1*^{-/-} mice [136].

1.9 The matrix vesicle theory of ECM mineralization

Matrix vesicles (MVs) are lipid enclosed vesicular bodies released by the matrix secreting cells in hard tissues. Although somewhat disputed, for a long time the theory of matrix vesicle-mediated initiation of mineralization has been thought to be a critical process in ECM mineralization in the skeletal and dental tissues. According to this theory, the initial seeding of hydroxyapatite crystals first occurs in the protected microenvironment of the MVs [137-140]. Although many different laboratories showed electron micrographs of MVs with mineral crystals, until recently a definitive molecular mechanism for this process has been elusive.

Recent findings suggesting the roles of SMPD3 and PHOSPHO1, two enzymes with their activities in the cytosolic compartment provided the first clue that these enzymes might be involved in MV-mediated initiation of ECM mineralization. This notion was further supported by the observations that none of the known factors regulating the extracellular progression of bone ECM mineralization is altered in SMPD3-deficient *fro/fro* or *Phospho1*^{-/-} mice, and in both models the initiation of embryonic bone and cartilage mineralization is markedly delayed [83, 132]. A more direct evidence supporting the involvement of these two enzymes in MV-mediated ECM mineralization came from a recent study describing the presence of both these enzymes in MV preparations.

In the MVs prepared from growth plate chondrocytes, it was shown that the amount of sphingomyelin is higher in the MVs in comparison to the chondrocytes from which they derive [141]. Sphingomyelin is also one of the lipids most rapidly degraded when MVs are incubated in synthetic cartilage lymph and allowed to mineralize [142]. Taken together, these findings suggest that a possible mechanism explaining MV-mediated ECM mineralization may involve the cleavage of sphingomyelin present in the MV lipid bi-layer by a sphingomyelinase. Because of its high level of expression in the mineralizing tissues, SMPD3 is the source of sphingomyelinase that is most likely to fit to this role.

A possible mechanism explaining MV-mediated ECM mineralization may involve the cleavage of sphingomyelin present in the MV lipid bi-layer by SMPD3 to generate phosphocholine as the first step. Phosphocholine can then be cleaved by soluble PHOSPHO1 present inside the MVs to release free P_i [133]. The increased P_i levels may promote spontaneous precipitation of calcium phosphate salts that may serve as a nidus for hydroxyapatite crystal nucleation. The crystal(s) may grow in size to finally rupture the MV wall to be released on the newly formed unmineralized collagen-rich matrix. These crystals may grow further and coalesce with each other as a result of the extracellular phase of ECM mineralization.

1.10 Rationale and Aim:

ECM mineralization in bones and teeth is a genetically regulated process. In most of these pathologic conditions one or more common determinants of ECM mineralization, such as the levels of mineral ions or mineralization inhibitors are altered. However, there might be unidentified genetic regulators that do not involve these common determinants. To identify the novel genetic regulators of ECM mineralization one can investigate mouse models in which bone mineralization defects are present without any alteration of the common determinants mentioned

above. Many regulators of ECM mineralization have been identified but the initiation of this process is not well-understood. This is why we became interested in the two enzymes SMPD3 and PHOSHO1. In the current thesis, I presented my findings in the form of three manuscripts. These manuscripts address several novel questions/topics in the field as outlined below.

In the first paper, we investigate the role of SMPD3 in skeletal development and mineralization. The overall aim of this paper is to understand the molecular basis of the bone mineralization defects in *fro/fro* mice. More specifically, we addressed several questions: What is the effect of the *fro* mutation on SMPD3 function, its membrane localization and the effect on the developing skeleton as a whole; and does SMPD3 affect bone mineralization locally?

In the second paper, we characterized the tooth phenotype in SMPD3-deficient mice. We examined whether the differentiation of odontogenic cells are affected in *fro/fro* mice causing the tooth phenotype and investigated the ultrastructural properties of the dentin matrix in these mice. We also investigated whether SMPD3 affects dentin mineralization locally.

Finally we examined the underlying pathways by which SMPD3 regulates ECM mineralization in the third paper. Using a combination of mouse genetics, histology and biochemistry, we investigated whether the SMPD3 products ceramides or phosphocholine, is involved in bone mineralization and whether SMPD3 and PHOSPHO1 act through the same pathway.

**Chapter 2: A Cell-Autonomous Role for Neutral Sphingomyelinase 2 in Bone
Mineralization**

A Cell-Autonomous Role for Neutral Sphingomyelinase 2 in Bone Mineralization

Zohreh Khavandgar^{1†}, Christophe Poirier^{2†}, Christopher J. Clarke^{3†}, Jingjing Li⁴, Nicholas Wang⁴, Marc D. McKee^{1,5}, Yusuf A. Hannun³ and Monzur Murshed^{1,4*}

¹Faculty of Dentistry, McGill University, Montreal, QC H3A 1A4, Canada; ²Medical College University of Georgia, Augusta, GA 30912, USA; ³Medical University of South Carolina, Charleston, SC 29425, USA; ⁴Department of Medicine, McGill University, Montreal, QC H3A 1A4, Canada; ⁵Department of Anatomy and Cell Biology, McGill University, Montreal, QC H3A 1A4, Canada

The Journal of cell biology, 2011 Jul 25; 194(2): 277-89

doi: 10.1083/jcb.201102051

2.1 Abstract

A deletion mutation called *fro* (*fragilitas ossium*) in the murine *Smpd3* (*sphingomyelin phosphodiesterase 3*) gene leads to a severe skeletal dysplasia. *Smpd3* encodes a neutral sphingomyelinase 2 (nSMase2), which cleaves sphingomyelin to generate bioactive lipid metabolites. We examined endochondral ossification in embryonic day 15.5 *fro/fro* mouse embryos and observed impaired apoptosis of hypertrophic chondrocytes and severely undermineralized cortical bones in the developing skeleton. In a recent study, it was suggested that nSMase2 activity in the brain regulates skeletal development through endocrine factors. However, we detected *Smpd3* expression in both embryonic and postnatal skeletal tissues in wild-type mice. To investigate whether nSMase2 plays a cell-autonomous role in these tissues, we examined the *in vitro* mineralization properties of *fro/fro* osteoblast cultures. The *fro/fro* cultures mineralized less than the control osteoblast cultures. We next generated *fro/fro;Colla1-Smpd3* mice, in which osteoblast-specific expression of *Smpd3* corrected the bone abnormalities observed in *fro/fro* embryos without affecting the cartilage phenotype. Our data suggest tissue-specific roles for nSMase2 in skeletal tissues.

2.2 Introduction

ECM mineralization in bones and teeth is a genetically regulated process. In humans, genetic mutations may lead to a variety of diseases affecting ECM mineralization in skeletal and dental tissues, which include X-linked hypophosphatemia, hypophosphatasia, rickets, and some forms of osteogenesis/dentinogenesis imperfect [26, 48, 80, 143, 144]. Although considered as a critical physiological process, the molecular mechanism of ECM mineralization is still not fully understood. Identification of novel genetic regulators of this process and elucidation of their modes of action may lead to effective interventions for genetic diseases associated with abnormal skeletal mineralization.

Our current understanding suggests that skeletal and dental ECM mineralization can be attributed to a large extent to the unique promineralization environment of these hard tissues. Two mineral ions, P_i and calcium, when present at physiological concentrations, will promote apatitic mineral crystal growth within and between newly synthesized collagen fibrils in the skeletal ECM [24]. Apart from the mineral ions themselves, extracellular levels of mineralization inhibitors can also affect ECM mineralization [30, 31, 145, 146]. For example, >40 year ago, it was shown that PP_i , a chemical derivative of P_i , can potently inhibit the mineralization process [28, 29]. More recently, it has been shown that matrix gla protein (MGP), a small extracellular protein, prevents ECM mineralization in the cartilage and vascular tissues [145, 146].

Type 1 collagen, a scaffolding ECM protein, and tissue-nonspecific alkaline phosphatase (ALPL [alkaline phosphatase, liver/bone/kidney]), an enzyme required for the cleavage of PP_i in the bone matrix, are both necessary for normal bone mineralization [24, 33, 39]. We recently demonstrated the importance of these key determinants of ECM mineralization in an *in vivo* mouse model, in which *Alpl* forced expression in the dermis, a fibrillar, collagen-rich soft connective tissue, resulted in ectopic mineralization of the skin [24]. Although these findings

established the concurrent requirements of a mineral-scaffolding protein matrix and phosphatase activities in skeletal ECM mineralization, they did not rule out the existence of other mechanisms working in concert to regulate this process. A recently identified mutation in a mouse model, which displays altered sphingolipid metabolism and poorly mineralized skeletal tissues, further enforces the likelihood that multiple mechanisms are involved in skeletal mineralization [83, 124].

Although initially considered as inert structural molecules, sphingolipids are now recognized as important mediators for signal transduction pathways affecting various cell functions [89, 147, 148]. Bone deformities in mouse models lacking a functional *Smpd3* (*sphingomyelin phosphodiesterase 3*) gene underscore the importance of sphingolipid metabolism in skeletal tissues [83, 125]. *Smpd3* encodes neutral sphingomyelinase 2 (nSMase2), a membrane-bound enzyme, which cleaves sphingomyelin to generate the lipid second messenger ceramide. Ceramide generated by sphingomyelinases or by a de novo pathway affects a wide range of cellular processes, including cell death, proliferation, and differentiation [96, 149, 150].

In recent years, studies have provided useful perspectives on novel physiological roles for nSMase2 [151-153]. Further insight into the functions of this enzyme came with the development of animal models lacking nSMase2 activity. Currently, there are two nSMase2-deficient mouse models available: one was generated by gene targeting (*Smpd3*^{-/-}), whereas the other carries a chemically induced deletion of 1,758 base pairs (bp) encompassing part of intron 8 and the adjacent exon 9 of the *Smpd3* gene [83, 125, 126]. The latter mutation known as *fragilitas ossium* or *fro* replaces the last 33 amino acids of nSMase2, resulting in a significant reduction of total neutral sphingomyelinase activities in the tissues of the *fro/fro* mice [83,125,126]. In their recent studies, [126] characterized the skeletal phenotypes of the *Smpd3*^{-/-}

mice as a chondrodysplasia and speculated a systemic role for neuronal *Smpd3* in the regulation of the skeletal development. Although both the *Smpd3*^{-/-} and *fro/fro* mutants show similar gross skeletal abnormalities, some phenotypic differences exist between these two models. For example, the skeletal phenotype appears to be milder in *Smpd3*^{-/-} mice. Also, no bone or tooth mineralization defects were reported in this gene-targeted model. These differences raise the possibility that additional, as yet unknown, mutations in the chemically mutagenized *fro/fro* model may cause the severe skeletal abnormalities.

The goals of our current study were to characterize the skeletal phenotype of *fro/fro* mice and to investigate the local role of *Smpd3* in osteoblasts. Toward these goals, we performed a detailed characterization of the skeletal tissues in *fro/fro* embryos and adult mice using skeletal preparations, microcomputed tomography (micro-CT), and histology/histomorphometric analysis. We demonstrate here that the *fro* mutation affects bone ECM mineralization in both embryos and in adult mice and that there is a delay of apoptosis in the hypertrophic chondrocytes in the developing *fro/fro* skeleton. We also show that osteoblast-specific expression of the *Smpd3* transgene in *fro/fro;Coll1a1-Smpd3* mice completely rescues the bone mineralization defects, whereas the cartilage phenotype that appears during early skeletal development remains unaffected. Our work establishes the *fro* mutation as the sole cause of skeletal abnormalities in the *fro/fro* mice and suggests a cell-autonomous, tissue-specific role for nSMase2 in the developing skeleton.

2.3 Results

2.3.1 Impaired bone mineralization in *fro/fro* mice

The *fro/fro* neonates are characterized by a shortened body stature with skeletal abnormalities [83]. As shown by the skeletal preparations of the newborn mice, both flat (intramembranous) and long (endochondral) bones are affected—the parietal suture was poorly mineralized, whereas both fore- and hind limbs were severely bent in the *fro/fro* mutants (Fig. 2.1 A and B). Further analysis by micro-CT revealed a reduction of mineralized tissue in the flat bones of the skull and alveolar bones in the jaw (Fig. 2.1 C).

To further confirm that the observed decrease in mineralized tissue was attributable purely to a mineralization defect, we examined WT and mutant mice for the presence of excess osteoid, the proteinaceous matrix secreted by osteoblasts, which subsequently becomes mineralized. Histological analysis of the parietal bones in the skullcap of 2-day-old *fro/fro* mice revealed a severely hypomineralized matrix at the suture (Fig. 2.1 D, top). Also, there was a marked reduction of mineralization in the alveolar bones from these mice (Fig. 2.1 D, bottom). By 1 mo of age, the trabecular bones of *fro/fro* mice showed an increase of ~5% in osteoid volume over total bone volume as measured by histomorphometry (Fig. 2.1 E and F). Similarly, there was a significant increase in the osteoid surface in the *fro/fro* bones (Fig. 2.1 G). These results indicate that osteoid ECM is indeed deposited but is not efficiently mineralized. None of these skeletal abnormalities were seen in *+/fro* mice; therefore, we used these mice as controls for our subsequent *in vivo* analyses.

2.3.2 The *fro* mutation abolishes nSMase2 activity but does not affect its membrane localization

The *fro* mutation causes a deletion in *Smpd3*, resulting in a replacement of the last 33 amino acids of nSMase2. In a previous study, reduced nSMase activity was reported in skin samples collected from *fro/fro* mice [83]. This reduced enzymatic activity can be caused by a loss of the catalytic site and/or by impaired membrane targeting of the enzyme. To investigate this, we generated two FLAG-tagged expression constructs *CMV-Smpd3* and *CMV-mSmpd3* encoding the WT and a mutated nSMase2 that carries the *fro* mutation, respectively (Fig. 2.2 A and B). The constructs were used to transfect MCF-7 cells, and the expression of both WT and mutated proteins was confirmed by Western blotting (Fig. 2.2 C). As shown in Fig. 2.2 D, there was a marked increase in nSMase activity in cells transfected with *CMV-Smpd3* but not with the *CMV-mSmpd3* construct. We next examined the membrane localization of the WT and mutated nSMase2 proteins by indirect immunofluorescence and confocal microscopy using an antibody raised against the FLAG tag. Importantly, there was no alteration in the membrane localization pattern of mutant nSMase2 when compared with the WT protein (Fig. 2.2 E). These data confirm that the mutation of the predicted active site is the sole reason for the loss of catalytic activity of this enzyme in *fro/fro* mice.

2.3.3 The *fro* mutation affects skeletal development

To investigate the effects of the *fro* mutation on the developing skeleton, we performed histological analysis of the long bones from embryonic day 15.5 (E15.5) *+fro* and *fro/fro* embryos. There was an increased presence of unmineralized collagenous matrix in the cortical bones of the humerus (a representative long bone) of the *fro/fro* embryos in comparison to the cortical bones of their *+fro* littermates (Fig. 2.3 A and

B). This poor mineralization was not attributable to impaired osteoblast differentiation, as osterix (SP7) immunopositive cells were present in the cortical bones of the *fro/fro* mice (Fig. 2.3 C and D). Also, alkaline phosphatase activity was detected within the unmineralized matrix of the *fro/fro* bones, further indicating that osteoblast differentiation was not affected (Fig. 2.3 E and F). We next prepared total RNAs from the bones of newborn WT and *fro/fro* mice and examined the effects of the *fro* mutation on the expression of *Runx2* and *Atf4*, encoding two key transcription factors involved in early and late osteogenic differentiation, respectively. In agreement with our histological analysis of the embryonic mice, quantitative real-time PCR (qRT-PCR) analysis showed that the expression of these osteoblast marker genes were not altered in *fro/fro* bones (Fig. S1).

Although osteoblast differentiation was not affected in *fro/fro* mice, we did not observe any osterix-positive cells in the marrow space in the long bones of *fro/fro* embryos, whereas infiltration of osteoblast progenitors into the marrow space was normal in their *+fro* littermates. Instead, we observed an unusual persistence of hypertrophic chondrocyte-like cells in the mid-shaft regions of the *fro/fro* long bones (Fig. 2.3 C and D). A possible explanation for this observation might be that the hypertrophic chondrocytes in these mutant bones were not undergoing apoptosis at a rate comparable with that of *+fro* hypertrophic chondrocytes. To investigate this possibility, we performed TUNEL assay on the humerus sections from both *+fro* and *fro/fro* embryos at E15.5. A decreased presence of TUNEL-positive nuclei in the *fro/fro* hypertrophic zones in comparison to the corresponding areas of the *+fro* bones confirmed that there was indeed a reduction of the apoptosis of *fro/fro* hypertrophic chondrocytes (Fig. 2.3 G and H).

The presence of ALPL activity in the developing *fro/fro* bones suggests normal PP_i hydrolysis in the ECM. However, the PP_i levels in the ECM may increase because of an up-

regulation of ectophosphodiesterase nucleotide phosphohydrolases (*Enpp1*) and progressive ankylosis (*Ank*), which encode two proteins critical for the maintenance of tissue homeostasis of this mineralization inhibitor [30, 33]. We analyzed the expression of these two genes by qRT-PCR and found that there was in fact a mild down-regulation of *Enpp1* expression in the bones of newborn *fro/fro* mice, whereas *Ank* expression was not altered (Fig. 2.3 I). Also, we did not observe any up-regulation of *Mgp* and *Colla1* expression (Fig. 2.3 I). We then used a fluorogenic sensor to measure PP_i levels in the bones of adult WT and *fro/fro* mice. We observed that PP_i was present at comparable levels in the bone samples from both genotypes (Fig. 2.3 J). Collectively, these data suggest that the hypomineralization defect seen in *fro/fro* mice was not caused by the increase of MGP or PP_i in the bone ECM.

2.3.4 Loss of nSMase2 in osteoblasts affects mineralization in vitro

We next examined *Smpd3* expression in late-stage mouse embryos and also in tissues collected from WT mice at the preweaning age. The sense and antisense probes generated from the *Smpd3* cDNA were hybridized separately on fixed whole-embryo paraffin sections prepared from E16.5 WT embryos. The in situ hybridization analysis performed with the antisense probe showed a high level of *Smpd3* expression in all bone types, cartilage, and in the brain (Fig. 2.4 A). A similar *Smpd3* expression pattern was also observed in 2-week-old mice (Fig. 2.4 B). Next, we examined *Smpd3* expression during the differentiation of MC3T3-E1 preosteoblasts cultured in the presence of ascorbic acid and β -glycerol phosphate. Under these culture conditions, we observed a progressive induction of *Smpd3* expression, which was down-regulated in fully mature osteoblasts (Fig. 2.4 C).

A high level of expression of *Smpd3* in embryonic and postnatal bones and in a differentiating osteoblastic cell line suggests a local role for this enzyme in bone. To examine

whether nSMase2 deficiency in *fro/fro* bones causes a reduction of total nSMase activity, we prepared calvarial bone extracts from both *+fro* and *fro/fro* mice and performed an *in vitro* enzymatic assay using ^{14}C -labeled sphingomyelin [154]. As a control experiment, we performed the same analysis on the extracts prepared from both *+fro* and *fro/fro* brain tissues. As shown in Fig. 2.4 D, there was a comparable decrease of nSMase activities in both brain and bone extracts from *fro/fro* mice.

We next investigated whether a loss of nSMase2 activity affects the *in vitro* mineralization capacities of cultured osteoblasts. First, we transfected MC3T3-E1 preosteoblasts with siRNA oligonucleotides to knock down *Smpd3* gene expression. Gene expression analysis by qRT-PCR revealed that there was ~60% reduction of *Smpd3* expression in the siRNA-transfected cells (Fig. 2.4 E). We cultured both control and *Smpd3* siRNA-transfected cells in the presence of ascorbic acid and β -glycerol phosphate to induce differentiation and mineralization. Upon culturing for 10 d in the aforementioned medium, cells were stained with Alizarin red, a calcium-binding dye. We observed reduced mineralization in the cultures with *Smpd3*siRNA-transfected cells in comparison to the cultures with control siRNA-transfected cells (Fig. 2.4 F). This observation was further confirmed in experiments performed with primary osteoblasts isolated from the newborn *+fro* and *fro/fro* mice. When cultured in the presence of ascorbic acid and β -glycerol phosphate, *fro/fro* osteoblast cultures showed reduced mineralization in comparison to the *+fro* cultures (Fig. 2.4 G).

2.3.5 Osteoblast-specific expression of *Smpd3* in *fro/fro* mice increases bone nSMase activity

Collectively, a decline of total nSMase activity in *fro/fro* bones and reduced *in vitro* mineralization by *fro/fro* osteoblasts (Fig. 2.4 D and G) strongly suggest a local and specific role for nSMase2 in bone. To investigate this *in vivo*, we overexpressed *Smpd3* specifically in the

bones of *fro/fro* mice. For this purpose, we generated a *Colla1-Smpd3* transgene construct using a 2.3-kb *Colla1* promoter fragment, earlier shown to be specifically expressed in osteoblasts (Fig. 2.5 A). Pronuclear injection of this construct into fertilized mouse eggs resulted in four founders, of which two showed bone-specific expression of the transgene. No transgene expression was detected in any other tissue in these founders (Fig. 2.5 B). These founders were then mated with *+/fro* mice to first generate *+/fro;Colla1-Smpd3* mice, which were mated again with *+/fro* mice to obtain *fro/fro;Colla1-Smpd3* mice.

By visual examination, there was no gross skeletal abnormalities in the *fro/fro;Colla1-Smpd3* mice. Also, these mice survived the perinatal death routinely seen in *fro/fro* mice (described in Fig. 2.6). In agreement with our transgene expression data, we observed a threefold increase of total nSMase activities in the bones of newborn *fro/fro;Colla1-Smpd3* mice in comparison to the bones of *fro/fro* mice, whereas brain nSMase activities remained indistinguishable between these two genotypes (Fig. 2.5 C). Interestingly, despite a significant increase of bone nSMase activities in *fro/fro;Colla1-Smpd3* mice, there was no detectable decrease of total bone sphingomyelin levels (Fig. 2.5 D). However, an increase of total ceramide levels in the bones of *fro/fro;Colla1-Smpd3* mice was observed when compared with the *fro/fro* bones (Fig. 2.5 E). Interestingly, we found a significant increase of several long-chain ceramide species (e.g., C16, C24, and C24:1) in the bones of the former genotype (Fig. 2.5 F). No significant alterations were observed in total dihydroceramide levels in the bone extracts prepared from any of the mouse models analyzed (Fig. 2.5 G). Also, several known serum parameters affecting ECM mineralization (e.g., calcium, P_i , and alkaline phosphatase levels) were unaltered in the *fro/fro;Colla1-Smpd3* mice (Fig. 2.5 H–J).

Finally, we compared the expression of *Enpp1*, *Ank*, *Mgp*, and *Colla1* by qRT-PCR in the parietal bones of newborn *fro/fro* and *fro/fro;Colla1-Smpd3* mice. We observed significant

up-regulation of *Enpp1* and *Ank*, but not *Mgp*, expression. *Colla1* gene expression was mildly up-regulated in *fro/fro;Colla1-Smpd3* bones in comparison with *fro/fro* bones (Fig. S2).

2.3.6 Normal bone mineralization in *fro/fro; Colla1-Smpd3* mice

We next examined the skeletal phenotype in *fro/fro;Colla1-Smpd3* mice. Micro-CT analysis of the humerus from 15.5-day-old *fro/fro* embryos showed poorly mineralized cortical bones, which were fully mineralized in the *fro/fro;Colla1-Smpd3* embryos at the same developmental stage. Interestingly, a reduced presence of mineral in the marrow compartment of both *fro/fro* and *fro/fro;Colla1-Smpd3* long bones was noted, indicating that the chondrocyte phenotype was largely unaffected in the latter genotype (Fig. 2.6 A). The aforementioned observation was further confirmed by Alcian blue staining of the humeri sections from WT, *fro/fro*, and *fro/fro;Colla1-Smpd3* mice. We observed that, as was the case in the long bones from the *fro/fro* mice, the marrow compartment in the long bones of *fro/fro;Colla1-Smpd3* mice was full of densely packed chondrocytes within a cartilage matrix (Fig. 2.6 B). We next examined the skeleton of newborn *fro/fro;Colla1-Smpd3* mice. Osteoblast-specific expression of *Smpd3* completely corrected the *fro/fro* skeletal abnormalities (Fig. 2.6 C). X-ray analysis showed that there was no recurrence of the skeletal abnormalities in the adult *fro/fro;Colla1-Smpd3* mice (Fig. 2.6 D). Also, we observed an absence of abnormally high osteoid volume in the bones of this latter model (Fig. 2.6 E).

We analyzed a total of 144 mice from the aforementioned breeding experiments, of which 17 were *fro/fro*. All of these mice had limb deformities, and 11 of them died perinatally. On the other hand, out of a total of 28 *fro/fro;Colla1-Smpd3* mice generated through this breeding, only three died perinatally, whereas none of them showed any kind of skeletal abnormalities (Fig. 2.6 F). We tested the significance of these data using the standard Pearson's

χ^2 test and found that for the rescue of both skeletal phenotype and perinatal death, the p-values were far below the commonly accepted 5% threshold for significance.

2.4 Discussion

Analysis of novel, genetically modified mouse models with skeletal and dental mineralization defects may provide critical information on as yet unidentified regulators of ECM mineralization and, thereby, improve our understanding of this important physiological process. Recently, a loss-of-function mutation in the *Smpd3* gene has been identified in a mouse model (*fro/fro*), which shows severe bone and tooth mineralization defects [83, 124]. The *fro/fro* skeletal abnormalities are similar to the skeletal pathology seen in patients with certain forms of osteogenesis imperfecta that do not involve any mutation in collagen genes [80]. As is the case with these patients, the most common parameters affecting ECM mineralization, e.g., serum calcium, P_i , and alkaline phosphatase levels, are not decreased in *fro/fro* mice. Furthermore, when analyzed by histology, the unmineralized bone matrix appears to be secreted normally in these mice. Collectively, these observations suggest that *Smpd3* might affect ECM mineralization through a novel mechanism.

In an earlier study, the skeletal phenotype of *Smpd3*^{-/-} mice has been described as a form of chondrodysplasia [125]. In agreement with this finding, we observed a significantly impaired apoptosis of hypertrophic chondrocytes, possibly caused by reduced ceramide levels during early skeletal development in *fro/fro* embryos. Additionally, we also observed poor mineralization of the matrix secreted by osteoblasts that severely affects the strength of the cortical bones in these embryos. This novel finding explains the long bone deformities in *fro/fro* mice.

Our data suggest that hypomineralization of bone ECM in *fro/fro* mice is not caused by the elevated levels of mineralization inhibitors MGP or PP_i (Fig. 2.3 I and J). We observed a mild down-regulation of *Enpp1* in *fro/fro* bones, whereas both *Ank* and *Enpp1* expressions were significantly up-regulated in the bones of *fro/fro;Coll1a1-Smpd3* mice. Interestingly, up-regulation of these two genes in the latter model did not prevent the rescue of the bone

mineralization defects. These data suggest that there might be a compensatory interplay between the positive (nSMase2) and negative (ANK and ENPP1) regulators of bone ECM mineralization.

Our current study establishes an osteoblast-specific role of *Smpd3* in bone mineralization and several lines of evidence suggest that the *Smpd3*-encoded enzyme nSMase2 acts as a local modulator of ECM mineralization in bone. First, *Smpd3* is highly expressed in bone, and its expression progressively increases as osteoblasts mature. Second, loss of *Smpd3* expression in both siRNA-treated MC3T3-E1 preosteoblasts and in *fro/fro* primary osteoblasts causes impaired mineral deposition in cultures. Finally, osteoblast-specific expression of *Smpd3* in *fro/fro* bones completely rescues the skeletal abnormalities. Collectively, all these findings provide unambiguous demonstration of a direct osteoblast/mineralization effect for the locally synthesized nSMase2 in osteoblasts. Furthermore, a normal skeletal appearance in *fro/fro;Colla1-Smpd3* mice suggests that the loss of nSMase2 activity in osteoblasts is the major cause of the *fro/fro* phenotype.

At this point, we cannot fully rule out an indirect systemic effect of nSMase2 enzymatic activity from other tissues on the developing skeleton. However, in view of our findings that osteoblast-specific expression of *Smpd3* in *fro/fro* mice corrects the bone but not the cartilage phenotype, we do not consider this as a likely possibility. This latter finding also suggests a tissue-specific role for nSMase2 in the developing skeleton with apparent independent roles in bone and cartilage.

Both *fro/fro* and the gene-targeted *Smpd3*^{-/-} mice share similar gross skeletal abnormalities, i.e., short-limbed dwarfism, deformation of long bones, abnormally formed rib cages, and abnormalities in growth plate cartilage. However, Stoffel *et al.* [125, 126], in their gene-targeted model, did not observe bone and tooth mineralization abnormalities, which are seen in all *fro/fro* mice. This apparent discrepancy can be explained by differences in the

analytical methods used to characterize the two mouse lines. Stoffel *et al.* [125, 126] analyzed the mineralization status of the *Smpd3*^{-/-} mice solely by bone mineral density analysis, which determines the total bone mineral content and is not suitable for detecting an increase in unmineralized bone matrix. In contrast, we analyzed the *fro/fro* bones using a histomorphometric technique on undecalcified samples, commonly used to detect skeletal mineralization defects.

Although Stoffel *et al.* [125, 126] suggested that the phenotypic variations in *fro/fro* and *Smpd3*^{-/-} mice can be attributable to the presence of any additional genetic alterations in the former strain, such mutations would have been fully segregated during the propagation of *fro/fro* mice in multiple laboratories over the last two decades. This inference, together with the observation that the fully penetrant *fro/fro* phenotype, including the severe hypomineralization defect, is always associated with the *Smpd3* deletion mutation reported by Aubin *et al.*, clearly identifies the loss of nSMase2 function as the sole cause of the *fro/fro* phenotype [83]. Indeed, our current data showing a complete rescue of the skeletal phenotypes in *fro/fro; Colla1-Smpd3* mice expressing *Smpd3* in osteoblasts rules out the possibility of the presence of any additional mutation in *fro/fro* mice that may cause the observed mineralization defects.

Our results demonstrate an intrinsic loss of nSMase activity attributable to the *fro* mutation. The translocation of nSMase2 from the Golgi compartment to the plasma membrane and its recycling back to the Golgi is a highly dynamic and regulated process. Notably, preventing nSMase2 recycling has been shown to increase nSMase activity and ceramide levels, suggesting adverse physiological consequences for alterations in localization of this enzyme [147]. Considering the critical nature of this process, we examined whether the reduced nSMase activities in *fro/fro* tissues are attributable to an impaired nSMase2 localization or are caused by the loss of its catalytic activity. Our cell culture data confirm that the mutant nSMase2 localizes

identically to WT nSMase2 and indicate that the reduced tissue nSMase activity in *fro/fro* mice is likely to be caused by the disruption of the enzyme's catalytic site.

nSMase2 cleaves sphingomyelin to generate the lipid second messenger ceramide [89, 148]. Thus, a loss of functional nSMase2 could have dual effects, i.e., both a decrease in ceramide levels and an increase in sphingomyelin levels in tissues in which *Smpd3* is normally expressed. Indeed, a recent study suggested a crucial role for sphingomyelin and its degradation in bone and dentin mineralization [143]. However, as sphingomyelin, being an integral component of all cell membranes, is present in all tissues in relatively high amounts and because only a small fraction of it is cleaved by the nSMase2 enzymatic activity, a loss-of-function mutation in *Smpd3* as such may not have any significant effects on the total tissue sphingomyelin levels. Indeed, we did not observe any difference in total sphingomyelin levels between *+fro* and *fro/fro* bones. This observation suggests that increased sphingomyelin levels in bone attributable to the loss of nSMase2 activity may not account for the ECM mineralization defects in *fro/fro* mice. Although we could not detect any significant alteration in tissue sphingomyelin levels, we found a remarkable decrease of various ceramide species, particularly those with long chains, in *fro/fro* bones in comparison to the control *+fro* bones. Currently, it is not clear how ceramide might affect bone ECM mineralization. Ceramide acting as a second messenger can affect several signaling pathways and may alter as yet unknown downstream regulators critical for bone ECM mineralization.

In conclusion, the *fro/fro* mice lacking a functional nSMase2 provide a unique opportunity to investigate a novel mechanism involved in vertebrate hard tissue mineralization. The data we present here suggest that a local nSMase2 function is required for a normal bone mineralization and for the normal apoptosis of hypertrophic chondrocytes in the cartilage during early skeletal development (Fig. 2.7). Collectively, these data demonstrate, for the first time, the

tissue-specific roles for this enzyme in the developing skeleton. Further analyses of the mouse models reported here may reveal the molecular mechanisms underlying the pathophysiology of certain forms of osteomalacia and osteogenesis imperfecta in humans.

2.5 Materials and Methods

2.5.1 DNA constructs

The DNA construct for osteoblast-specific expression of the *Smpd3* transgene was generated using a 2.3-kb *Colla1* promoter fragment [155]. A full-length *Smpd3* cDNA (American Type Culture Collection) preceded by a rabbit β -globin intron was inserted in between the *Colla1* promoter fragment and a SV40 polyadenylation signal. The transgene sequence was released from the plasmid backbone by SacII restriction digestion and was used for pronuclear injection. A PCR-based technique was used to introduce the *fro* mutation into the WT cDNA. Both WT and mutant (*fro*) *Smpd3* cDNAs were cloned in pIRES-hrGFP-1 α (Agilent Technologies).

2.5.2 Mice

Generation of *fro/fro* mice was described previously [83]. Transgenic founders were generated by pronuclear injections at the McIntyre Cancer Center Transgenic Core Facility at McGill University following standard techniques. All mice were maintained in a pathogen-free standard animal facility, and the experimental procedures were performed following an animal use protocol approved by the Animal Care Committee of McGill University. Genotypes were determined by PCR on genomic DNAs isolated from the tail biopsies. The following primers were used for the genotyping of the *fro* mutation: 5'-GGGACGACGTCTGCCTCAGG-3', 5'-TTAGAGGTCCCAACCACAGG-3', and 5'-CCCAGGTGCTGGGCAGAAGG-3'. With these three primers, it is possible to amplify specific WT (145 bp) and mutant (189 bp) DNA fragments. The *Colla1-Smpd3* transgene integration was detected using the following primer

pair specific for the SV40 polyadenylation signal: 5'-CAGCTCTCCATCAAGATGGT-3' and 5'-CCGGTTTGGACTCAGAGTAT-3'.

2.5.3 Gene expression analysis

Gene expression analyses were performed using a qRT-PCR system (model 7500; Applied Biosystems). Total RNA was extracted from different tissues with TRIZOL reagent (Invitrogen) and subjected to DNase I (Invitrogen) treatment. The first-strand cDNA synthesis and qRT-PCR were performed using a high-capacity cDNA reverse transcription kit (Applied Biosystems) and SYBR green quantitative PCR master mix (Maxima; Fermentas), respectively. The following primer pairs were used: 5'-AGAAACCCGGTCCTCGTACT-3' and 5'-CCTGACCAGTGCCATTCTTT-3' for *Smpd3* expression and 5'-AAGCAGGAGGGCAATAAGGT-3' and 5'-CAAGCAGGGTTAAGCTCACA-3' for *Bglap1* expression. For in situ hybridization analyses, embryos were fixed in 4% PFA, embedded in paraffin, and sectioned at 5- μ m thickness. A full-length *Smpd3* cDNA was used to generate ³⁵S-labeled sense and antisense riboprobes.

2.5.4 Skeletal preparation and histologic analysis

Skeletal tissues from newborn and adult mice were fixed overnight in 95% ethanol, stained in 0.015% Alcian blue dye (Sigma-Aldrich) in a 1:4 solution of glacial acetic acid and absolute ethanol for 24 h, and treated with 2% potassium hydroxide until the soft tissues were dissolved. The mineralized tissues were stained by 0.005% Alizarin red (Sigma-Aldrich) solution in 1% potassium hydroxide and clarified in 1% potassium hydroxide/20% glycerol for ≥ 2 d. For plastic sectioning, vertebrae were fixed overnight in 4% PFA/PBS, embedded in methyl

methacrylate, and sectioned (7- μm thickness), and von Kossa and van Gieson staining was applied. Unmineralized bone sections were analyzed using Osteomeasure software (Osteometrics, Inc.). Mouse embryos were fixed in 4% PFA/PBS, pH 7.4, overnight and embedded in paraffin. 5- μm -thick sections were submitted to von Kossa, Alcian blue, and van Gieson staining. Images were taken at room temperature using a light microscope (DM200; Leica) with a 20 \times (numerical aperture of 0.40) or 40 \times (numerical aperture of 0.65) objective. All histological images were captured using a camera (DP72; Olympus), acquired with DP2-BSW software (XV3.0; Olympus), and processed using Photoshop (Adobe). The TUNEL assay was performed on E15.5 embryos to evaluate *in vivo* chondrocyte apoptosis as per the manufacturer's instructions (Deadend Fluorometric TUNEL System kit; Promega).

2.2.5 Immunofluorescence and confocal microscopy

MCF-7 cells (15×10^4 /dish) were seeded in 35-mm confocal dishes (MatTek), and after 24 h, cells were transiently transfected with 1 μg *Smpd3* or *mSmpd3* cloned in the pIRES-hrGFP-1 α expression vector. After 24 h, cells were fixed with 3.7% PFA for 10 min, permeabilized with 100% methanol for 5 min at -20°C , and blocked with 2% human serum in PBS for 30 min at room temperature. Cells were probed with or without anti-FLAG (1:1,000; Sigma-Aldrich) antibody in 2% serum for 2 h at room temperature, washed with 3 \times PBS, and probed with fluorescent secondary antibody (1:200 anti-mouse Alexa Fluor 555; 30–45 min at room temperature). After washing with 3 \times PBS, nuclei were visualized with DRAQ5 staining (1:500 in PBS). Images were captured with a confocal microscope (LSM 510 Meta; Carl Zeiss).

2.2.6 Immunoblotting

Protein samples were separated on 4–20% gradient Tris-HCl gels (Bio-Rad Laboratories) at a constant current of 40 mA before transfer to nitrocellulose membrane in Tris/glycine buffer (100 V for 30 min at 4°C). Membranes were blocked (5% milk in 0.1% Tween in PBS for 30 min) and incubated overnight at 4°C with anti-FLAG (Sigma-Aldrich), anti-nSMase2 (Santa Cruz Biotechnology, Inc.), or antiactin (Sigma-Aldrich) primary antibodies at a 1:1,000, 1:500, or 1:20,000 dilution, respectively. Membranes were washed (3× in 0.1% Tween in PBS), probed with HRP-conjugated mouse or rabbit secondary antibody (1:5,000 in 5% milk in 0.1% Tween in PBS) for 30–45 min at room temperature, and washed (3× in 0.1% Tween in TBS). Proteins were visualized by enhanced chemiluminescence (Thermo Fisher Scientific).

2.5.7 Transient transfection with siRNAs, cell culture, and in vitro mineralization

MC3T3-E1 cells were transfected with 50 ng/μl of *Smpd3* (SI01426999; QIAGEN) or control (1027284; QIAGEN) annealed double-stranded siRNAs and cultured in α-MEM (Invitrogen) supplemented with 10% FBS (PAA Laboratories) and 100 U/ml penicillin-streptomycin at 37°C under 5% CO₂ in a humidified incubator. Primary osteoblast isolation from calvaria, *in vitro* differentiation and culture, and Alizarin red staining for mineral deposition were performed as described previously [156].

2.5.8 Radiography and micro-CT analysis

Radiography and micro-CT analyses of the skeletal samples were performed at the Centre for Bone and Periodontal Research Core Facility at McGill University using an X-ray imaging system (XPRT; Kubtec) and micro-CT system (SkyScan), respectively. For micro-CT analyses,

the X-ray source was operated at 45 kV and at 222 μ A (maximum power). Images were captured using a 12-bit, cooled charge-coupled device camera (1,024 by 1,024 pixels) coupled by a fiber optics taper to the scintillator. Samples were scanned at a magnification resulting in a pixel size of 4.79 μ m. Using a rotation step of 0.9° and an exposition time of 2,240 ms for each step, images were generated, giving a scanning time of 30 min. The cross sections along the specimen long axis were reconstructed using NRecon software (SkyScan), with a distance between each cross section of 9.58 μ m. Each cross section was reduced in half-size to facilitate the analysis, giving of a voxel of 9.58 \times 9.58 \times 9.58 μ m³. CT-Analyser and 3D Creator software (both from SkyScan) were used to analyze and to perform 3D rendering, respectively.

2.5.9 Serum biochemistry

Serum calcium and P_i levels were measured using commercially available kits (Diagnostic Chemicals Limited). Serum ALPL levels were measured as described previously [156], whereas tissue PP_i levels were measured using a fluorogenic sensor following the manufacturer's instructions (Advancing Assay Technologies Bioquest, Inc.).

2.5.10 Sphingomyelinase assays and lipid measurements

Limbs and skullcaps were snap frozen in liquid nitrogen and crushed before further homogenization in 20 mM Tris buffer containing protease inhibitors using an autohomogenizer. Brain tissue was homogenized directly in the same buffer. Aliquots of homogenate were removed for the estimation of protein concentration by the Bradford assay. *In vitro* analysis of nSMase activity was performed using a mixed micelle assay as described previously [154]. In brief, duplicate aliquots (20–30 μ g protein) of homogenate were diluted to 100 μ l in neutral

buffer containing 25 mM Tris, pH 7.4, 5 mM EDTA, 0.2% Triton X-100, and protease inhibitors. The reaction was started by adding 100 μ l assay buffer containing 200 μ M sphingomyelin, 100 μ M phosphatidylserine, and 100,000 cpm 14 C-labeled methyl-sphingomyelin reconstituted in 25 mM Tris, pH 7.4, 10 mM MgCl₂, 5 mM DTT, and 0.2% Triton X-100. After incubation for 30 min at 37°C, reactions were stopped by the addition of 1.5 ml chloroform/methanol (2:1). 400 μ l of water was added, and samples were vortexed and spun at 3,000 rpm for 5 min at room temperature. Next, 800 μ l of the upper phase was added to 4 ml scintillation fluid, vortexed, and counted. 10 μ l assay buffer, representing 2 nmol sphingomyelin, was also counted to allow conversion of results from counts per minute to picomoles of ceramide per milligram of protein per hour. For lipid analysis by mass spectrometry, after homogenization, lysate containing 200 μ g–1 mg protein was analyzed for sphingomyelin, ceramide, and dihydroceramide levels by tandem liquid chromatography/mass spectrometry as previously described [157]. Lipid levels were normalized to cellular protein.

2.6 Data analysis

All results are shown as means \pm the standard deviation. Statistical analyses were performed by Student's *t* test, with $P < 0.05$ considered significant as indicated by a single asterisk (**, $P < 0.01$). Standard Pearson's χ^2 test was used to test the significance of the rescue of both skeletal phenotype and perinatal death.

2.7 Acknowledgements

We thank Drs. Geoffrey Hendy and Houman Homayoun for critical reading of the manuscript.

This work was supported by operating grant 216548 from the Canadian Institutes of Health Research and a seed grant from the Osteogenesis Imperfecta Foundation to M. Murshed. Z. Khavandgar receives a stipend from the McGill University Health Centre Research Institute, and M. Murshed receives salary support from the Fonds de la Recherche en Santé du Québec grant 16302. Additional support for this work was provided by National Institutes of Health grant GM43825 to Y.A. Hannun. M. Murshed and M.D. McKee are members of the Centre for Bone and Periodontal Research, and additional support is gratefully acknowledged from the Fonds de la Recherche en Santé du Québec Réseau de Recherche en Santé Buccodentaire et Osseuse.

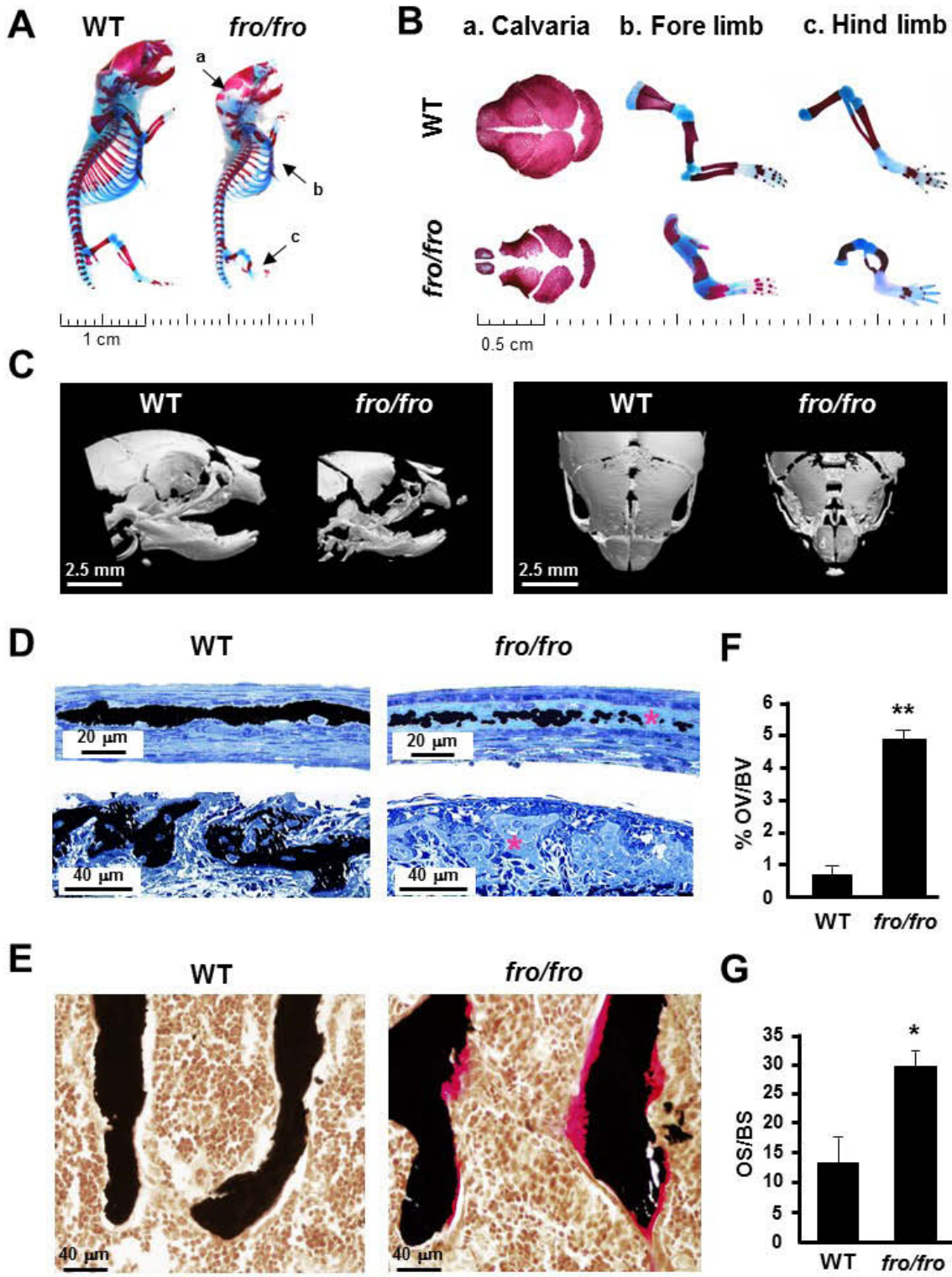


Figure 2.1: Skeletal abnormalities in *fro/fro* mice.

(A and B) Alizarin red (stains mineralized tissues)– and Alcian blue (stains cartilage matrix)–stained skeletal preparations of 2-day-old WT and *fro/fro* mice showing hypomineralization of the calvaria (a) and short (b) and bent (c) fore- and hind limbs in the latter genotype. **(C)** Micro-CT analysis of 2-day-old WT and *fro/fro* heads confirming severe hypomineralization of various head skeletal elements as seen from the dorsal (left) and the lateral (right) views. **(D)** Light micrographs of von Kossa–stained mineral (black) in parietal (top) and alveolar bone (bottom) sections of a 2-day-old WT mouse and its *fro/fro* littermate. There is a marked decrease in mineralization, revealed by extensive areas of unmineralized osteoid (asterisks) in the *fro/fro* bones. **(E)** Von Kossa and van Gieson staining of vertebral bones from 1-month-old WT and *fro/fro* littermates demonstrating a marked increase of unmineralized bone volume (pink staining) in the latter genotype ($n = 5$). **(F and G)** Comparison of the percentage of osteoid volume over total bone volume (OV/BV) and osteoid surface over bone surface (OS/BS) in WT and *fro/fro* mice ($n = 5$). Error bars represent standard deviations. *, $P < 0.05$; **, $P < 0.01$.

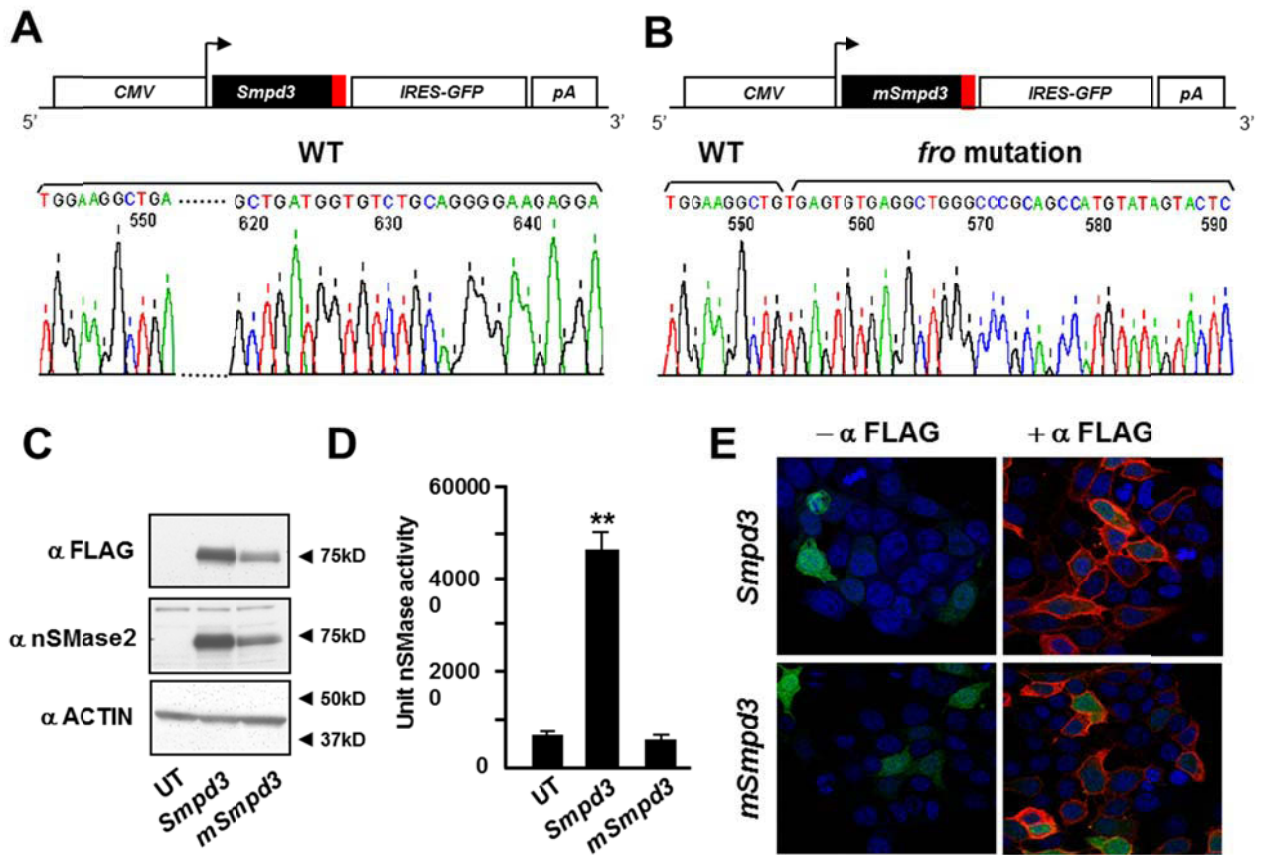


Figure 2.2: Effects of *fro* mutation on nSMase2 activity and localization.

(A and B) Schematic depiction of WT (*Smpd3*; A) and mutant *Smpd3* (*mSmpd3*; carries *fro* mutation; B) expression constructs. The red boxes represent the FLAG coding sequence (CMV, cytomegalovirus promoter; IRES, internal ribosome entry site; and pA, SV40 polyadenylation signal). **(C)** Western blots showing expression of WT and mutant nSMase2 in transfected MCF-7 cells. FLAG-tagged proteins from the transfected cells were detected using an anti-FLAG (top) or an anti-mouse nSMase2 (middle) antibody. UT, untransfected. **(D)** A mixed micelle assay using ¹⁴C-labeled methyl-sphingomyelin shows that mutated nSMase2 does not have any nSMase activity. Error bars represent standard deviations. **(E)** Indirect immunofluorescence microscopy analyses showing comparable cell membrane localization of WT and mutated nSMase2 (shown in red) in transfected MCF-7 cells. The green and blue stains represent GFP localization and the nucleus, respectively. **, P < 0.01.

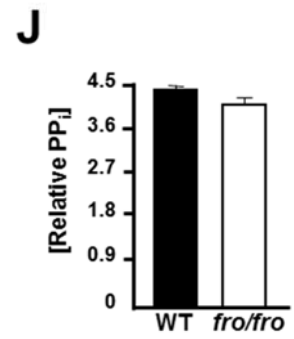
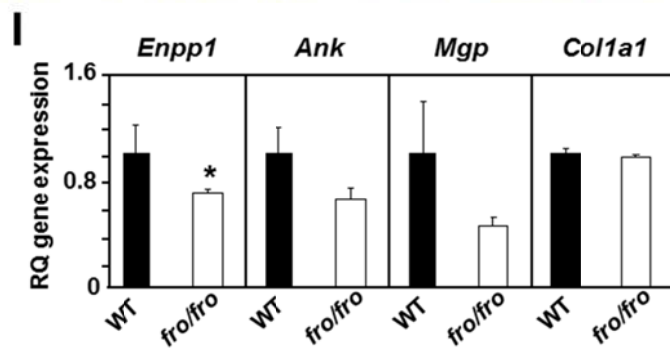
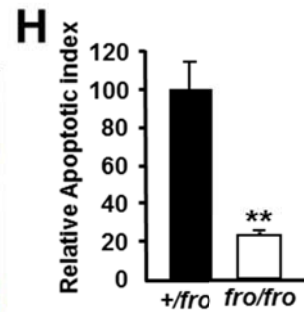
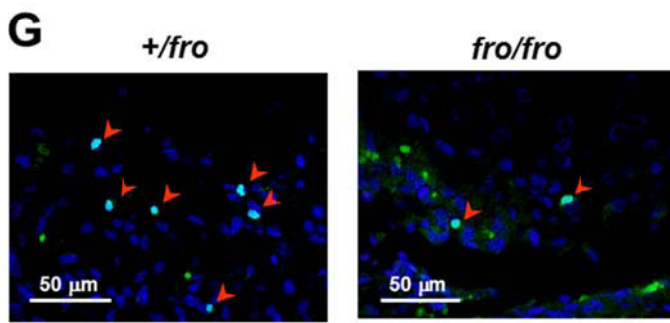
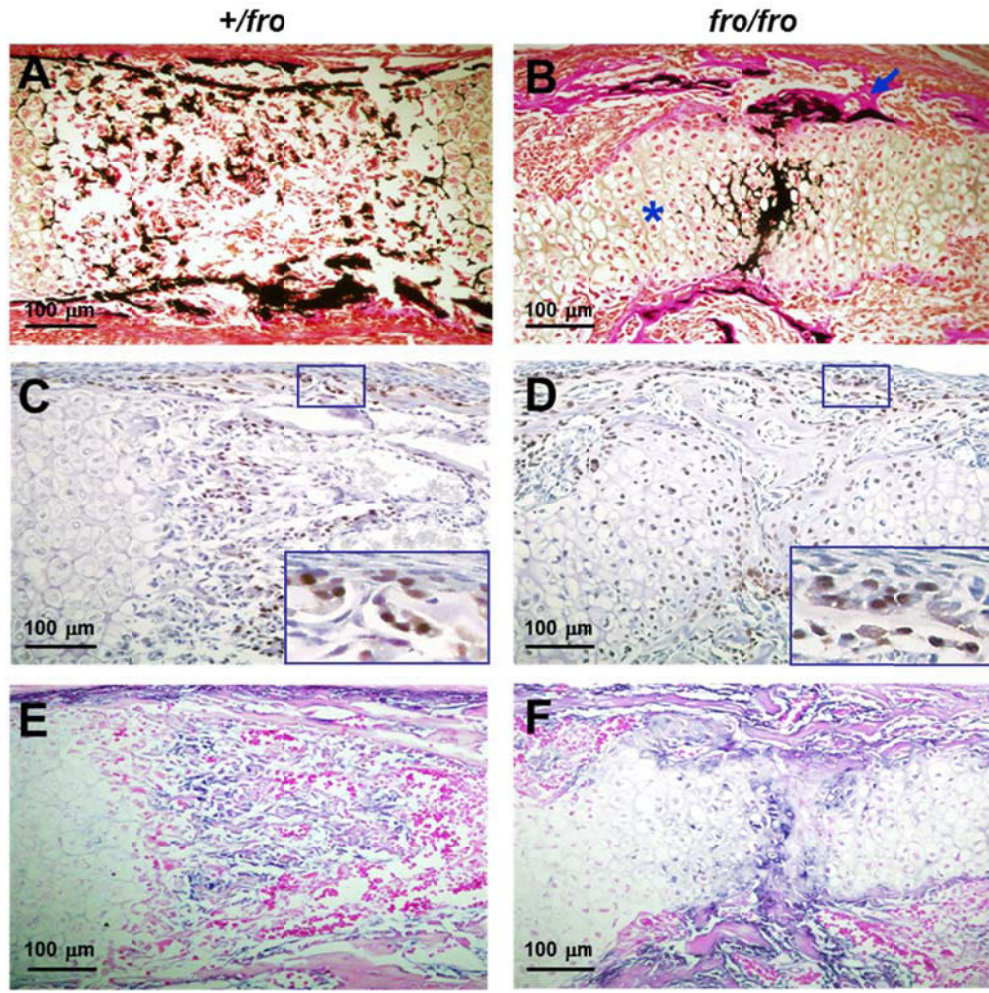


Figure 2.3: Effects of *fro* mutation on the developing skeleton.

(A and B) Von Kossa and van Gieson staining of the humerus from E15.5 *+fro* and *fro/fro* embryos. Note the unmineralized cortical bones (arrow) and the expanded hypertrophic zone (asterisk) in the *fro/fro* mice. **(C and D)** Immunostaining of humerus sections from E15.5 *+fro* and *fro/fro* embryos using an antiosterix antibody shows osteoblast differentiation is unaffected in the latter genotype. For each panel, a magnified view of the marked area has been shown in the insets. **(E and F)** Incubation with a chromogenic substrate solution demonstrates the comparable presence of alkaline phosphatase activities in the *+fro* and *fro/fro* bone sections. **(G and H)** TUNEL assay showing impaired apoptosis of hypertrophic chondrocytes in developing *fro/fro* endochondral bones ($n = 4$). Arrowheads indicate the TUNEL-positive cell nuclei. **(I)** qRT-PCR showing a mild down-regulation of *Enpp1* expression in the parietal bones from *fro/fro* mice. Note that there is no significant alteration of *Ank*, *Mgp*, and *Colla1* expression in *fro/fro* bones. RQ, relative quantification. **(J)** PP_i levels are comparable in both WT and *fro/fro* bone samples. Error bars represent standard deviations. *, $P < 0.05$; **, $P < 0.01$.

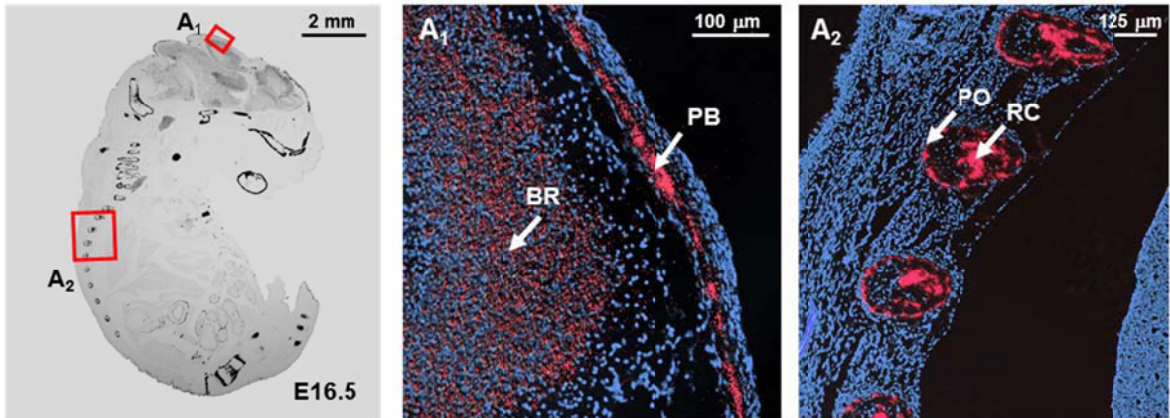
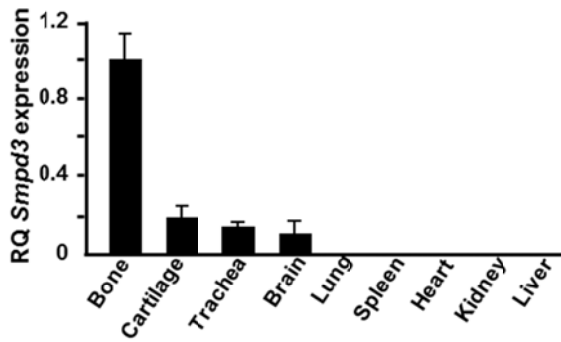
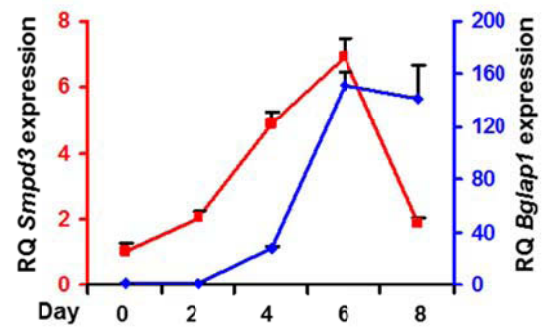
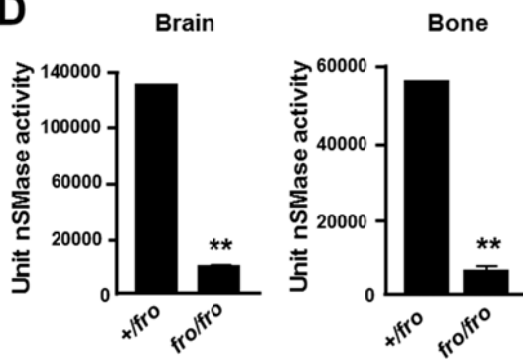
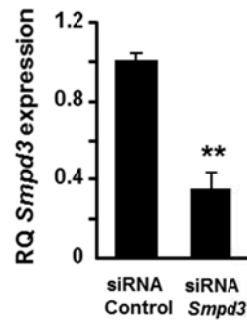
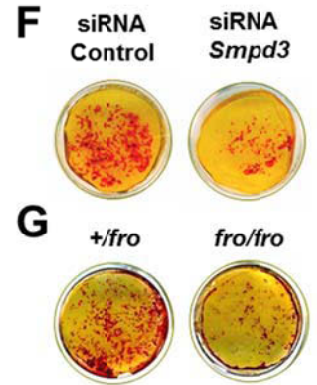
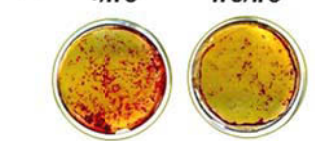
A**B****C****D****E****F****G**

Figure 2.4: *Smpd3* expression and function in osteoblasts

(A) In situ hybridization showing *Smpd3* expression in different skeletal elements in an E16.5 WT mouse embryo. The magnified views of the areas in red boxes are shown in A₁ and A₂ (PB, parietal bone of the skull cap; BR, brain; PO, periosteum in the rib; and RC, rib cartilage). Red stain represents the localization of the *Smpd3* transcript, whereas the blue stain represents the nucleus. (B) qRT-PCR showing high levels of *Smpd3* expression in bone, brain, and cartilage. Tissues were collected from a 2-week-old WT mouse. All expression analyses were performed using *hypoxanthine guanine phosphoribosyl transferase* (*Hprt*) expression in the tissue as an internal control and *Smpd3* expression in the bone as a calibrator (RQ, relative quantification). (C) *Smpd3* and *Bglap1* (red and blue lines, respectively) gene expression analysis in differentiating MC3T3-E1 preosteoblasts at five different time points. *Smpd3* expression reaches its peak by day 6. Late osteoblast marker *Bglap1* expression was used to monitor terminal differentiation of the MC3T3-E1 cells. (D) A mixed micelle assay using ¹⁴C-labeled methyl-sphingomyelin shows a significant decrease in nSMase activity in both brain and bone tissues collected from the *fro/fro* mice. (E) *Smpd3* knockdown by using siRNA technique in MC3T3-E1 preosteoblasts. (F) Alizarin red staining shows reduced *in vitro* mineral deposition in cultures of MC3T3-E1 cells transfected by *Smpd3* siRNAs in comparison with the control group. (G) Alizarin red staining shows reduced mineral deposition in cultures of differentiated *fro/fro* osteoblasts in comparison with the *+/fro* osteoblasts. The cultures were grown for 10 d in an osteogenic medium containing ascorbic acid and β-glycerol phosphate. Error bars represent standard deviations. **, P < 0.01.

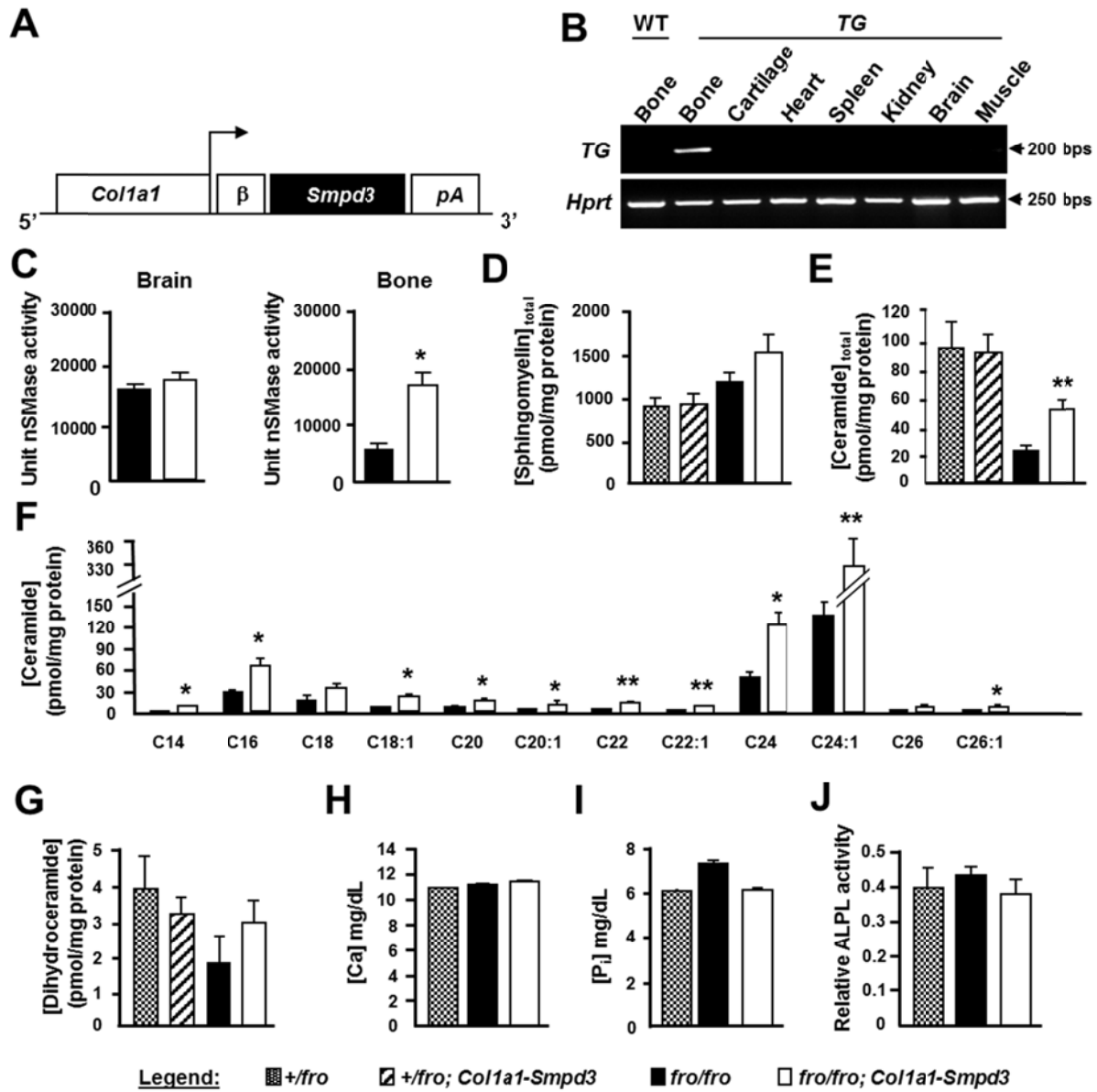
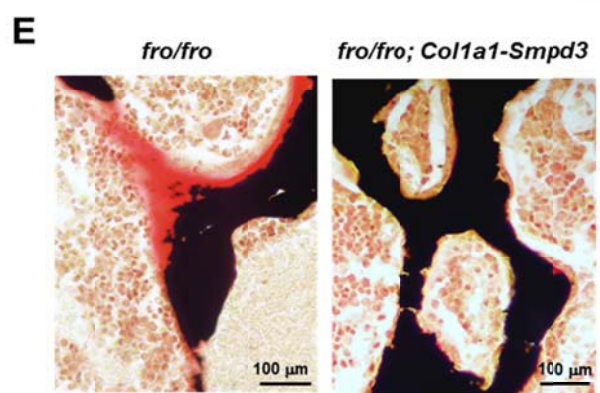
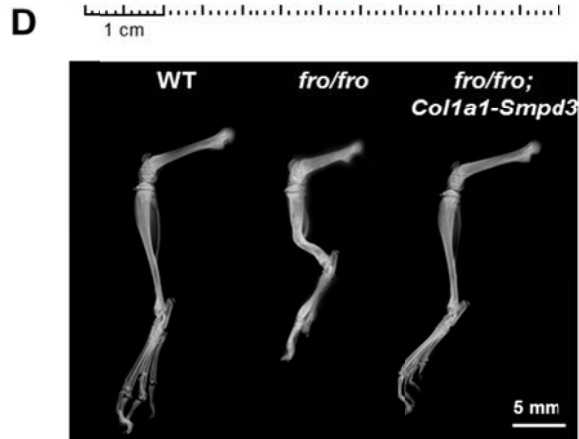
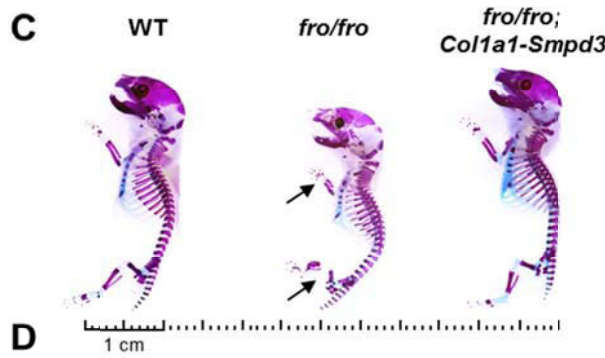
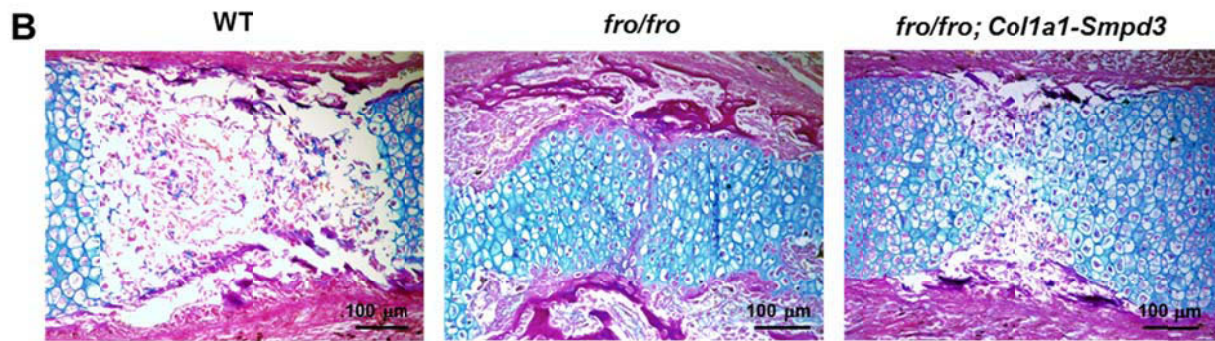
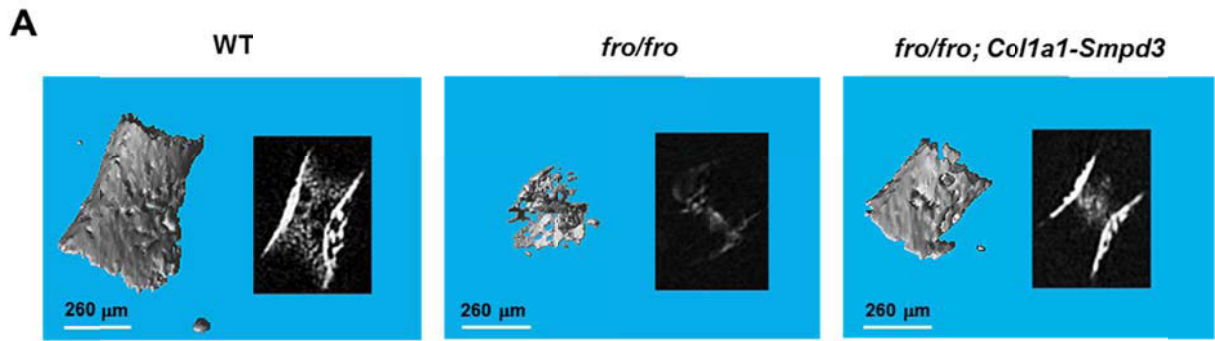


Figure 2.5: Biochemical analysis of bone tissue and serum samples from *fro/fro;Colla1-Smpd3* mice.

(A) Schematic representation of the *Colla1-Smpd3* transgene construct. **(B, to p)** Semiquantitative PCR analysis confirming bone-specific expression of the transgene (*TG*). (bottom) *Hprt* expression analysis has been shown as a control for the cDNA amount. Amplicon sizes in base pairs are indicated on the left. **(C)** Enzymatic assays using ^{14}C -labeled methyl-sphingomyelin shows no change in nSMase activity in *fro/fro;Colla1-Smpd3* brain samples. As expected, in *fro/fro;Colla1-Smpd3* bone samples, the nSMase activity is increased in comparison with the *fro/fro* bone samples. **(D–G)** Lipid analysis using liquid chromatography/mass spectrometry of sphingomyelin **(D)**, total ceramide **(E)**, individual ceramide species **(F)**, and dihydroceramide **(G)**. A significant increase of total ceramide levels is caused by the increase of several long-chain ceramide species in *fro/fro* bones ($n = 4$). **(H–J)** Serum calcium **(H)**, P_i **(I)**, and alkaline phosphatase **(J)** activities are comparable in *+fro*, *fro/fro*, and *fro/fro;Colla1-Smpd3* mice ($n = 5$). Error bars represent standard deviations. *, $P < 0.05$; **, $P < 0.01$.



F

Total Genotyped 144			
<i>fro/fro</i> 17		<i>fro/fro; Col1a1-Smpd3</i> 28	
Perinatal death 11	Limb deformities 17	Perinatal death 3	Limb deformities 0

Figure 2.6: Analysis of *fro/fro;Coll1a1-Smpd3* bones

(A) Micro-CT analysis of E15.5 *fro/fro* humerus showing a poorly mineralized bone collar and cartilage matrix. Although bone collar mineralization defects are completely rescued in *fro/fro;Coll1a1-Smpd3* embryos, mineralization defects in the cartilage matrix are still present. Insets show the cross-sectional X-ray images of the analyzed bones. (B) Alcian blue and van Gieson staining of humerus sections from E15.5 *fro/fro* embryos confirm the micro-CT findings. Note the abnormal presence of the hypertrophic chondrocyte-like cells in the shaft region of the *fro/fro* humerus. This latter phenotype is largely unaffected in the *fro/fro;Coll1a1-Smpd3* long bones. (C) Skeletal preparations indicate a full rescue of the *fro/fro* bone deformities (arrows) in the newborn *fro/fro;Coll1a1-Smpd3* mice. (D) Radiographical analysis shows that the limb abnormalities are absent in 1-month-old *fro/fro;Coll1a1-Smpd3* mice. (E) Von Kossa and van Gieson staining of vertebral bone sections from 1-month-old *fro/fro* and *fro/fro;Coll1a1-Smpd3* littermates demonstrate a complete rescue of the mineralization defects in the latter genotype. (F) Table showing genotyping data. Skeletal abnormalities were not seen in any of the *fro/fro;Coll1a1-Smpd3* mice analyzed.

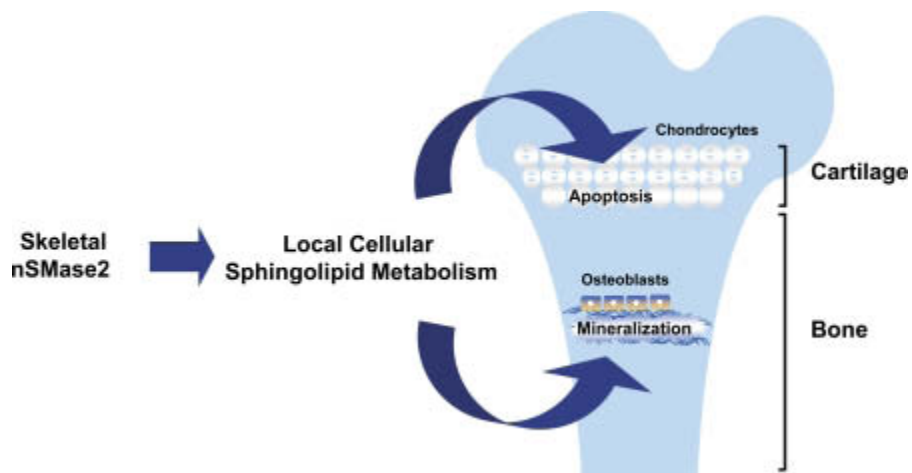


Figure 2.7: A model depicting the local activities of nSMase2 in skeletal tissues.

The cell-autonomous activity of nSMase2 in bone promotes ECM mineralization. In the cartilage, nSMase2 enzymatic activity is necessary for the normal apoptosis of hypertrophic chondrocytes.

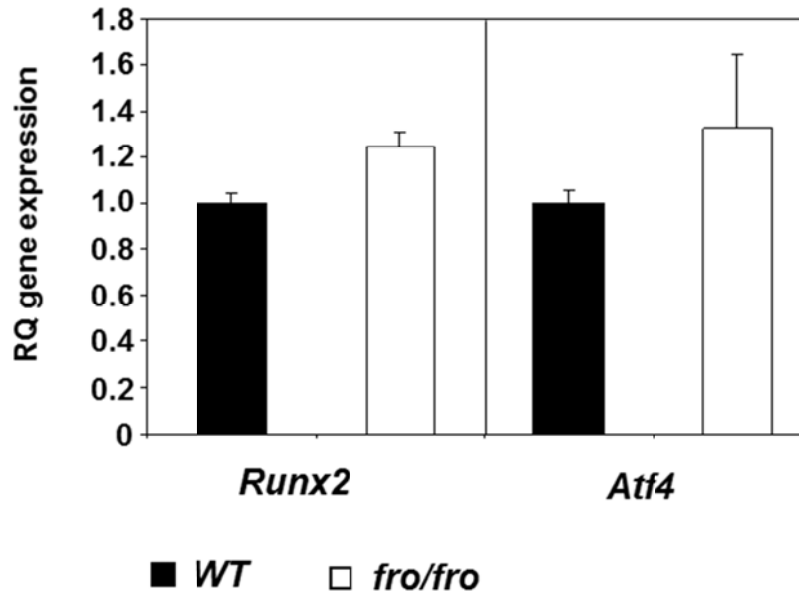


Figure S1: qRT-PCR analysis of *Runx2* and *Atf4* expression in newborn *fro/fro* bones.

The qRT-PCR expression analysis of total RNA shows that *Runx2* and *Atf4* expression in the bones from newborn *fro/fro* mice are normal. Error bars represent standard deviations. RQ, relative quantification.

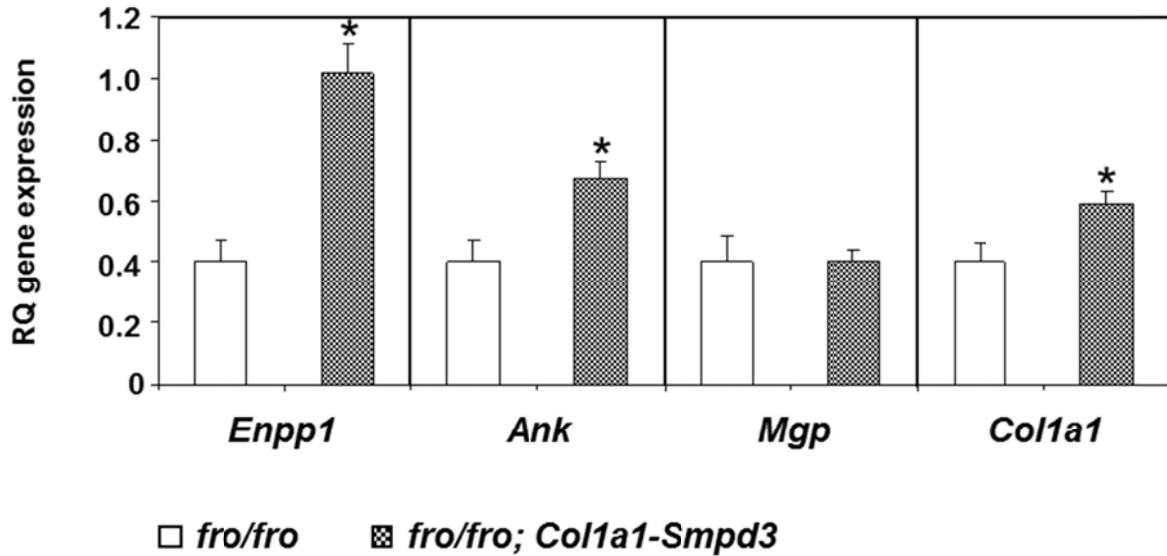


Figure S2: The comparative expression analysis of *Enpp1*, *Ank*, *Mgp*, and *Col1a1* by qRT-PCR in the parietal bones of *fro/fro* and *fro/fro;Col1a1-Smpd3* mice.

Enpp1 expression is ~2.5-fold up-regulated, whereas there is a mild but significant up-regulation of *Ank* and *Col1a1* expression in the bones from newborn *fro/fro;Col1a1-Smpd3* mice in comparison with that of their *fro/fro* littermates. *Mgp* expression remains unchanged. Error bars represent standard deviations. *, $P < 0.05$. RQ, relative quantification.

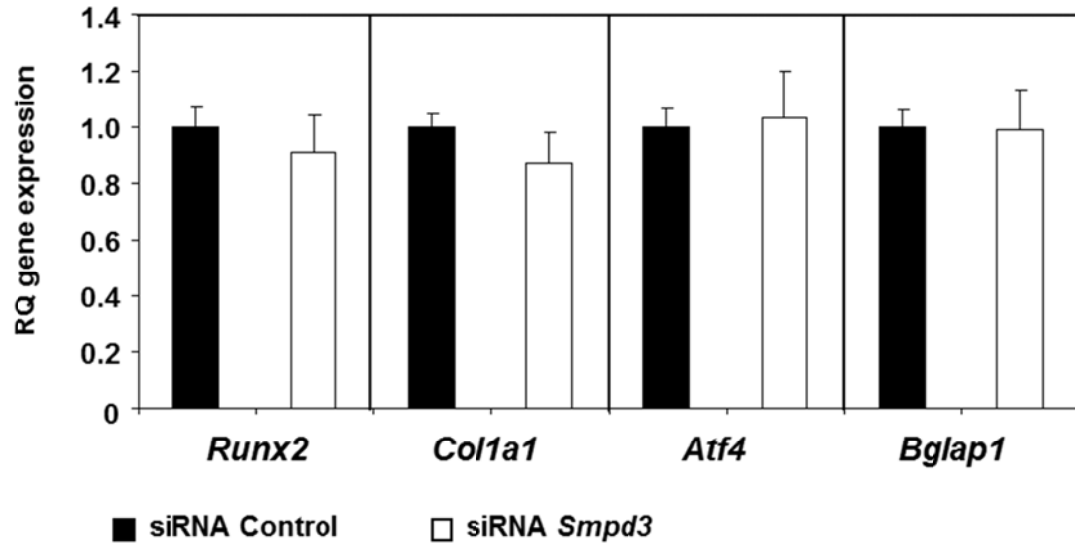
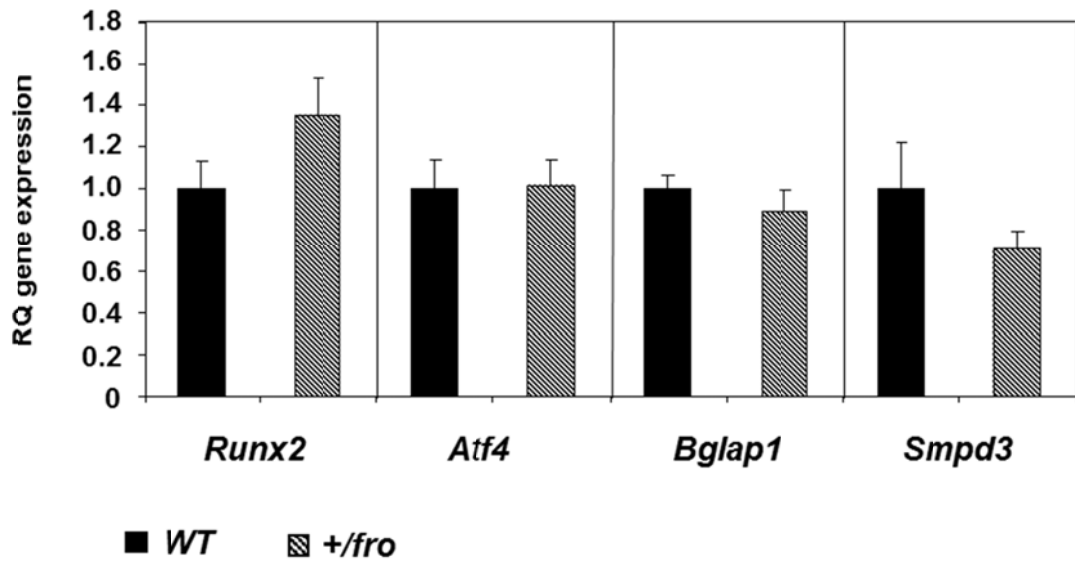
A**B**

Figure S3: qRT-PCR analysis of *Runx2*, *Colla1*, *Atf4*, and *Bglap1* expression in the control and *Smpd3* siRNA-treated MC3T3-E1 cells and *Runx2*, *Atf4*, *Bglap1*, and *Smpd3* expression in WT and *+fro* mice.

(A) *Runx2*, *Colla1*, *Atf4*, and *Bglap1* expressions are not altered in *Smpd3* siRNA-transfected MC3T3-E1 cells, in comparison with the control siRNA-transfected cells. **(B)** No significant alteration of *Runx2*, *Atf4*, *Bglap1*, and *Smpd3* expression was seen in the *+fro* bones when compared with those from their WT littermates. The qRT-PCR expression analysis was performed on the total RNA extracted from the parietal bones of the newborn mice. Error bars represent standard deviations. RQ, relative quantification.

Chapter 3: Local Regulation of Tooth Mineralization by Sphingomyelin

Phosphodiesterase 3

Local Regulation of Tooth Mineralization by Sphingomyelin Phosphodiesterase 3

Zohreh Khavandgar¹, Sharifa Alebrahim¹, Hazem Eimar¹, Faleh Tamimi¹, Marc D. McKee^{1,2} and

Monzur Murshed^{1,3}

¹Faculty of Dentistry; ²Department of Anatomy and Cell Biology; and ³Department of Medicine,

McGill University, Montreal, Quebec, Canada.

Journal of dental research, 2013 Apr; 92(4): 358-64

doi:10.1177/0022034513478429

3.1 Abstract

Sphingomyelin phosphodiesterase 3 (*Smpd3*) encodes a membrane-bound enzyme that cleaves sphingomyelin to generate several bioactive metabolites. A recessive mutation called *fragilitas ossium (fro)* in the *Smpd3* gene leads to impaired mineralization of bone and tooth extracellular matrix (ECM) in *fro/fro* mice. In teeth from *fro/fro* mice at various neonatal ages, radiography and light and electron microscopy showed delayed mantle dentin mineralization and a consequent delay in enamel formation as compared with that in control *+/fro* mice. These tooth abnormalities progressively improved with time. Immunohistochemistry showed expression of SMPD3 by dentin-forming odontoblasts. SMPD3 deficiency, however, did not affect the differentiation of these cells, as shown by osterix and dentin sialophosphoprotein expression. Using a transgenic mouse rescue model (*fro/fro; Colla1-Smpd3*) in which *Smpd3* expression is driven by a murine *Colla1* promoter fragment active in osteoblasts and odontoblasts, we demonstrate a complete correction of the tooth mineralization delays. In conclusion, analysis of these data demonstrates that *Smpd3* expression in odontoblasts is required for tooth mineralization.

3.2 Introduction

While extracellular matrix (ECM) mineralization in bones and teeth is driven by developmentally distinct cell types, the mineralization process appears to be regulated by several common determinants. Indeed, the mechanisms underlying bone ECM mineralization and those of tooth dentin and cementum are so similar that genetic diseases affecting bone mineralization often also manifest as tooth mineralization defects [39, 158-160].

In an attempt to identify the novel regulators of hard-tissue mineralization and to understand their modes of action, we are investigating mouse models with bone and tooth mineralization defects in which the known determinants of ECM mineralization are unaffected. These critical determinants of ECM mineralization include 2 mineral ions, inorganic phosphate (P_i) and calcium, the mineralization inhibitor inorganic pyrophosphate (PP_i), and alkaline phosphatase (ALPL), an ectoenzyme that regulates tissue PP_i levels [24, 29, 33, 161]. We recently reported the cell-autonomous requirement of sphingomyelin phosphodiesterase 3 (SMPD3) in osteoblasts for bone ECM mineralization [95]. SMPD3 cleaves sphingomyelin in the cell membrane and generates phosphocholine and ceramide [89], 2 bioactive metabolites that, in turn, affect a variety of cellular activities. A recessive mutation in *Smpd3* called *fragilitas ossium* (*fro*) leads to poor bone and tooth mineralization, impaired apoptosis of hypertrophic chondrocytes, and severe skeletal dysplasia in *fro/fro* mice [83, 95, 124, 162]. Interestingly, the known factors important in influencing ECM mineralization appear to be unaffected in this model [95], thus making it useful for deciphering the direct effects of SMPD3 on mineralization.

The objectives of the present study were to characterize the tooth mineralization defects in *fro/fro* mice and to determine, in transgenic mice, whether SMPD3 regulates tooth mineralization locally. Herein we report on the temporal appearance (and recovery) of tooth

mineralization delays in young *fro/fro* mice. Analysis of the radiographic and histological data suggests that the tooth mineralization delays caused by the *fro* mutation are attributable not to abnormal cell differentiation and patterning, but rather to altered mineralization caused by a local effect of the absence of SMPD3 activity (from odontoblasts) in the dentin ECM. Finally, we show that transgenic expression of *Smpd3* in odontoblasts in *fro/fro* mice completely corrects the neonatal tooth abnormalities.

3.3 Results

3.3.1 Transient tooth mineralization delay in *fro/fro* mice

Since skeletal mineralization is normal in *+fro* mice, we used these and wild-type (WT) mice interchangeably as controls. We first used radiography to analyze the mandibles of 3-day-old control *+fro* and *fro/fro* mice. Both molars and incisors were smaller and hypomineralized (more radiolucent) in *fro/fro* mice in comparison with those of their *+fro* littermates (Fig. 3.1 A). Although tooth and alveolar bone mineralization improved by day 14, tooth sizes remained slightly smaller.

We next performed von Kossa and van Gieson staining of plastic sections of 1-, 3-, and 7-day-old teeth from *+fro* and *fro/fro* mice. Light microscopy confirmed the smaller size of the *fro/fro* teeth, and showed normal organization of ameloblasts and odontoblasts in the molars of both *+fro* and *fro/fro* mice at all stages analyzed. Although crown cusp and root patterning of the molars were overtly comparable in both genotypes, some *fro/fro* molars showed differences in cusp shapes (Fig. 3.1 B).

In 1-day-old *+fro* mice, a distinct and normal-looking layer of odontoblasts was observed associated with the adjacent mineralizing dentin matrix at the cusp tips (Fig. 3.1 B). In *fro/fro* littermates, however, no trace of mineral deposition was apparent in the mantle dentin secreted by the odontoblasts at this stage.

In 3-day-old *+fro* mice, the crown dentin was well-mineralized throughout, and mineralized enamel appeared as a thin layer in opposition to the dentin. However, although the crown dentin ECM was fully formed in the 3-day-old mutant *fro/fro* mice, its mineralization was reduced and discontinuous, and no mineralized enamel had formed (Fig. 3.1 B and C).

By day 7, both *+fro* and *fro/fro* littermates had overtly comparable, continuous tooth mineralization in the crown (Fig. 3.1 B and C). In addition to the smaller tooth size, the total

thickness of the mineralized tissue (dentin and enamel combined) was less in 7-day-old *fro/fro* mice compared with that in age- and gender-matched *+/fro* littermates (Fig. 3.1 B).

As with the molars, we observed a significant delay in the mineralization of the incisors of *fro/fro* mice in comparison with that in *+/fro* littermates (Fig. 3.1 D). Although the dental organs were indistinguishable at day 1 in *+/fro* and *fro/fro* mice, by day 3 we observed a striking difference in their mineralization status, with the thinner layer of dentin being completely unmineralized in the incisors of the *fro/fro* mice. Ameloblasts were comparably organized in both genotypes.

3.3.2 SMPD3 localization in odontoblasts

Immunohistochemistry performed on 3-day-old WT molar sections showed that SMPD3 was expressed in odontoblasts, but not in ameloblasts (Fig. 3.2 A). We next examined whether the lack of SMPD3 activity in *fro/fro* odontoblasts affected the expression of osterix (OSX), a transcription factor required for odontogenic differentiation from mesenchymal precursor cells [47]. OSX expression was not altered in the mutant odontoblasts (Fig. 3.2B). Similarly, dentin sialophosphoprotein (DSPP) localization in the odontoblasts was comparable in WT and *fro/fro* mice. Also, ameloblasts from *fro/fro* mice expressed comparable amounts of amelogenin (AMELX), the major enamel matrix protein (Fig. 3.2 B) [163].

3.3.3 Normal mineral structure and ECM architecture in fro/fro teeth

Ultrastructural analysis of molar mantle dentin by TEM revealed a similar matrix structure for both *+/fro* and *fro/fro* mice. In both cases, matrix vesicles were dispersed throughout the collagenous matrix, and evidence of matrix vesicle mineralization was clearly observed (Fig. 3.3 A)

Crystallographic dimensions in enamel and dentin in the incisors of 14-day-old WT and *fro/fro* mice were determined from XRD spectra (Fig. 3.3 B). Crystallographic dimensions in enamel along both the *c*-axis (6.57 ± 1.39 nm) and the *a*-axis (6.43 ± 1.59 nm) in WT mice were significantly larger ($p < 0.05$) than in *fro/fro* mice (*c*-axis, 3.73 ± 1.58 nm; *a*-axis, 3.59 ± 1.05 nm) (Fig. 3.3 C). Crystallographic dimensions in dentin along the *c*-axis (5.72 ± 1.79 nm) in WT mice were significantly larger ($p < 0.05$) than in *fro/fro* mice (3.32 ± 0.88 nm) (Fig. 3.3 C), but no difference was observed for the *a*-axis dimension (WT, 5.98 ± 1.09 nm; *fro/fro*, 4.59 ± 1.17 nm).

3.3.4 A cell-autonomous requirement of SMPD3 in tooth mineralization

The specific localization of SMPD3 in odontoblasts (Fig. 3.2 A) prompted us to examine whether restoration of *Smpd3* expression in these cells could prevent the tooth mineralization delays in *fro/fro* mice. We previously reported a mouse strain *fro/fro;Colla1-Smpd3* that expressed the *Smpd3* transgene under an osteoblast-/odontoblast-specific *Colla1* promoter fragment (Fig. 3.4 A) [95]. The *Colla1* promoter activity in the tooth is evident from the blue β -galactosidase activity in the mandible of the *Colla1-lacZ* reporter transgenic mouse (Fig. 3.4 B) [155].

Radiographic and histologic assessment of 3-day-old teeth revealed well-developed, continuous mineralization in the crown dentin of the rescued *fro/fro;Colla1-Smpd3* mice, as compared with the reduced and discontinuous mineralization seen in the *fro/fro* mice (Fig. 3.4 C, D, E). Finally, as shown by micro-CT analysis, while *fro/fro* incisors still appeared to be smaller at 1 month of age, by 3 months, their size became largely comparable with those in *+/fro* mice. The sizes of the *fro/fro;Colla1-Smpd3* incisors were comparable with those of *+/fro* mice at both time-points analyzed (Fig. 3.4 F).

3.4 Discussion

SMPD3 is a novel regulator of ECM mineralization. The *fro* mutation does not affect SMPD3 membrane localization, but completely ablates its activity. In the current study, we describe the effects of the *fro* mutation on the transient tooth mineralization delays in *fro/fro* mice and also characterize the mineral properties of the tooth of these mice.

In general, teeth in *fro/fro* neonates were smaller in comparison with those in their *+fro* littermates; however, this was partly corrected as these mice approached their weaning age. The smaller tooth size could be a result of the generally smaller body size of the *fro/fro* strain, most likely caused by hormonal abnormalities in these mice [126].

Analysis of our data suggests that the development of the dental organ is generally not affected in *fro/fro* mice, indicating that the *fro* mutation does not affect cell differentiation and the general tooth developmental pattern. Also, the expression of odontogenic markers OSX and DSPP is not altered in *fro/fro* odontoblasts. The conclusion that odontoblast differentiation and function is preserved in *fro/fro* teeth is supported by the seemingly normal production of a dentin matrix layer with normal ultrastructure.

We observed that there was a significant delay in the mineralization of mantle dentin in *fro/fro* mutants. Since mantle dentin mineralization induces enamel mineralization, there was a concomitant delay in enamel mineralization, all occurring in the presence of seemingly normal cell structure and organization. Additionally, in both WT and *fro/fro* ameloblasts, the comparable expression of amelogenin indicated that there were no overt changes in ameloblast differentiation and function in the latter genotype. Analysis of our data indicates that mineral type and morphology of the enamel and dentin apatite crystals of *fro/fro* and WT mice are similar, with the smaller crystals being expected in the *fro/fro* mice, since tooth development is delayed and since crystals grow in size over time [164].

SMPD3 is specifically produced by normal odontoblasts, and we observed a complete rescue of the *fro/fro* (lacking functional SMPD3) tooth mineralization delays in juvenile *fro/fro;Coll1a1-Smpd3* mice in which *Smpd3* expression had been restored in the odontoblasts [95]. A recent study has reported on *Smpd3*^{-/-} mice – a gene-targeted model of SMPD3 deficiency [126] – describing skeletal deformities similar to those seen in *fro/fro* mice, but it did not report on any bone and tooth mineralization defects. The phenotypic differences between the 2 mouse models have been attributed to variations in genetic background and/or the possibility of additional genetic alterations in *fro/fro* mice. While the effects of genetic background cannot be fully ruled out, the complete rescue of the bone and tooth mineralization defects in our *fro/fro;Coll1a1-Smpd3* mice suggests that the *fro* mutation, and not any other genetic alteration, is the cause of this observed phenotype. One possible explanation for fact that the tooth phenotype was not detected in the *Smpd3*^{-/-} mice could be that older mice were analyzed when the defect had largely been corrected.

Analysis of our TEM data suggests that matrix vesicles, small extracellular vesicular bodies involved in mantle dentin mineralization [165], still show an ability to mineralize in the *fro/fro* mice. This indicates that factors beyond the matrix vesicle that are involved in dentin mineralization are likely to be affected by missing or inactive SMPD3.

Phospholipid metabolism has been associated with tooth mineralization [143]. Phospholipids, abundantly present in the cell membrane, may act as sources of P_i, a critical determinant of ECM mineralization. During the initiation of ECM mineralization, enzymatic processing of phospholipids may generate free phosphate and increase its local concentration within the tissue microenvironment. We hypothesized that phosphocholine generated from the cleavage of sphingomyelin can be processed further inside matrix vesicles by the intracellular enzyme PHOSPHO1 and extracellularly by ALPL to generate free phosphate [133]. This

hypothesis is supported by the observation that both *Phospho1*^{-/-} and *Alpl*^{-/-} mice show bone and tooth mineralization defects. Interestingly, the severity of the skeletal mineralization phenotype of *Phospho1*^{-/-};*Alpl*^{-/-} double-knockout mice is similar to that seen in *fro/fro* mice [136]. Additional work is required to examine the epistatic interactions among SMPD3, PHOSPHO1, and ALPL in phospholipid-mediated ECM mineralization.

3.5 Materials and Methods

3.5.1 Mice

The generation of mice has been described previously [95]. All mice were maintained following an animal use protocol approved by McGill University. Primer sequences used for the genotyping of tail biopsies are available upon request. Mice were analyzed at post-natal days 1, 3, 7, and 14 by X-ray and/or histological analysis, and at 1 and 3 months of age by micro-CT.

3.5.2 Radiography and micro-CT

X-ray analyses of the mandibles were performed at the Centre for Bone and Periodontal Research core facility at McGill University, with an XPERT X-Ray imaging system (Kubtec, Milford, CT, USA). Micro-CT scanning of mouse mandibles was performed with a SkyScan model 1072 instrument (SkyScan, Kontich, Belgium) set at a resolution of 8.0 μm and 0.5-mm Al filter. Micro-CT image processing and analysis was performed with Version 2.2f of the manufacturer's software (SkyScan).

3.5.3 Histology

Mandibles were fixed overnight in 4% PFA/PBS (paraformaldehyde in phosphate-buffered saline) and embedded in methyl methacrylate and sectioned (7 μm), followed by von Kossa (for mineral) and van Gieson staining. Light microscopy images were taken by means of a Leica DM200 light microscope equipped with an Olympus DP72 camera and DP2-BSW software (XV3.0, Olympus, Tokyo, Japan). For immunohistochemistry, similarly fixed mandibles were first decalcified in EDTA prior to being embedded in paraffin and sectioned (5 μm). Sections were blocked with 5% bovine serum albumin (Fisher, Pittsburgh, PA, USA) in TBS Triton, followed by incubation with anti-SMPD3, anti-osterix (OSX), and anti-AMELX

(amelogenin) antibodies from Abcam (Cambridge, MA, USA) and anti-DSPP antibody, kindly provided by Dr. Larry W. Fisher. Detection was by horseradish-peroxidase-conjugated secondary antibody (Abcam).

3.5.4 Transmission electron microscopy

Transmission electron microscopy (TEM) was performed on fixed (as above) samples that were post-fixed in osmium tetroxide and embedded in Epon epoxy resin (Cedarlane, Burlington, ON, Canada). Thin sections (80 nm) of undecalcified teeth were cut with a Leica Ultracut E microtome followed by conventional staining with uranyl acetate and lead citrate. Samples were viewed in an FEI Technai 12 transmission electron microscope (Philips, Eindhoven, the Netherlands) operating at 120 kV and equipped with a 792 Bioscan 1k × 1k wide-angle multiscan CCD camera (Gatan, Pleasanton, CA, USA).

3.5.5 X-ray diffraction

Microtome-cut smooth surfaces of methyl-methacrylate-embedded incisors of 14-day-old mice from the *fro/fro* and WT strains were analyzed by X-ray diffraction (XRD) in a D8-DISCOVER diffractometer (Bruker, Billerica, MA, USA) allowing for spot-size (50 μm) placement on either the enamel or dentin layer, with XRD parameters adjusted to those described previously [166]. We used DIFFRAC-plus EVA software (AXS, Bruker) to analyze the data obtained from each XRD spectrum. We used the (002) and (310) Bragg peaks from each XRD spectrum to obtain average crystallographic dimensions along the *c*- and *a*-axes (based on Scherrer's formula) to calculate the crystal aspect ratio (*c*-axis : *a*-axis) and the crystal lattice parameters in enamel and dentin.

3.5.6 X-gal staining

Mouse heads were dissected and fixed for 5 min in 2% formalin and 0.2% glutaraldehyde in PBS containing 5 mM EGTA and 2 mM MgCl₂. Fixed tissues were rinsed with PBS containing 2 mM MgCl₂ and 0.2% IGEPAL[®] CA 630 and stained overnight at 37°C in the same buffer supplemented with 5 mM each of K₃Fe(CN)₆ and K₄Fe(CN)₆.3H₂O and 25 mg/mL X-Gal.

3.6 Statistical analysis

All results are shown as means with standard deviation values. Statistical analyses were performed by the Student's *t* test, with $p < 0.05$ considered significant, as indicated by a single asterisk.

3.7 Acknowledgements

The authors thank L. Malynowsky for help with the electron microscopy. This work was supported by operating grants from the Canadian Institutes of Health Research (CIHR) Fund # 123310 to MM and from the Natural Sciences and Engineering Research Council of Canada (NSERC) and the Fondation de l'Ordre des Dentistes du Québec (FODQ) to FT. ZK, SA, and HE receive studentships from CIHR, the Ministry of Higher Education of Saudi Arabia, and the FRQS Réseau de Recherche en Santé Buccodentaire et Osseuse (RSBO), respectively. MM is an FRQ-S Chercheur-boursier.

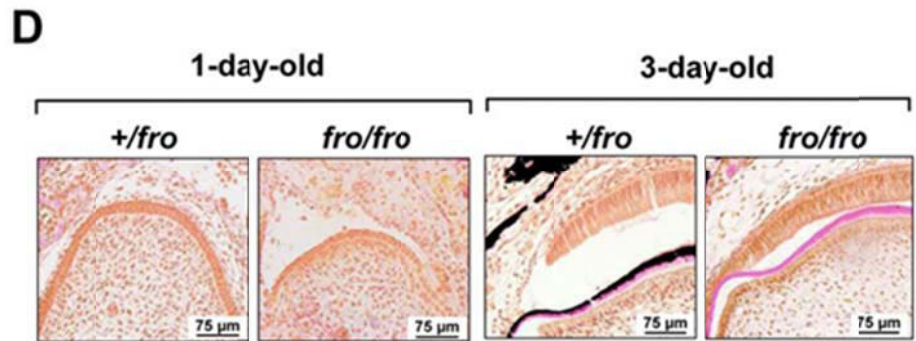
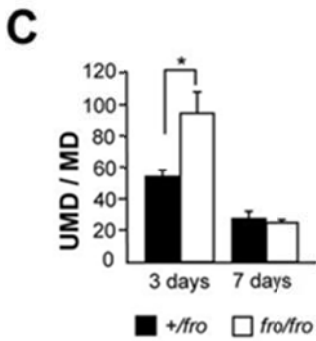
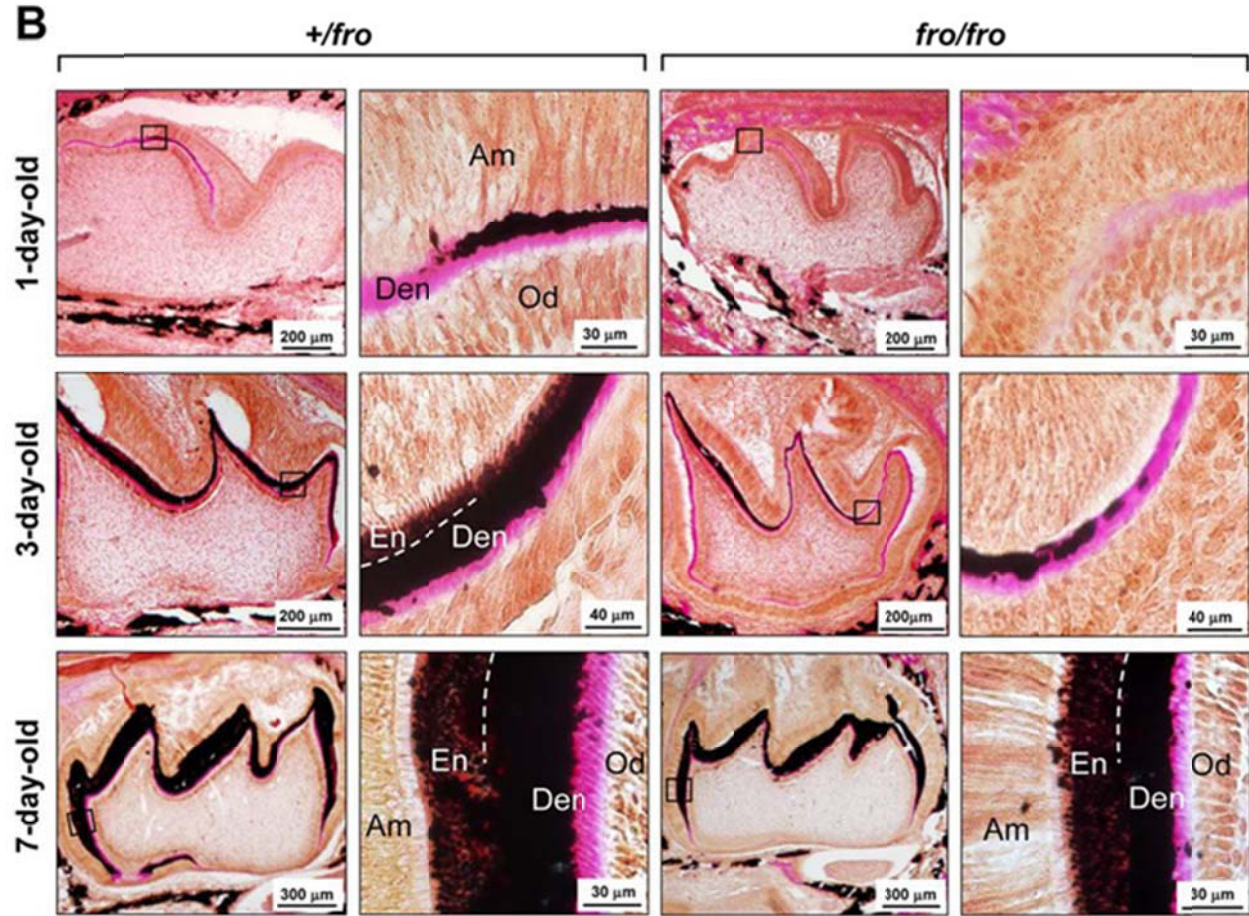
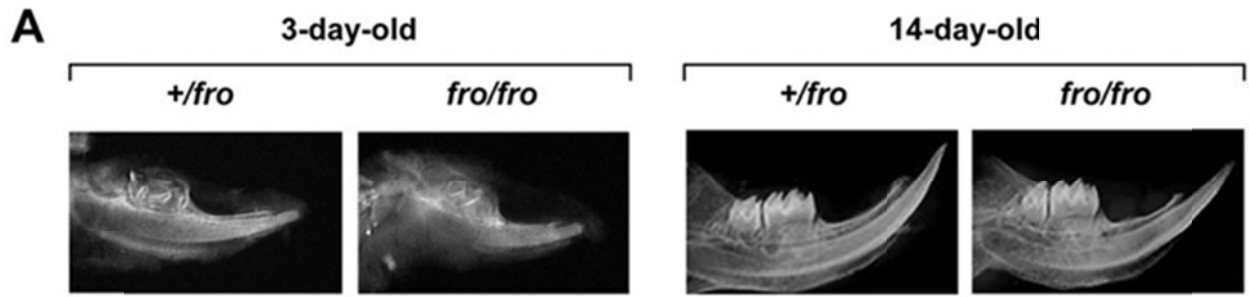


Figure 3.1: Effects of the *fro* mutation on developing teeth.

(A) X-ray images of 3-day-old mandibles from *fro/fro* mice showing overall smaller mandibular size, and smaller and poorly mineralized incisors and molars in comparison with those in *+fro* controls. These defects were largely corrected by 14 days of age for the *fro/fro* mice. (B) von Kossa and van Gieson staining of sagittal sections of molars from 1-, 3-, and 7-day-old *+fro* and *fro/fro* mice showing smaller-sized molars at all time-points with a significant delay in tooth mineralization (dentin and enamel) that was corrected with age. The magnified views of the area indicated by the black boxes are shown to the right next to each panel. (C) Histomorphometric quantification shows a significant increase of unmineralized dentin (UMD) over mineralized dentin (MD) in the molars of 3-day-old *fro/fro* mice in comparison with that of *+fro* littermates. However, UMD/MD in the molars of 7-day-old *fro/fro* and *+fro* mice were comparable (n = 3 for each genotype). (D) von Kossa and van Gieson staining of coronal sections of incisors from 1- and 3-day-old *+fro* and *fro/fro* mice showing smaller-sized incisors at both ages, and with a significant delay in mineralization seen at day 3.

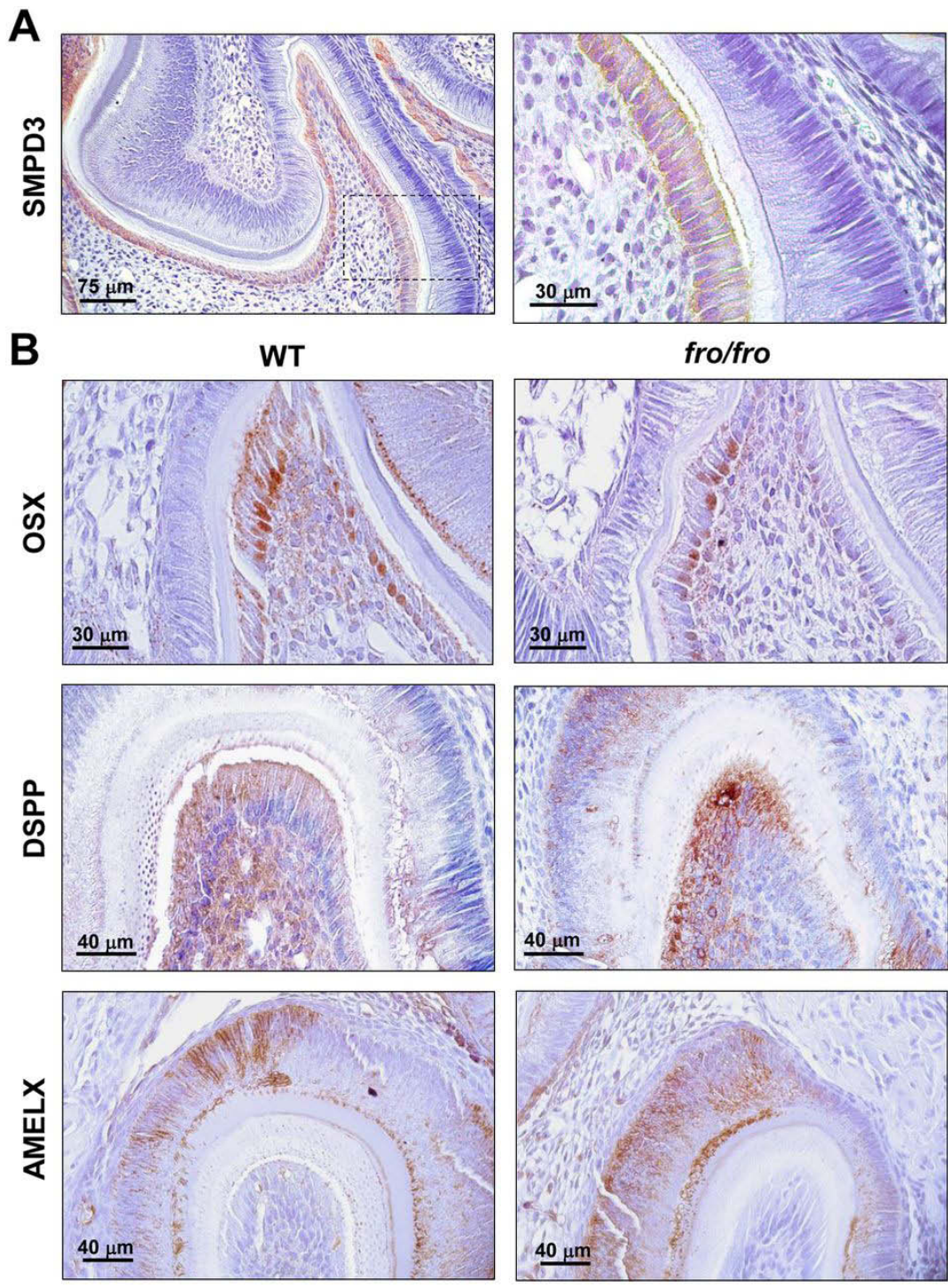


Figure 3.2: Localization of SMPD3, OSX, DSPP, and AMELX in tooth cells.

(A) Immunostaining of decalcified molars of 3-day-old WT mice with anti-SMPD3 antibody, showing the localization of this enzyme in odontoblasts only. The area indicated by the box on the left panel is magnified in the panel to the right. (B) Immunostaining of decalcified molars of 3-day-old WT and *fro/fro* mice with anti-OSX (top panels) and anti-DSPP (middle panel) antibody shows comparable expression (brown stain) of these odontogenic markers in both genotypes. Immunostaining of the tooth sections with anti-AMELX antibody (bottom panels) shows comparable amelogenin localization in ameloblasts (brown stain) in both genotypes, indicating that the differentiation of ameloblasts was not affected by the *fro* mutation.

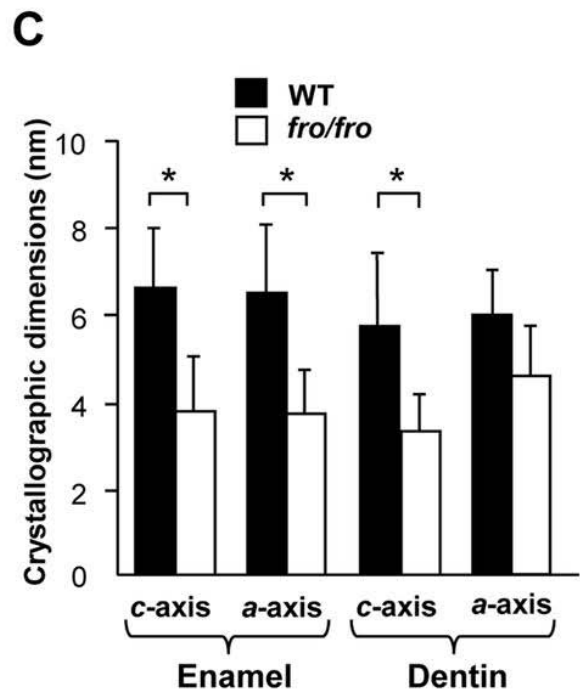
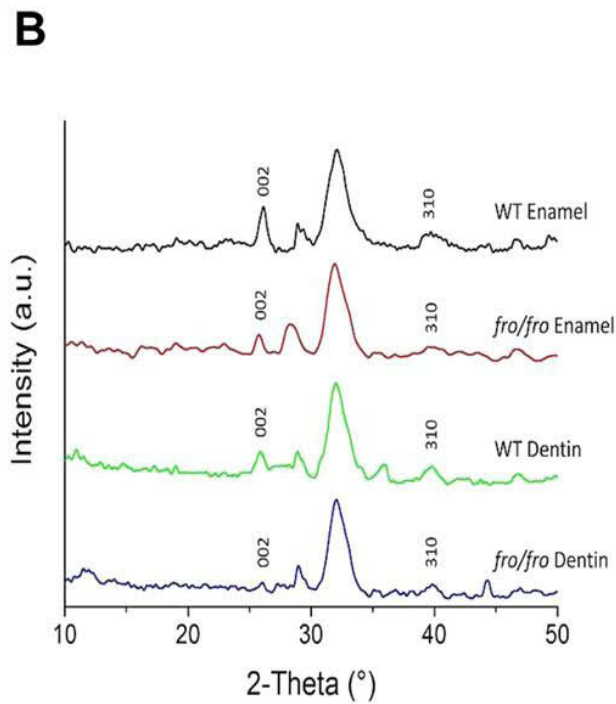
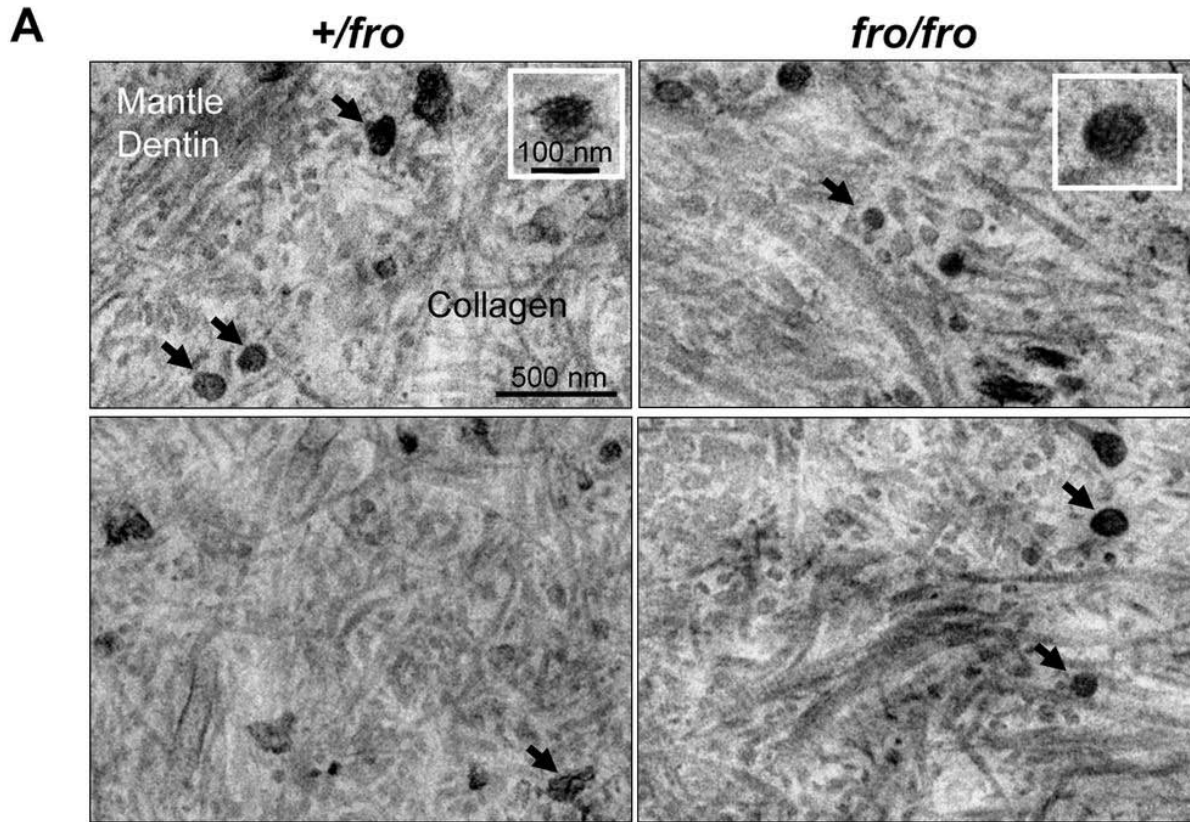


Figure 3.3: TEM and X-ray diffraction of 14-day-old molars.

(A) Ultrastructural features of mantle dentin in 14-day-old molars of *+/fro* and *fro/fro* mice. In both genotypes, abundant matrix vesicles (arrows) with electron-dense deposits were found throughout the collagenous matrix, with some containing mineral crystals (insets). (B) XRD spectra of enamel and dentin in WT and *fro/fro* mice demonstrated differences in height and width of the (002) and (310) Bragg peaks, indicating different crystallographic dimensions. (C) Bar graphs illustrating crystallographic dimensions along the *c*-axis and the *a*-axis of enamel and dentin crystals in WT and *fro/fro* mice, with crystals generally being smaller in the mineralized dental tissues of the *fro/fro* mice, as anticipated from the delayed development and delayed mineralization of these teeth ($*p < 0.05$).

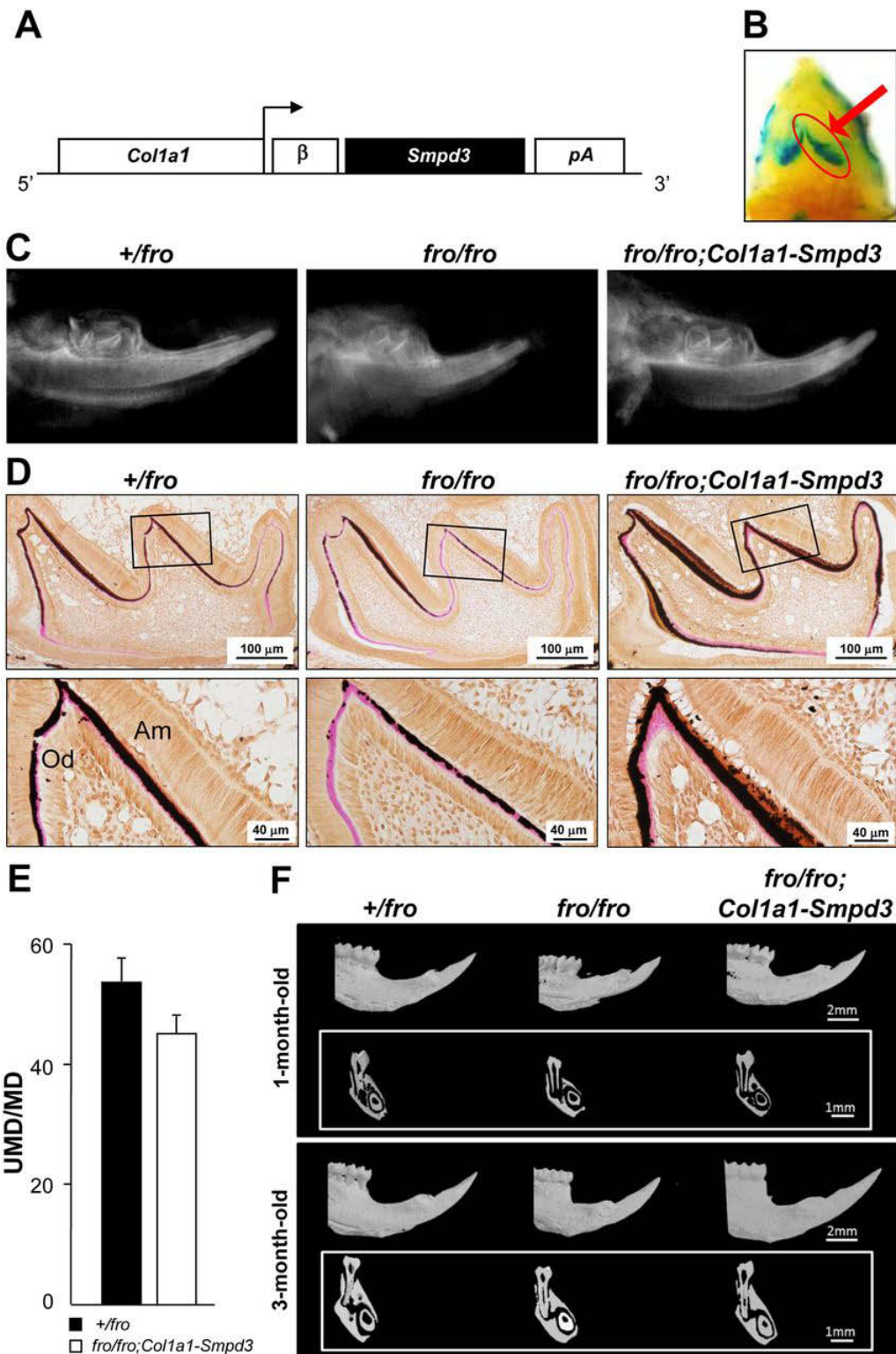


Figure 3.4: Correction of the fro tooth phenotype in *fro/fro;Colla1-Smpd3* transgenic mice.

(A) Schematic representation of the *Colla1-Smpd3* transgene construct. (B) X-Gal staining (blue) of a newborn *Colla1-LacZ* mouse showing the activity of the 2.3-kb *Colla1* promoter driving bacterial β -galactosidase (*lacZ*) expression in the incisor and mandibular bone (red arrow). (C) X-rays of mandibles from 3-day-old *fro/fro* mice, showing smaller, poorly mineralized alveolar bone and teeth in comparison with the *+/fro* mandibles. These abnormalities are not present in *fro/fro;Colla1-Smpd3* mandibles. (D) von Kossa and van Gieson staining of molars from 3-day-old *+/fro*, *fro /fro*, and *fro/fro;Colla1-Smpd3* mice. Note the correction of the *fro* mutation phenotype in the *fro/fro;Colla1-Smpd3* molars, which confirms the radiographic findings. For each panel, a magnified view of the indicated area (black box) is shown below. (E) Histomorphometric quantification shows a comparable UMD/MD in the molars of 3-day-old *+/fro* and *fro/fro;Colla1-Smpd3* mice (n = 3 for each genotype). (F) Micro-CT analysis shows that the incisors are smaller in 1-month-old *fro/fro* mice in comparison with those in *+/fro* mice. This difference became marginal when samples from both genotypes were compared at 3 months of age. At both time-points, *fro/fro;Colla1-Smpd3* incisors were comparable with those of *+/fro* mice. Insets: cross-sectional view through the first molar of respective mandibles.

Chapter 4: Sphingomyelin Phosphodiesterase 3 and Phosphatase, Orphan 1

Acts in a Relay to Promote Bone Mineralization

**Sphingomyelin Phosphodiesterase 3 and Phosphatase, Orphan 1 Acts in a Relay to
Promote Bone Mineralization**

Zohreh Khavandgar¹, Christopher J. Clarke², Scott A. Summers³, Colin Farquharson⁴, José Luis Millán⁵ and Monzur Murshed^{1,6,7}

¹Faculty of Dentistry, McGill University, Montreal, QC H3A 1A4, Canada.

²Department of Medicine, Stony Brook University, Stony Brook, NY, United States.

³Program in Cardiovascular and Metabolic Disorders, Duke-National University of Singapore Graduate Medical School, Singapore.

⁴The Roslin Institute and Royal (Dick) School of Veterinary Studies, University of Edinburgh, Easter Bush, Roslin, Midlothian, Edinburgh, EH25 9RG, UK.

⁵Sanford Children's Health Research Center, Sanford-Burnham Medical Research Institute, La Jolla, CA, United States.

⁶Department of Medicine, McGill University, Montreal, Quebec, Canada.

⁷Shriners Hospital for Children, McGill University, Montreal, Quebec, Canada

Manuscript in Preparation

4.1 Abstract

Sphingomyelin phosphodiesterase 3 (SMPD3), an enzyme critical for mineralized hard tissue development, hydrolyzes sphingomyelin present in the cell membrane to generate ceramide, a bioactive lipid molecule, and phosphocholine, an essential nutrient. SMPD3-deficient *fro/fro* mice show a decrease of tissue ceramide levels. Ceramide level is also decreased upon the inactivation of the alternative *de novo* pathway of ceramide synthesis in dihydroceramide desaturase 1 -deficient (*Des1*^{-/-}) mice. However, we found that *Des1*^{-/-} mice do not show any bone mineralization defects. This observation raises the possibility that the other SMPD3 metabolite, phosphocholine, might play a role in bone mineralization. The deficiency of phosphatase, orphan 1 (PHOSPHO1), an intracellular enzyme that cleaves phosphocholine to generate free phosphate and choline, has been associated with poor bone and tooth mineralization. We found similar hypomineralized skeletal tissues in both *fro/fro* and *Phospho1*^{-/-} embryos. Our histological analyses of the bones of 4-week-old *fro/fro;Phospho1*^{-/-} compound homozygotes showed that the osteoid amount did not differ from that of control *fro/fro* bones, suggesting that SMPD3 and PHOSPHO1 might act through the same pathway. However, unlike in *fro/fro* mice, ceramide levels were not altered in *Phospho1*^{-/-} mice. Further, restoration of SMPD3 activity in *fro/fro* osteoblasts via a transgenic approach corrected the bone mineralization defects, while no such correction was observed when *Smpd3* was overexpressed in the osteoblasts of *Phospho1*^{-/-} mice. In the cells, apart from the sphingomyelinase pathway, phosphocholine can also be generated by cytosolic choline kinases that can convert choline to phosphocholine. Based on this finding, we fed both *fro/fro* and *Phospho1*^{-/-} mice a 2%-choline diet. This choline-rich diet raised the serum choline levels and corrected the bone mineralization defects in *fro/fro* mice, but not in *Phospho1*^{-/-} mice. Taken together, our data suggest that

SMPD3 acts upstream of PHOSPHO1 and confirms the importance of choline metabolism in hard tissue mineralization.

4.2 Introduction

Mineralization of the hard tissue extracellular matrix (ECM) is a salient feature of vertebrate organisms that has unique evolutionary and biological roles. The importance of ECM mineralization in the skeletal tissues has already been demonstrated by several classic genetic mutations that affect this process and cause life-threatening diseases such as hypophosphatasia, rickets and some forms of osteogenesis imperfecta [26, 48, 80, 143, 144]. The study of these mutations in human patients and genetically modified animal models provided unique opportunities to understand the complex mechanisms underlying hard tissue mineralization.

According to a well-accepted model explaining ECM mineralization, two mineral species – inorganic phosphate (P_i) and ionic calcium, when present at physiologic concentrations, will promote hydroxyapatite [$Ca_{10}(PO_4)_6(OH)_2$] crystal growth within and between newly synthesized collagen fibrils in the skeletal ECM [24]. It has also been shown that inorganic pyrophosphate (PP_i) and polyphosphates, chemical derivatives of P_i , can inhibit the mineralization process [28, 29]. Additionally, proteins belonging to the SIBLING family such as osteopontin has been suggested to play a direct role in the regulation of ECM mineralization [167].

Although the above model explains the progression of ECM mineralization in the extracellular space, it does not address the mechanism of initiation of this process per se. A growing body of experimental evidences suggests that the initiation of ECM mineralization may occur inside the protected environment of the matrix vesicles (MVs), which are lipid bilayer-enclosed vesicular bodies that are released by the cells in the mineralizing tissues [137, 139, 142, 168]. The breakdown of the MVs releases the calcium phosphate crystals in the ECM. These calcium phosphate crystals are deposited on and around the fibrillar collagen serving as nidi for the initiation of ECM mineralization [133].

The recently characterized recessive mutation *fragilitas ossium (fro)* , in the murine *Smpd3* gene identifies sphingolipid metabolism as a novel effector of ECM mineralization in the skeletal tissues [83, 95]. In the MVs obtained from growth plate chondrocytes, it was shown that the amount of sphingomyelin is higher in the MVs in comparison to chondrocytes from which they were prepared from [141]. Sphingomyelin is also one of the lipids most rapidly degraded when MVs are incubated in synthetic cartilage lymph and allowed to mineralize [142]. Taken together, these findings suggest that a possible mechanism explaining MV-mediated ECM mineralization may involve the cleavage of sphingomyelin present in the MV membrane by a sphingomyelinase. Because of its high level expression in the mineralizing tissues and its presence in the MVs, SMPD3 is the sphingomyelinase that is most likely to fit to this role [169].

SMPD3 cleaves sphingomyelin in the cell membrane and generates phosphocholine and ceramide [88, 89]. These two bioactive metabolites in turn affect a variety of cellular activities including proliferation, differentiation, apoptosis and energy metabolism [96, 149, 150, 170]. In a previous study, we examined endochondral ossification in E15.5 *fro/fro* embryos and observed impaired apoptosis of hypertrophic chondrocytes and severely undermineralized cortical bones in the developing skeleton [95]. Following transgenic approaches, we showed that local SMPD3 activity in osteoblasts is necessary for a normal bone mineralization [95]. Taken together, our published data clearly demonstrated the importance of SMPD3-mediated sphingolipid metabolism in the mineralization of the developing skeletal tissues.

Both ceramides and phosphocholine can be generated by multiple metabolic pathways. The various species of ceramides in the cells are mainly generated by two different mechanisms- the *de novo* and the sphingomyelinase pathway [89, 171, 172]. In the *de novo* pathway, dihydroceramide desaturase 1 (DES1) is the final enzyme that converts dihydroceramide to ceramide. In the sphingomyelinase pathway, sphingomyelinases are the sole family of enzymes

which cleave sphingomyelin to generate ceramide and phosphocholine. Phosphocholine can also be generated from dietary choline by two isoforms of choline kinases [173]. Phosphocholine can then be cleaved by PHOSPHO1, an intracellular phosphatase [132]. Our data showed that PHOSPHO1-deficient mice have similar bone mineralization defects as seen in *fro/fro* mice. The phenotypic similarities between these two mutant strains further suggest that phosphocholine metabolism may directly regulate ECM mineralization in the skeletal tissues.

The goal of the current paper was to identify which SMPD3 metabolite has a role in bone mineralization. Toward this goal, we performed X-ray and histology/histomorphometric analyses of *Des1*^{-/-} mice showing impaired ceramide synthesis and demonstrated that despite a decrease in ceramide level, these mice do not show any bone mineralization defects. We also showed that while the solitary loss of PHOSPHO1 or SMPD3 activity causes similar bone mineralization defects, the loss of both of these enzymes in a compound mutant did not result in an additive increase of the osteoid volume. Interestingly, there was no reduction of ceramide levels in *Phospho1*^{-/-} limbs. Taken together, this study suggests that SMPD3 and PHOSPHO1 works in concert to regulate bone mineralization, and phosphocholine metabolism may play a critical role in this process.

4.3 Results

4.3.1 Normal bone mineralization in *Des1*^{-/-} mice

In order to examine the involvement of ceramide in bone mineralization, we examined the skeletal phenotype of mice lacking DES1, an enzyme that generates ceramide from dihydroxyceramide via the *de novo* pathway of ceramide synthesis (Fig. 4.1 A). It has been demonstrated that ceramide levels are reduced in these mice [174]. We first examined the bones of one-month-old *Des1*^{-/-} mice by X-ray. As shown in Fig. 4.1 B, both tibia and femora appear to be normal in *Des1*^{-/-} mice. In order to examine the mineralization status of the trabecular bones, we next prepared thin plastic sections of the vertebral bones (L3 and L4) and stained with von Kossa and van Gieson. There was no bone mineralization defect as shown by the absence of increased unmineralized collagen (osteoid) in *Des1*^{-/-} vertebra sections (Fig. 4.1 C).

4.3.2 Bone and cartilage abnormalities in *fro/fro*, *Phospho1*^{-/-} and compound mutant mice

We next investigated whether SMPD3 and PHOSPHO1 work in the same pathway to regulate ECM mineralization. We first analyzed the skeletal phenotype of E15.5 and E18.5 *fro/fro*, *Phospho1*^{-/-} and *fro/fro;Phospho1*^{-/-} embryos. Von Kossa-van Gieson (upper panel) and von Kossa-Alcian blue (lower panel) staining showed very similar phenotypic abnormalities in single and compound mutants. Both SMPD3 and PHOSHO1 deficiencies resulted in poor mineralization of the developing bone collars and the cartilage matrix secreted by the hypertrophic chondrocytes (Fig. 4.2 A). As reported by us before, we also observed an accumulation of hypertrophic chondrocyte-like cells in the mid-shaft region of the humeri in all three mutant models, but not in the WT control. We next examined the bone mineralization status of one-month-old *fro/fro*, *Phospho1*^{-/-} and *fro/fro;Phospho1*^{-/-} mice by histology. Von

Kossa and van Gieson staining showed a comparable increase of osteoid volume/bone volume (OV/BV) in *fro/fro* and *Phospho1*^{-/-} mice. Interestingly, we did not observe any additive increase of osteoid volume in *fro/fro;Phospho1*^{-/-} compound bones (Fig. 4.2 B).

4.3.3 Sphingolipids and ceramide measurements in the *fro/fro* and *Phospho1*^{-/-} embryos

We next investigated whether there is any alteration of sphingolipid metabolism in the developing *Phospho1*^{-/-} skeleton. Using tandem liquid chromatography/mass spectrometry we measured sphingosine, dihydrosphingosine, sphingosine-1 phosphate, dihydrosphingosine-1 phosphate and ceramide levels in the developing proximal and distal skeletons of E16.5 WT, *fro/fro* and *Phospho1*^{-/-} embryos. We detected a significant decrease of sphingosine levels in the skeletal tissue extracts prepared from both *fro/fro* and *Phospho1*^{-/-} embryos (Fig. 4.3 A). No significant alterations were observed in dihydrosphingosine, sphingosine-1 phosphate and dihydrosphingosine-1 phosphate levels (Fig. 4.3 B-D). Interestingly, despite a significant decrease of skeleton and brain ceramide levels in *fro/fro* mice, we did not observe any significant changes of ceramide levels in any of these tissue in *Phospho1*^{-/-} (Fig. 4.3 E-H).

4.3.4 Osteoblast-specific expression of *Smpd3* in *Phospho1*^{-/-} mice does not rescue the mineralization defect

Previously, using a transgenic approach, we showed that over-expression of *Smpd3* specifically in the osteoblasts of *fro/fro* mice rescues the bone mineralization defects. For this experiment, we generated a *Colla1-Smpd3* transgene construct using a 2.3 kb *Colla1* promoter fragment, earlier shown to be specifically expressed in osteoblasts [95]. We used the same transgenic line to generate *Phospho1*^{-/-};*Colla1-Smpd3* mice. Von Kossa and van Gieson staining of the humeri of 15.5 day-old *phospho1*^{-/-};*Colla1-Smpd3* embryos showed

unmineralized bone and cartilage matrix similar to that of *Phospho1*^{-/-} embryos (Fig. 4.4 A). We also measured osteoid volume in one-month-old *Phospho1*^{-/-};*Colla1-Smpd3* mice. In agreement with the data obtained from the analyses of the embryos, we did not observe any significant difference in the OV/BV in adult *Phospho1*^{-/-} and *Phospho1*^{-/-};*Colla1-Smpd3* mice (Fig. 4.4 B).

4.3.5 High choline diet corrects the bone mineralization defects in fro/fro mice

2%-choline diet has been shown to raise the tissue choline and phosphocholine levels in experimental models [130, 131]. Based on these studies, we next examined whether this diet can correct the bone mineralization defects in *fro/fro* mice. We fed 1-month-old *fro/fro* mice with a high-choline or normal diet for 6 weeks. This diet increased the serum choline levels (Fig 4.5 A). Interestingly, there was a mild but significant increase of bone volume/tissue volume (BV/TV), trabecular thickness and mineral apposition rates in the mice on the high-choline diet (Fig 4.5 B-D). As shown in Fig 4.5 E and F, there was a remarkable reduction of OV/BV in *fro/fro* mice that were fed the 2%-choline diet in comparison to those fed the regular diet. On the other hand, there was no change in OV/BV in *Phospho1*^{-/-} mice that were on the same 2%-choline diet (Fig 4.5 G and H).

4.4 Discussion

Mouse models for hard tissue mineralization defects are proven invaluable tools to study the mechanisms of ECM mineralization in vertebrates. The reported *fro* mutation in the murine *Smpd3* gene and its association with poor hard tissue mineralization have provided a unique opportunity to extend our understanding of ECM mineralization further [83, 125]. The *fro/fro* mouse is particularly interesting as the mineralization defects seen in this model does not affect the known regulators of ECM mineralization [95].

Although the cell autonomous role of SMPD3 in hard tissue mineralization is now well-established, it is not clear how ceramide and/or phosphocholine, two byproducts of the SMPD3-catalyzed reaction might affect this process. Our data presented here indicate that of these two products, ceramide may not be involved in bone mineralization. The primary indication of this inference came from our observation that *Des1*^{-/-} mice that show a reduction of tissue ceramide levels [174], do not show any bone mineralization defect or skeletal deformities. On the other hand, mice lacking PHOSPHO1, a phosphatase that cleaves phosphocholine, show a strikingly similar skeletal phenotype to that of *fro/fro* mice [83, 95, 134]. As is the case in *fro/fro* embryos, *Phospho1*^{-/-} embryos show poor bone mineralization. Interestingly, these mineralization defects are present without any apparent alteration of the ceramide levels in *Phospho1*^{-/-} skeletal tissues.

Until now, although there is no experimental evidence that suggests a role for ceramide in bone mineralization, the reported decrease in apoptosis in the late-stage chondrocytes in *fro/fro* mice might be caused by ceramide deficiency [95]. In fact, in several studies ceramide has been suggested to be involved in apoptosis in multiple cell types [96, 102, 170, 175]. A recent study suggested SMPD3 present in the membrane of the endoplasmic reticulum (ER) induce apoptosis via ER-mitochondria membrane swapping resulting in the release of cytochrome C from the mitochondria [98]. Interestingly, as is the case in *fro/fro* embryos, the long bones of *Phospho1*^{-/-}

embryos also show an abnormal presence of hypertrophic chondrocyte-like cells in the mid-shaft region. Our finding that ceramide levels are not reduced in *Phospho1*^{-/-} mice, raises the possibility that the altered phosphocholine levels might cause the abnormal chondrocyte phenotype in these mice. In support of this notion, we recently showed that the loss of choline kinase β , a cytosolic enzyme that converts choline to phosphocholine, show similar abnormal presence of hypertrophic chondrocyte-like cells in the developing *Chkb*^{-/-} long bones [176]. However, further work will be needed to establish whether proliferation or apoptosis of hypertrophic chondrocytes is affected in *Phospho1*^{-/-} and *Chkb*^{-/-} mice.

SMPD3 is attached to the inner leaflet of the cell membrane [177], while PHOSPHO1 is localized in the cytosol [178]. The presence of these two enzymes in the same cellular compartment and their involvement in phosphocholine metabolism suggest that their activities might be directly linked. Furthermore, the common metabolic pathway involving these two enzymes indicates that SMPD3 acts upstream of PHOSPHO1. Several lines of experiments presented in this study support this possibility. Firstly, we did not observe any additive effects of the combined SMPD3 and PHOSPHO1 mutation on OV/BV in *fro/fro;Phospho1*^{-/-} mice. Secondly, overexpression of *Smpd3* in the osteoblasts did not reduce OV/BV in *Phospho1*^{-/-}; *Colla1-Smpd3* mice. Finally, feeding a choline-rich diet that has been shown to increase tissue phosphocholine levels reduced the osteoid volume in *fro/fro* mice but not in *Phospho1*^{-/-} mice. Taken together, these findings provide strong indications that SMPD3 acts upstream of PHOSPHO1.

A critical question remains unanswered: How intracellular phosphocholine metabolism by SMPD3 and PHOSPHO1 can affect ECM mineralization, essentially an extracellular event. One possible answer to this question may come from the matrix vesicle theory of ECM mineralization. According to this theory the initiation of ECM mineralization may occur within

the protected environment of MVs [140, 168]. Wu *et al.* showed that extensive phospholipid degradation occurs in the mineralizing MVs with a concomitant increase of free fatty acids, indicative of the presence of phospholipase activity [142]. This study provided the early evidence that linked phospholipid metabolism to the initiation of mineralization. Phospholipase activity generates phosphocholine and phosphoethanolamine, which can be cleaved by PHOSPHO1 releasing free phosphate inside the MVs and promoting mineral nucleation. SMPD3 may cleave sphingomyelin present in the MV membrane to generate additional phosphocholine to further facilitate this process [178]. This later possibility is supported by the observation that both PHOSPHO1 and SMPD3 are present in MV preparations [133, 142].

Our data demonstrates that SMPD3 is a critical regulator of ECM mineralization. The proposed mechanism of SMPD3 action extends the existing model of ECM mineralization in which both SMPD3 and PHOSPHO1 work in concert to initiate this process (Fig 4.6). Once initiated the progression of ECM mineralization is regulated by the extracellular levels of P_i , ionic calcium and mineralization inhibitors, and the synthesis of the mineral scaffolding proteins. This work has important tissue engineering aspects as modulation of SMPD3 and PHOSPHO1 activities may promote faster initiation of mineralization in bone grafts and help better healing of fractured bones. Additionally, it may provide clues to the yet unknown mechanism(s) underlying several idiopathic bone mineralization disorders.

4.5 Materials and Methods

4.5.1 Mice

The *fro/fro* mice were obtained from Dr. Christophe Poirier [83]. The *Phospho1*^{-/-} and *Dec1*^{-/-} mice were provided by Drs. José Luis Millán [136] and Scott A. Summers [171] respectively. Generation of transgenic mice were previously described [95]. The *fro/fro* and *Phospho1*^{-/-} mice had free access to either a standard diet (0.2% CC) containing choline chloride 2.0 (g/kg) Protein 17.7 (% by weight) Carbohydrate 65 (% by weight) Fat 5.0 (% by weight) or choline supplemented Diet (2% CC) containing choline chloride 20.0 (g/kg) Protein 17.7 (% by weight) Carbohydrate 63.2 (% by weight) Fat 5.0 (% by weight) (TD.03119, Harlan Teklad Premier Laboratory Diets). All mice were maintained in a pathogen-free standard animal facility and the experimental procedures were performed following an Animal Use Protocol approved by the Animal Care Committee of McGill University.

4.5.2 Histologic analysis

Vertebrae from one-month-old were fixed overnight in 4% PFA/PBS, embedded in methyl methacrylate, sectioned (7 µm thickness), and von Kossa and van Gieson staining was applied. Unmineralized bone sections were analyzed using Osteomeasure software (Osteometrics Inc.). Mouse embryos were fixed in 4% PFA/PBS overnight and embedded in paraffin. 5-µm-thick sections were submitted to von Kossa, Alcian Blue and van Gieson staining. Images were taken using a light microscope (model DM200; Leica) using an Olympus DP 72 camera, acquired with DP2-BSW software XV3.0 (Diagnostic Instruments), and processed using Adobe Photoshop[®].

4.5.3 Lipid measurements

Limbs and brains were snap frozen in liquid nitrogen and crushed prior to further homogenization in 20 mM Tris buffer containing protease inhibitors utilizing an auto homogenizer. Brain tissue was homogenized directly in the same buffer. Aliquots of homogenate were removed for estimation of protein concentration by the Bradford assay. For lipid analysis by mass spectrometry, following homogenization, lysate containing 200 µg-1 mg protein was analyzed for sphingosine, sphingosine 1 phosphate, dihydrosphingosine, dihydrosphingosine 1 phosphate and ceramide levels by tandem LC/MS mass spectrometry as described [157]. Lipid levels were normalized to cellular protein.

4.6 Data analysis

All results are shown as means of the standard deviation. Statistical analyses were performed by Student's *t* test or one way ANOVA, with $P < 0.05$ considered significant as indicated by a single asterisk and $P < 0.005$ by double asterisks. Bonferroni correction was performed whenever more than two groups were compared.

4.7 Acknowledgements

This work was supported by Operating Grant 216548 from the Canadian Institutes of Health Research and a Seed Grant from the Osteogenesis Imperfecta Foundation to MM. ZK receives a stipend from the Canadian Institutes of Health Research and MM receives salary support from the Fonds de la recherche en *Santé* du Québec (FRSQ, Grant 16302).

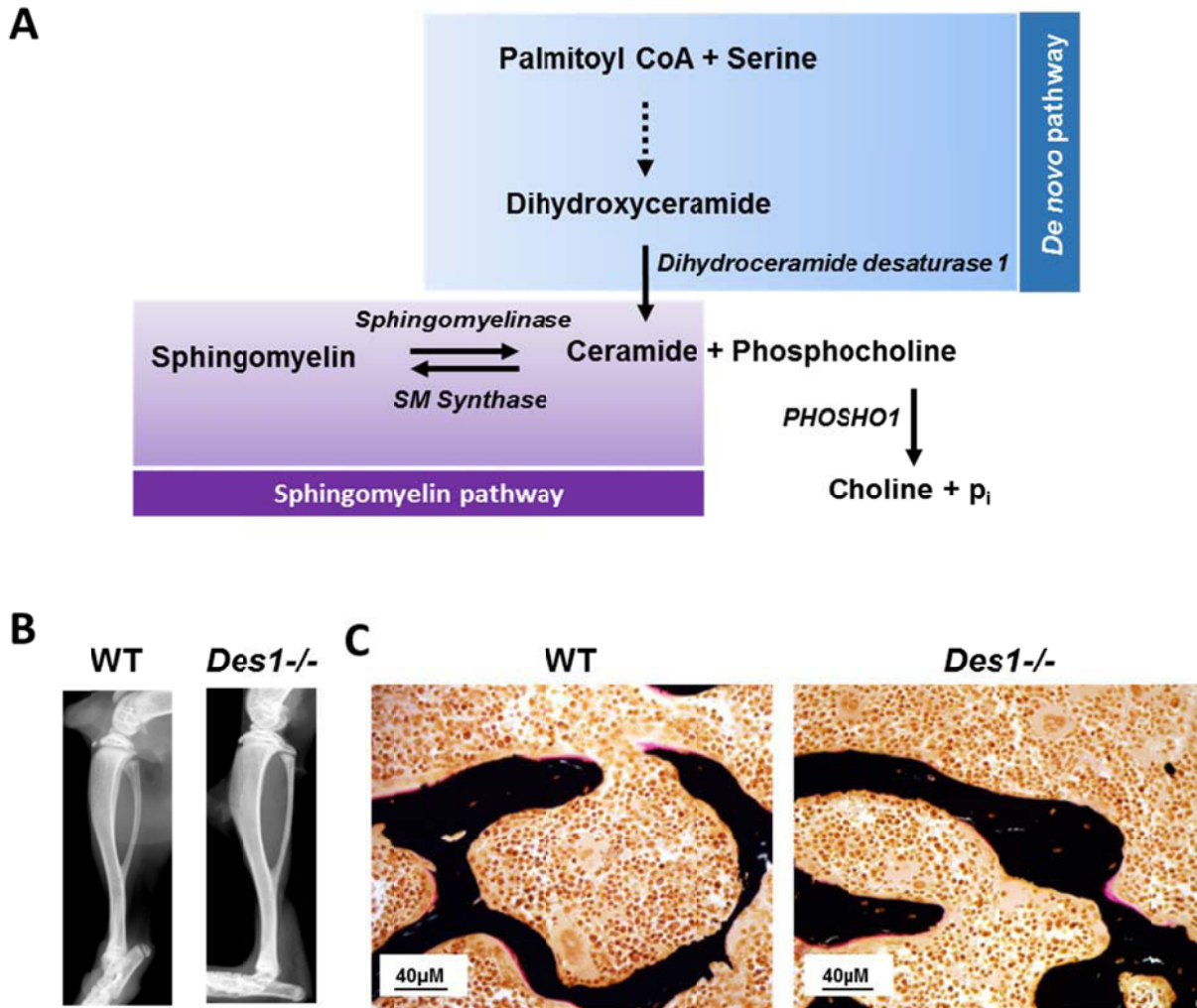


Figure 4.1: Ceramide biosynthesis by SMPD3 and DES1 and the skeletal analyses of *Des1*-deficient mice.

(A) Schematic diagram showing the *de novo* and sphingomyelinase pathways for the synthesis of ceramide. (B) Radiographic analysis shows no limb abnormalities in *Des1*^{-/-} mice. (C) Von Kossa and van Gieson staining of vertebral sections demonstrate a normal bone mineralization in *Des1*^{-/-} mice.

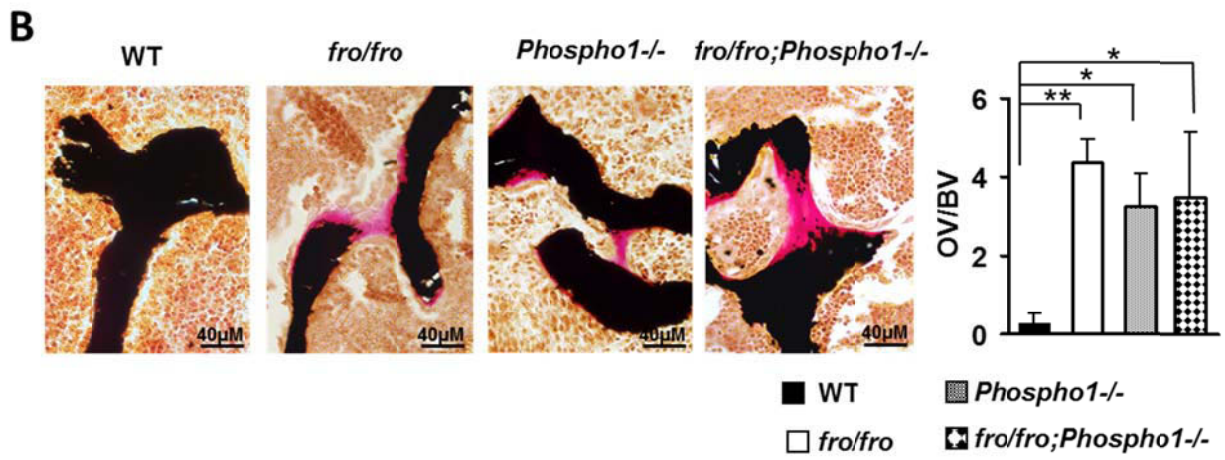
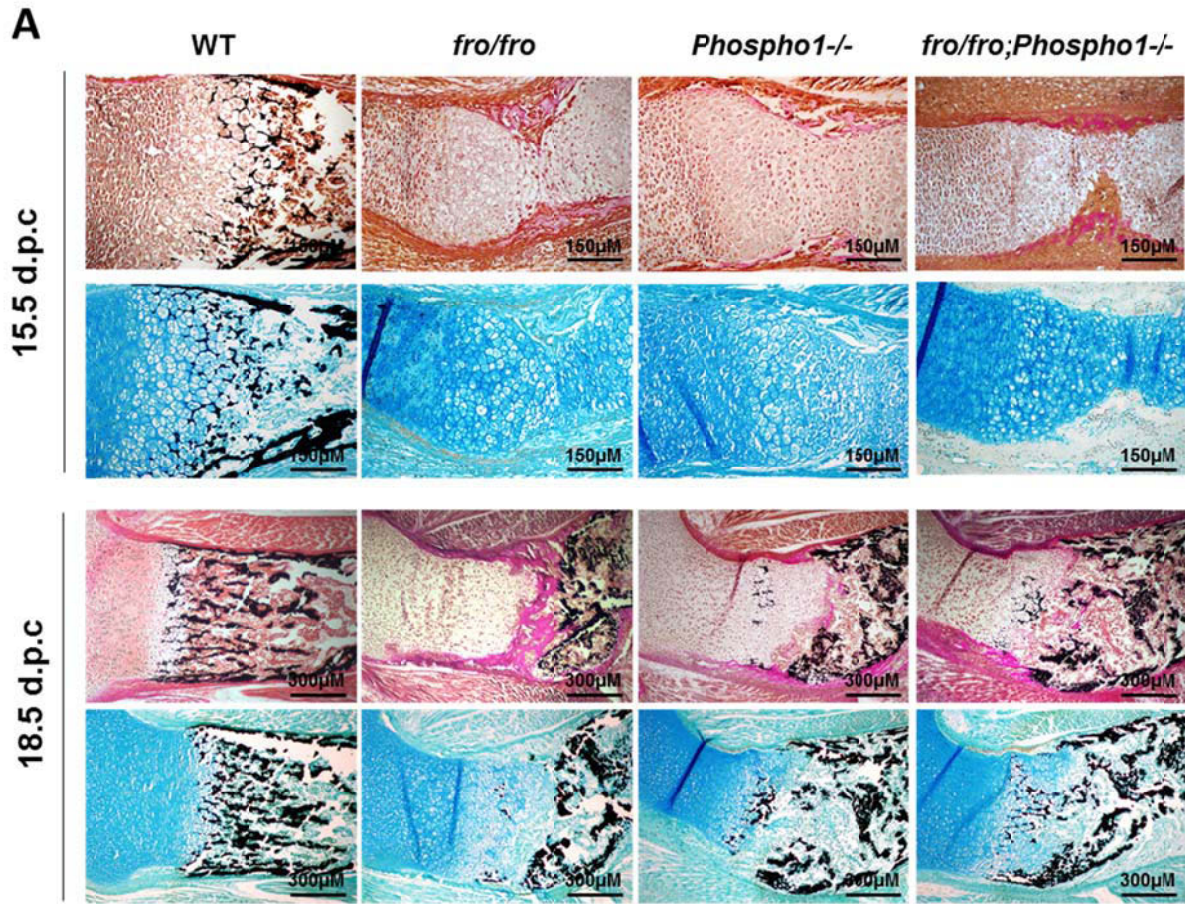


Figure 4.2: Bone and cartilage abnormalities in *fro/fro*, *Phospho1*^{-/-} and *fro/fro*;*Phospho1*^{-/-} compound mutant mice.

(A) Von Kossa-van Gieson (upper panel) and von Kossa-Alcian blue (lower panel) staining of humeri of 15.5 and 18.5 day-old embryos. Note a similar unmineralized cortical bone in *fro/fro* mice which is similar to *Phospho1*^{-/-} and *fro/fro*;*Phospho1*^{-/-} mice. **(B)** Von Kossa and van Gieson staining of vertebral bones of 1-month-old *fro/fro*, *Phospho1*^{-/-} and *fro/fro*;*Phospho1*^{-/-} mice littermates demonstrating increased OV/BV in comparison to their WT littermates. No additional increase of OV/BV was observed in the compound mutants.

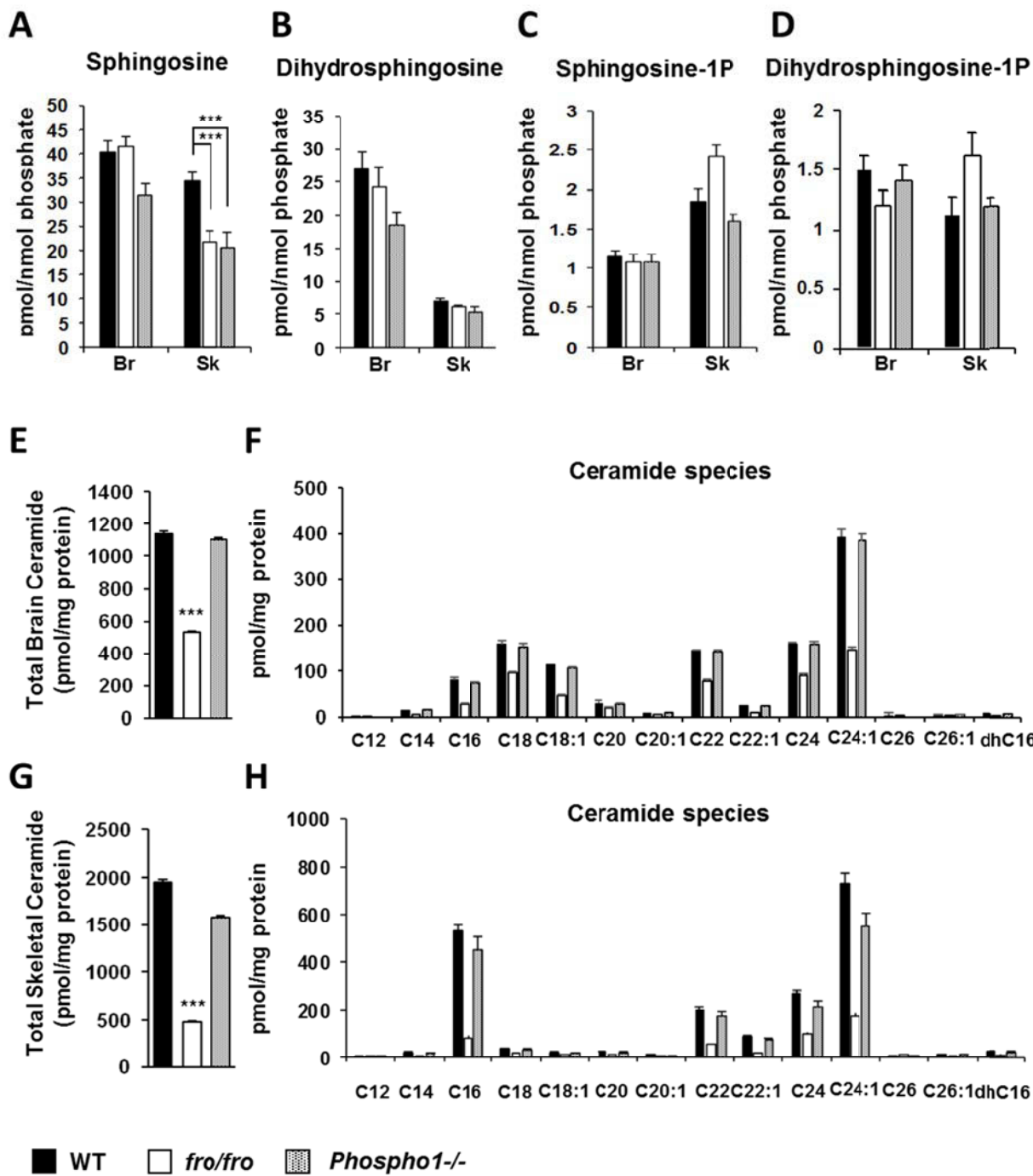


Figure 4.3: Phospholipid and ceramide measurements in the E17.5 WT, *fro/fro* and *Phospho1*^{-/-} embryos.

(A) Lipid analysis using liquid chromatography/mass spectrometry shows sphingosine level is decreased in the proximal and distal skeleton (Sk), but not in brain (Br) of the *fro/fro* and *Phospho1*^{-/-} mice. **(B-D)** Dihydrosphingosin, sphingosine-1P and dihydrosphingosine-1P levels are not significantly changed in the brain (Br) and skeletons (Sk) of *fro/fro* and *Phospho1*^{-/-} mice. **(E and F)** The levels of total ceramide and individual ceramide species with different chain lengths were significantly decreased in *fro/fro*, but not in *Phospho1*^{-/-} brain tissues. **(G and H)** Similar results were obtained when the levels of total ceramide and individual ceramide species in the skeletal tissues were compared in these genotypes.

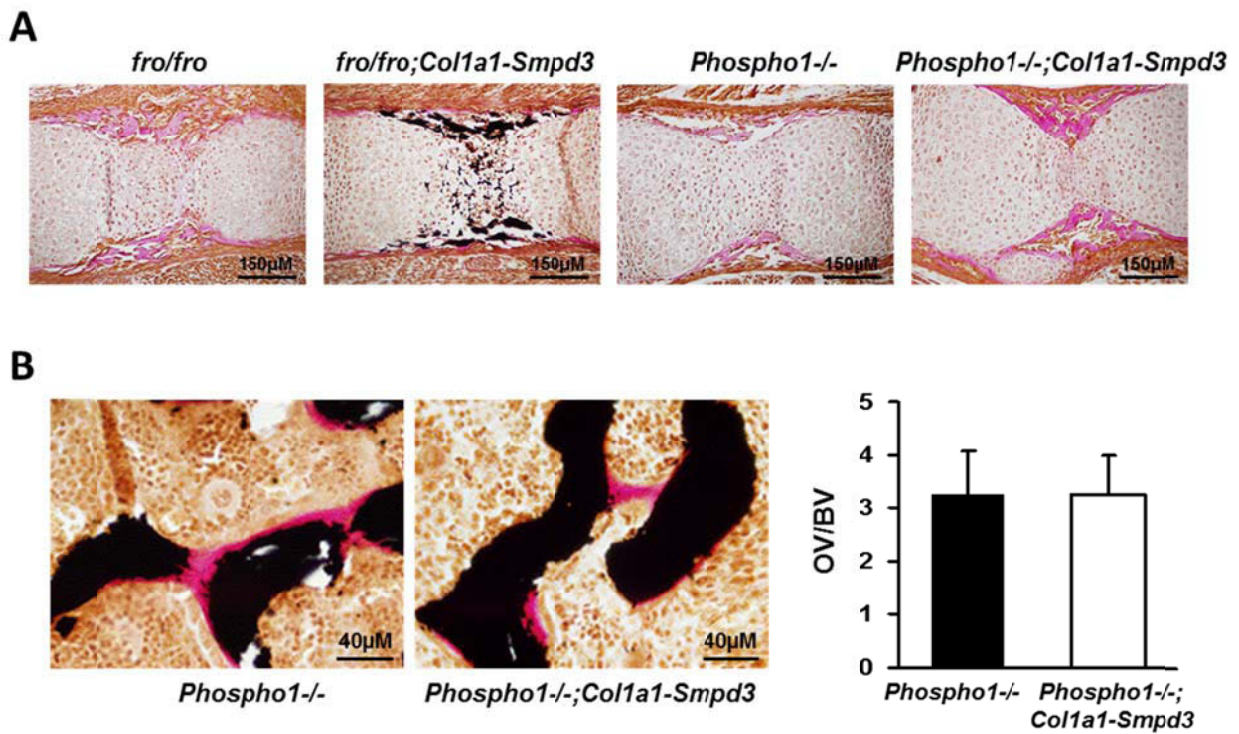


Figure 4.4: Analysis of *Phospho1-/-;Colla1-Smpd3* bones.

(A) Von Kossa and van Gieson staining of humeri sections from E15.5 *fro/fro;Colla1-Smpd3* and *Phospho1-/-;Colla1-Smpd3* mice demonstrate a rescue of the bone mineralization defects in the former but not in the later genotype. (B) Von Kossa and van Gieson staining of vertebral sections of 1-month-old *Phospho1-/-* and *Phospho1-/-;Colla1-Smpd3* mice show comparable osteoid volume over bone volume (OV/BV).

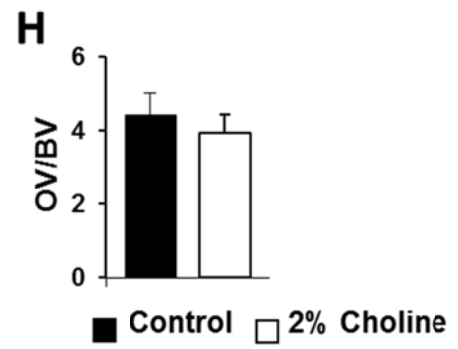
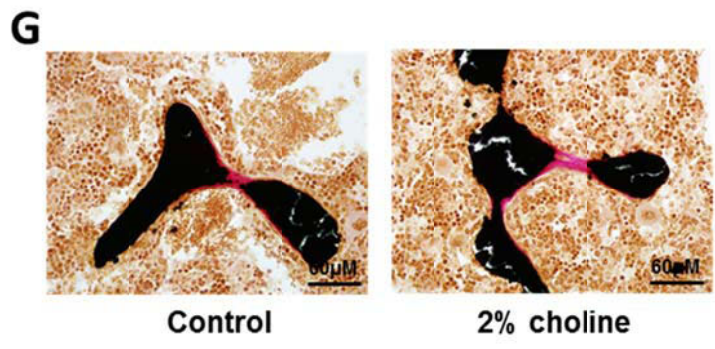
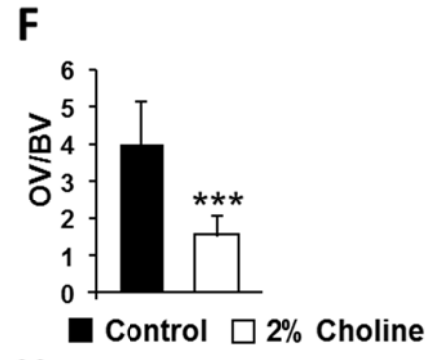
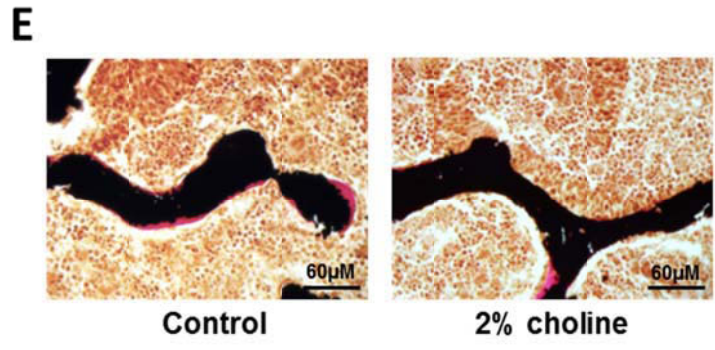
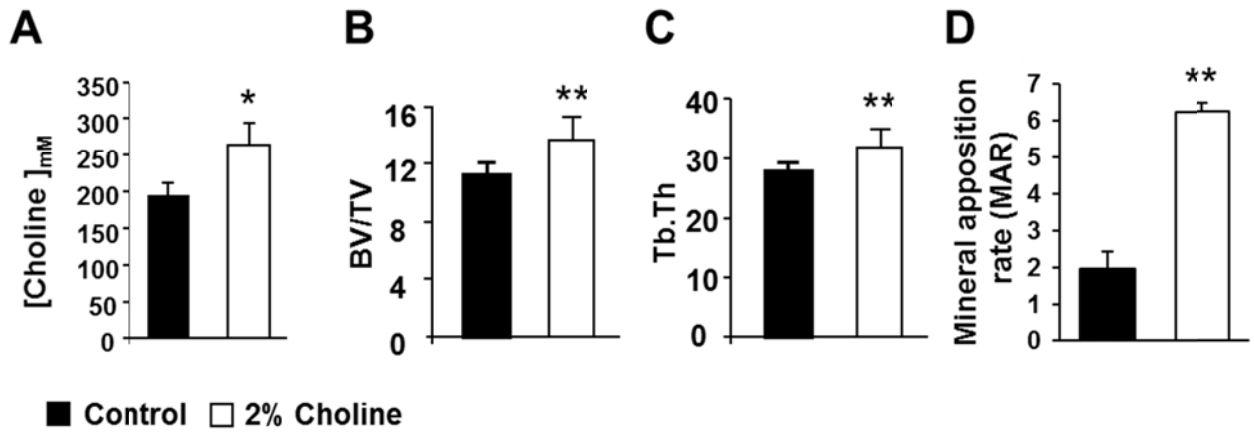


Figure 4.5: Effect of a 2%-choline diet on mineralization in *fro/fro* and *Phospho1*^{-/-} mice.

(A) 2%-choline diet significantly increased serum choline level in WT mice (B-D) 2%-choline diet increases bone volume (BV/TV), trabecular thickness (Tb.Th) and mineral apposition rate (MAR) in these mice. (E and F) *fro/fro* mice fed a 2%-choline diet for six weeks have significantly less unmineralized bone in comparison to *fro/fro* mice fed the normal diet as shown by von Kossa and van Gieson staining. (G and H) The choline-rich diet did not rescue the bone mineralization defects in *Phospho1*^{-/-} mice.

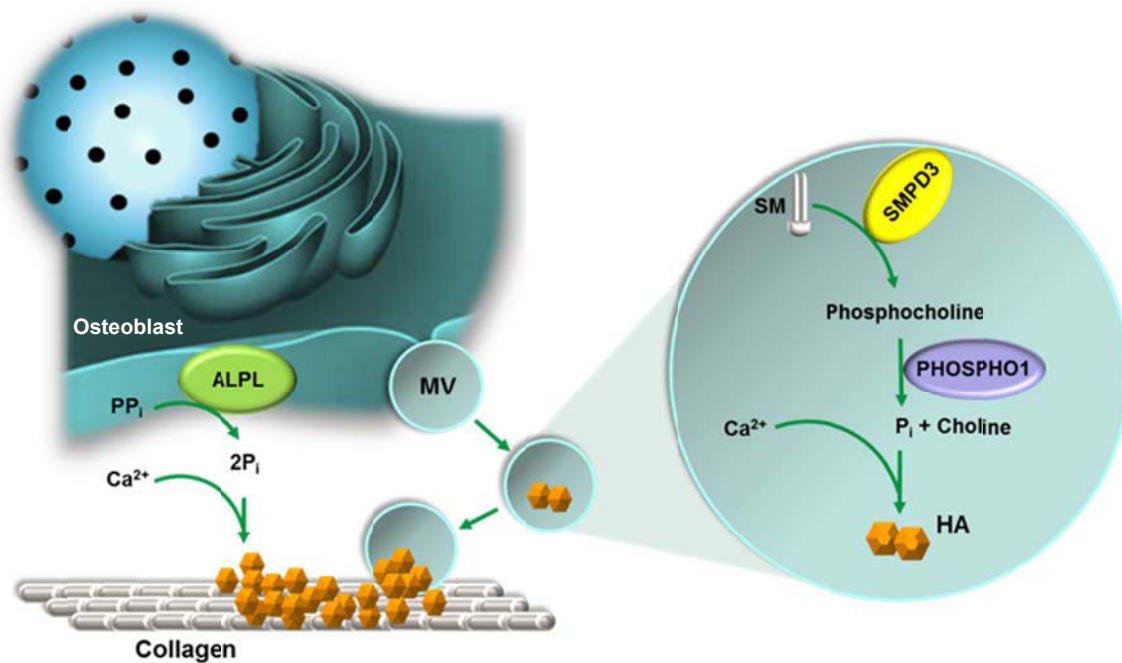


Figure 4.6: A model depicting ECM mineralization in bone.

Bone forming osteoblasts secrete a matrix rich in Type I collagen. Matrix vesicles (MVs) are released from osteoblasts which provide a microenvironment for the initial nucleation of hydroxyapatite (HA) crystals. Once the initial crystals grow in size the MVs are ruptured and minerals are unloaded into the ECM. The mineral crystals grow in size and coalesce with each other as extracellular inorganic phosphate (P_i) and calcium ions are deposited on them. Ectoenzyme alkaline phosphatase (ALPL) cleaves mineralization inhibitor pyrophosphate (PP_i) and other phospho-compounds (e.g. polyphosphates and phosphoproteins) and generates additional P_i in the mineralizing bone microenvironment. As an extension to the above mechanism, we propose that inside the MVs, SMPD3 cleaves sphingomyelin (SM) to generate phosphocholine, which is cleaved by PHOSPHO1 to increase the P_i levels, which in turn promotes the initial nucleation of HA crystals.

Chapter 5: General Discussion

5.1 General Discussion

ECM mineralization in vertebrates is a physiologic process primarily restricted to the skeletal and dental tissues. This unique feature provides evolutionary advantages including large body size, fast mobility and the ability to perform complex load-bearing tasks. Apart from its bio-mechanical roles, mineralized skeleton serves as a readily available reservoir for P_i and ionic calcium required for body's metabolic activities. Considering the importance of the pro-survival roles played by the mineralized tissues, it is not surprising that poor mineralization of the skeleton caused by various genetic mutations often lead to debilitating conditions.

For a long time, ECM mineralization in bones and teeth has been considered as a passive process [179]. However, recent studies involving human patients and mouse models have established that this process is highly regulated by genetic pathways in a spatiotemporal manner. Interestingly, although ECM mineralization is genetically regulated and primarily restricted to skeletal and dental tissues, so far no skeletal or dental tissue-specific gene has been identified as an initiator of this process. Instead, the available data suggest that the mineralization process is largely regulated by the unique co-expression of tissue non-specific genes in these hard tissues. For example, in bone and dentin, Type I collagen provides an essential protein scaffold that can trap the hydroxyapatite minerals [24]. However, *Colla1* and *Colla2*, the two genes encoding Type I collagen are expressed in a large number of tissues [180]. Similarly, ALPL is a key enzyme that is required for both dentin and bone mineralization and its expression is not restricted to the mineralizing hard tissues only [36]. In these tissues, ALPL liberates P_i from a variety of substrates including phosphoproteins, polyphosphates and PP_i . The cleavage of PP_i , a potent mineralization inhibitor, by ALPL and the generation of free P_i is essential to promote ECM mineralization [35].

The homeostasis of P_i and ionic calcium, two components of hydroxyapatite minerals, acts as a key regulator of ECM mineralization. Human metabolic diseases and mouse models that show impaired homeostasis of these components, inevitably leads to poor hard tissue mineralization hallmarked by an increase of unmineralized collagen in bone and dentin [48, 181]. It is therefore understandable that for a normal deposition of minerals on hard tissue, the formation rate of hydroxyapatite minerals needs to be matched by the rate of collagen synthesis. Failure to achieve this may result in a reduction of mineralized tissue mass. Indeed in a genetic model, it has been shown that reduced Type I collagen synthesis leads to lesser amount of mineralized bone formation [78]. Apart from the minerals and the mineral scaffolding matrix, the process of hard tissue mineralization is also regulated by the levels of mineralization inhibitors in the tissues, which is carefully regulated by multiple genetic factors [30, 31, 145, 146]. Mineralization inhibitors play the role of chaperones to prevent excessive mineral deposition in the hard tissues. However, their critical roles appear to lie in the soft tissues, where ectopic calcification can be detrimental.

The nucleation of hydroxyapatite minerals in the hard tissues might be initiated *de novo* at multiple foci and then progress rapidly to coalesce and form a continuous entity [182]. Although the mechanism underlying the progression of mineralization is relatively well-understood, the mechanism/factors regulating the initiation of mineralization is still not clear. One way to identify such factor(s) would be to study mouse models that show bone and tooth mineralization defects without any alterations in the already known factors that regulate the progression of ECM mineralization in the hard tissues. As outlined above, these factors include the levels of circulating/extracellular P_i and ionic calcium, mineral scaffolding collagen-rich matrix and the levels of known mineralization inhibitors. In the current thesis, I conducted

studies on *fro/fro* mice, which show poor bone and tooth mineralization without any alterations in factors mentioned above.

The role of SMPD3 as a regulator of skeletal development was first demonstrated by Stoffel *et al.* who reported a gene targeted model of *Smpd3* (*Smpd3*^{-/-} mice) [125]. Although these mice show skeletal deformities, no mineralization defects in the hard tissues were reported. Almost at the same time, the mutation in *fro/fro* mice was reported that showed a deletion of 1,758 bp in the *Smpd3* locus resulting in an inactive enzyme [83]. This later study reported hard tissue mineralization defects in *fro/fro* mice. The discrepancies in the reported phenotype of *Smpd3*^{-/-} and *fro/fro* mice might be caused by the methods used in the analyses of their mineralization phenotype. For example, the skeletal phenotype in *Smpd3*^{-/-} mice was examined by X-ray analysis, while the histological techniques were used to study the bone and tooth mineralization status in *fro/fro* mice. SMPD3, a cell-/ER membrane-bound enzyme cleaves sphingomyelin to generate ceramides and phosphocholine. At present it is not clear whether ceramide or phosphocholine or both of these products generated from the SMPD3-catalyzed reaction are involved in bone mineralization.

In the first manuscript, I addressed several key questions related to SMPD3 biology. I first wanted to investigate the cause of the limb deformities in *fro/fro* mice. I examined the limbs of *fro/fro* embryos at E15.5 and observed poorly mineralized cortical bones which lead to their deformities. Additionally, for the first time, I reported an abnormal presence of hypertrophic chondrocyte-like cells in the mid-shaft region of the long bones. I demonstrated that the apoptosis process of the matured chondrocytes was affected in *fro/fro* mice. These data suggested that both poorly mineralized cortical bones and the abnormal presence of the hypertrophic chondrocytes delay the normal trabecular bone formation resulting in the limb deformities seen in *fro/fro* mice.

Next, I examined the effects of the *fro* mutation on the membrane localization of SMPD3. In a cell culture experiment, I demonstrated that the mutated SMPD3 was localized to the cell membrane in a comparable manner to that of the native protein. However, as reported by Aubin *et al.* the mutated protein did not show any enzymatic activity [83]. This finding confirmed the requirement of the C-terminal end of SMPD3 for its functional properties.

The most critical experiment described in my first manuscript was the *in vivo* rescue experiment to restore *Smpd3* expression in the osteoblasts and examine how it affects the overall skeletal development and mineralization. The rationale to perform this experiment originally came from the manuscript published by the group of Dr. Stoffel. In this manuscript it was suggested that the *fro* mutation caused by a chemical mutagen might have mutated another locus causing the bone and tooth mineralization defects in *fro/fro* mice [125]. Although possible, such a mutation would have been segregated during many generations of breeding experiments in several laboratories working with the *fro/fro* mice. Nevertheless, the dispute centering the *fro/fro* mice as a valid model for an SMPD3-deficient mouse model and the role of SMPD3 in skeletal mineralization have been a major issue in the field. We thought that the most acceptable way to solve this issue would be to perform a genetic rescue to restore *Smpd3* expression in the skeletal tissues.

While designing this experiment, we took into account two key observations: 1) *Smpd3* is expressed in the osteoblasts both in embryonic and adult mice; and 2) SMPD3-deficient *fro/fro* osteoblasts show impaired *in vitro* mineralization capacities. Considering this, we used the murine 2.3 kb *Colla1* proximal promoter fragment to drive *Smpd3* expression in the osteoblasts. Once validated for its bone/osteoblast-specific expression of *Smpd3*, *Colla1-Smpd3* mice were used in breeding experiments to generate *fro/fro;Colla1-Smpd3* mice. The correction of all the bone mineralization defects and the skeletal deformities in both *fro/fro;Colla1-Smpd3* embryos

and adult mice confirmed that the inactivation of SMPD3 is the cause of the hard tissue mineralization defects and the associated skeletal abnormalities in *fro/fro* mice. Additionally, this critical experiment established that SMPD3 acts locally in the osteoblasts to regulate bone mineralization. Expectedly, we did not observe a correction of the cartilage abnormalities in the *fro/fro* embryos, suggesting that SMPD3 acts in a cell autonomous manner in the skeletal tissues.

My second manuscript was an extension of the first manuscript in which I characterized the tooth phenotypes in *fro/fro* mice and demonstrated that as is the case in bone, a local expression of *Smpd3* in the odontoblasts and cementoblasts also corrects the dentin and cementum mineralization defects caused by SMPD3 deficiency. I was able to use the *fro/fro;Coll1a1-Smpd3* mice since the 2.3 kb *Coll1a1* promoter fragment is also active in both odontoblasts and cementoblasts. Additionally, I demonstrated that the differentiation of odontogenic cells were not affected in *fro/fro* mice and the cause of impaired amelogenesis was due to impaired dentin mineralization in these mice. I also provided ultrastructural analyses showing the normal collagen matrix in these mice.

The main objective of the third manuscript (unpublished) has been to investigate how SMPD3 affects bone mineralization. More specifically, we examined whether ceramide or phosphocholine metabolism play a role in the process of bone mineralization. We showed that *Des1^{-/-}* mice lacking dihydroceramide desaturase 1, which generates ceramide from dihydroxyceramide via the *de novo* pathway of ceramide synthesis, show impaired ceramide metabolism but no bone mineralization defects and/or skeletal abnormalities. This finding indicates that phosphocholine metabolism might be the factor involved in bone mineralization. This inference was further supported by the bone mineralization defects in *Phospho1^{-/-}* mice lacking PHOSPHO1, a key enzyme in phosphocholine metabolism. Interestingly, we found that there was no increase of bone mineralization defects in the compound *fro/fro;Phospho1^{-/-}* mice

suggesting that these two enzymes work in the same pathway. Indeed, both SMPD3 and PHOSPHO1 are co-localized in matrix vesicles, which has been proposed as key sites for the initiation of ECM mineralization. We propose that phosphocholine generated by SMPD3 can be cleaved by PHOSPHO1 to locally increase the levels of P_i in the protected environment of matrix vesicles in which the initial seeding of hydroxyapatite crystals take place.

As described above, the extracellular regulators of ECM mineralization are better understood than the regulators that are involved in the initiation of this process. My work suggests a possible mechanism of SMPD3 action in matrix vesicle-mediated initiation of ECM mineralization. Indeed, the involvement of SMPD3 during the initiation of bone mineralization is supported by our observation that bone mineralization is most/severely impaired during the early stage of bone formation in the *fro/fro* mice compared to the remodelling stage. Taken together, this work establishes a critical role for SMPD3 in skeletal development, more particularly in ECM mineralization in the skeletal and dental hard tissues and demonstrates that the *fro/fro* mouse is a valid model to study SMPD3 biology. Additionally, my findings demonstrate that SMPD3 does not affect the known regulators of ECM mineralization and may possibly act in concert with a downstream enzyme, PHOSPHO1, to regulate this process.

5.2 Future directions

Despite the published data from numerous cell culture studies showing the role of lipid metabolites in chondrocytes, osteoblasts and osteoclasts, the *in vivo* validation of these studies is still missing. At present, limited *in vivo* data are available on the roles of sphingolipid metabolizing enzymes in the skeletal tissues. One possible reason for this could be that most of the mutant mouse models that show altered sphingolipid metabolism do not show any overt skeletal phenotype during their adulthood. Nevertheless, a systematic analysis of these mice

during embryonic development using histology and histomorphometric techniques may provide further clues on the function of sphingolipids in skeletal development. The chemical mutagenesis and targeted mutations in the murine SMPD3 gene have given us a unique opportunity to explore the role of this lipid metabolizing enzyme in the skeletal tissues. Further studies involving mouse models with tissue-specific inactivation of *Smpd3* are needed to decipher the local versus systemic contribution of this enzyme to skeletal development and growth. More specifically, these studies are expected to elucidate the role of this pleiotropic enzyme in the brain and how its activity might contribute to the hypothalamic regulation of skeletal growth. Additionally, novel mechanistic studies may shed light on the specific roles of the two products of the SMPD3-catalyzed reaction in the skeletal tissues. The *de novo* pathway of sphingolipid metabolism, more particularly ceramide metabolism, has been shown to regulate energy expenditure and a similar role is expected for the sphingomyelinase pathway of ceramide synthesis [171, 183, 184]. An important aspect would be to investigate how various species of ceramides generated by SMPD3 in the osteoblasts and chondrocytes might contribute to the overall energy metabolism in the body. This work is particularly relevant as osteocalcin, an osteoblast-specific protein has been recently shown to regulate energy metabolism [2].

5.3 Significance

The importance of ECM mineralization in the skeletal tissues has been demonstrated by several genetic mutations that affect this process and cause life-threatening diseases such as hypophosphatasia, rickets and some forms of osteogenesis imperfecta [26, 48, 80, 143, 144]. The recently characterized *fro* mutation in murine *Smpd3* gene identifies sphingolipid metabolism as a novel regulator of ECM mineralization in the skeletal tissues [83, 95]. Until now, no known mutation in the human SMPD3 gene has been identified. However, apart from the well-

characterized human diseases with bone and tooth mineralization defects, there are human disease of unknown etiology that are associated with poor bone mineralization and/or skeletal dysplasia. In some cases, although the genetic mutation is known, the exact mode of action of the protein is still missing. My study may provide a possible link to these idiopathic bone mineralization defects. The knowledge generated through this study will help to identify new therapeutic targets and may in turn improve the care and quality of life of patients with some forms of skeletal dysplasia.

5.4 Conclusion

The *fro/fro* mouse model is one of the first animal model to demonstrate a role for sphingolipids in skeletal development and homeostasis. Although a cell-autonomous role for SMPD3 in bone and tooth mineralization is now well established, the precise mechanism of its action in hard tissue mineralization is still unknown. SMPD3 metabolites, phosphocholine and different species of ceramides, may have distinct roles in the cells of the developing skeleton. A thorough understanding of the mode of actions of these two metabolites will be required to fully appreciate the complex process that regulates vertebrate skeletogenesis.

References

1. Horton, W.A. and C.R. Degen, *FGFs in endochondral skeletal development*. Trends Endocrinol Metab, 2009. **20**(7): p. 341-8.
2. Karsenty, G., *Bone endocrine regulation of energy metabolism and male reproduction*. C R Biol, 2011. **334**(10): p. 720-4.
3. Karsenty, G., *The complexities of skeletal biology*. Nature, 2003. **423**(6937): p. 316-8.
4. Karsenty, G., H.M. Kronenberg, and C. Settembre, *Genetic control of bone formation*. Annu Rev Cell Dev Biol, 2009. **25**: p. 629-48.
5. Mackie, E.J., L. Tatarczuch, and M. Mirams, *The skeleton: a multi-functional complex organ: the growth plate chondrocyte and endochondral ossification*. J Endocrinol, 2011. **211**(2): p. 109-21.
6. DiGirolamo, D.J., T.L. Clemens, and S. Kousteni, *The skeleton as an endocrine organ*. Nat Rev Rheumatol, 2012. **8**(11): p. 674-83.
7. Xiong, J. and C.A. O'Brien, *Osteocyte RANKL: new insights into the control of bone remodeling*. J Bone Miner Res, 2012. **27**(3): p. 499-505.
8. Saini, V., et al., *Parathyroid hormone (PTH)/PTH-related peptide type 1 receptor (PPR) signaling in osteocytes regulates anabolic and catabolic skeletal responses to PTH*. J Biol Chem, 2013. **288**(28): p. 20122-34.
9. Kollar, E.J. and G.R. Baird, *Tissue interactions in embryonic mouse tooth germs. I. Reorganization of the dental epithelium during tooth-germ reconstruction*. J Embryol Exp Morphol, 1970. **24**(1): p. 159-71.

10. Mina, M. and E.J. Kollar, *The induction of odontogenesis in non-dental mesenchyme combined with early murine mandibular arch epithelium*. Arch Oral Biol, 1987. **32**(2): p. 123-7.
11. Lumsden, A.G., *Spatial organization of the epithelium and the role of neural crest cells in the initiation of the mammalian tooth germ*. Development, 1988. **103 Suppl**: p. 155-69.
12. Thesleff, I., et al., *Interference of tooth differentiation with interposed filters*. Dev Biol, 1977. **58**(1): p. 197-203.
13. Thesleff, I. and K. Hurmerinta, *Tissue interactions in tooth development*. Differentiation, 1981. **18**(2): p. 75-88.
14. Matthiessen, M.E. and P. Romert, *Ultrastructure of the human enamel organ. II. Internal enamel epithelium, preameloblasts, and secretory ameloblasts*. Cell Tissue Res, 1980. **205**(3): p. 371-82.
15. Matthiessen, M.E. and P. Romert, *Ultrastructure of the human enamel organ. I. External enamel epithelium, stellate reticulum, and stratum intermedium*. Cell Tissue Res, 1980. **205**(3): p. 361-70.
16. Matthiessen, M.E., P. Vedtofte, and P. Romert, *Morphology of a simple ameloblastoma related to the human enamel organ*. Scand J Dent Res, 1980. **88**(3): p. 181-6.
17. Leblond, C.P., *Synthesis and secretion of collagen by cells of connective tissue, bone, and dentin*. Anat Rec, 1989. **224**(2): p. 123-38.
18. Wang, X.J., et al., *Characterization of dentin and enamel by use of optical coherence tomography*. Appl Opt, 1999. **38**(10): p. 2092-6.
19. Warshawsky, H., *Organization of crystals in enamel*. Anat Rec, 1989. **224**(2): p. 242-62.
20. Doi, Y., et al., *Inhibition of seeded growth of enamel apatite crystals by amelogenin and enamelin proteins in vitro*. J Dent Res, 1984. **63**(2): p. 98-105.

21. Reith, E.J., *The ultrastructure of ameloblasts during matrix formation and the maturation of enamel.* J Biophys Biochem Cytol, 1961. **9**: p. 825-39.
22. Drezner, M.K., *PHEX gene and hypophosphatemia.* Kidney Int, 2000. **57**(1): p. 9-18.
23. Kato, S., et al., *In vivo function of VDR in gene expression-VDR knock-out mice.* J Steroid Biochem Mol Biol, 1999. **69**(1-6): p. 247-51.
24. Murshed, M., et al., *Unique coexpression in osteoblasts of broadly expressed genes accounts for the spatial restriction of ECM mineralization to bone.* Genes Dev, 2005. **19**(9): p. 1093-104.
25. Shimada, T., et al., *Targeted ablation of Fgf23 demonstrates an essential physiological role of FGF23 in phosphate and vitamin D metabolism.* J Clin Invest, 2004. **113**(4): p. 561-8.
26. Tanaka, Y. and H.F. Deluca, *Role of 1,25-dihydroxyvitamin D3 in maintaining serum phosphorus and curing rickets.* Proc Natl Acad Sci U S A, 1974. **71**(4): p. 1040-4.
27. Tenenhouse, H.S. and Y. Sabbagh, *Novel phosphate-regulating genes in the pathogenesis of renal phosphate wasting disorders.* Pflugers Arch, 2002. **444**(3): p. 317-26.
28. Fleisch, H. and S. Bisaz, *Mechanism of calcification: inhibitory role of pyrophosphate.* Nature, 1962. **195**: p. 911.
29. Terkeltaub, R.A., *Inorganic pyrophosphate generation and disposition in pathophysiology.* Am J Physiol Cell Physiol, 2001. **281**(1): p. C1-C11.
30. Ho, A.M., M.D. Johnson, and D.M. Kingsley, *Role of the mouse ank gene in control of tissue calcification and arthritis.* Science, 2000. **289**(5477): p. 265-70.
31. Okawa, A., et al., *Mutation in Npps in a mouse model of ossification of the posterior longitudinal ligament of the spine.* Nat Genet, 1998. **19**(3): p. 271-3.

32. Eaton, R.H. and D.W. Moss, *Kinetic studies on the orthophosphatase and iorganic pyrophosphatase activities of human alkaline phosphatase*. *Enzymologia*, 1968. **35**(3): p. 168-78.
33. Hesse, L., et al., *Tissue-nonspecific alkaline phosphatase and plasma cell membrane glycoprotein-1 are central antagonistic regulators of bone mineralization*. *Proc Natl Acad Sci U S A*, 2002. **99**(14): p. 9445-9.
34. Mornet, E., *Hypophosphatasia: the mutations in the tissue-nonspecific alkaline phosphatase gene*. *Hum Mutat*, 2000. **15**(4): p. 309-15.
35. Mornet, E., et al., *Structural evidence for a functional role of human tissue nonspecific alkaline phosphatase in bone mineralization*. *J Biol Chem*, 2001. **276**(33): p. 31171-8.
36. Taillandier, A., et al., *Twelve novel mutations in the tissue-nonspecific alkaline phosphatase gene (ALPL) in patients with various forms of hypophosphatasia*. *Hum Mutat*, 2001. **18**(1): p. 83-4.
37. Taillandier, A., et al., *Characterization of eleven novel mutations (M45L, R119H, 544delG, G145V, H154Y, C184Y, D289V, 862+5A, 1172delC, R411X, E459K) in the tissue-nonspecific alkaline phosphatase (TNS-ALP) gene in patients with severe hypophosphatasia*. *Mutations in brief no. 217. Online*. *Hum Mutat*, 1999. **13**(2): p. 171-2.
38. Fedde, K.N., et al., *Alkaline phosphatase knock-out mice recapitulate the metabolic and skeletal defects of infantile hypophosphatasia*. *J Bone Miner Res*, 1999. **14**(12): p. 2015-26.
39. Waymire, K.G., et al., *Mice lacking tissue non-specific alkaline phosphatase die from seizures due to defective metabolism of vitamin B-6*. *Nat Genet*, 1995. **11**(1): p. 45-51.
40. Fincham, A.G., J. Moradian-Oldak, and J.P. Simmer, *The structural biology of the developing dental enamel matrix*. *J Struct Biol*, 1999. **126**(3): p. 270-99.

41. Aoba, T., et al., *Enamel mineralization and an initial crystalline phase*. Connect Tissue Res, 1998. **38**(1-4): p. 129-37;discussion 139-45.
42. Pittenger, M.F., et al., *Multilineage potential of adult human mesenchymal stem cells*. Science, 1999. **284**(5411): p. 143-7.
43. Thomas, H.F., *Root formation*. Int J Dev Biol, 1995. **39**(1): p. 231-7.
44. Wang, Y., et al., *BMP activity is required for tooth development from the lamina to bud stage*. J Dent Res, 2012. **91**(7): p. 690-5.
45. Porntaveetus, T., et al., *Expression of fibroblast growth factors (Fgfs) in murine tooth development*. J Anat, 2011. **218**(5): p. 534-43.
46. Camilleri, S. and F. McDonald, *Runx2 and dental development*. Eur J Oral Sci, 2006. **114**(5): p. 361-73.
47. Chen, S., et al., *Runx2, osx, and dspp in tooth development*. J Dent Res, 2009. **88**(10): p. 904-9.
48. Whyte, M.P., *Hypophosphatasia and the role of alkaline phosphatase in skeletal mineralization*. Endocr Rev, 1994. **15**(4): p. 439-61.
49. van den Bos, T., et al., *Cementum and dentin in hypophosphatasia*. J Dent Res, 2005. **84**(11): p. 1021-5.
50. Narisawa, S., N. Frohlander, and J.L. Millan, *Inactivation of two mouse alkaline phosphatase genes and establishment of a model of infantile hypophosphatasia*. Dev Dyn, 1997. **208**(3): p. 432-46.
51. McKee, M.D., et al., *Enzyme replacement therapy prevents dental defects in a model of hypophosphatasia*. J Dent Res, 2011. **90**(4): p. 470-6.
52. Millan, J.L., et al., *Enzyme replacement therapy for murine hypophosphatasia*. J Bone Miner Res, 2008. **23**(6): p. 777-87.

53. Whyte, M.P., et al., *Enzyme-replacement therapy in life-threatening hypophosphatasia*. *N Engl J Med*, 2012. **366**(10): p. 904-13.
54. Teitelbaum, S.L., *Pathological manifestations of osteomalacia and rickets*. *Clin Endocrinol Metab*, 1980. **9**(1): p. 43-62.
55. Durmaz, E., et al., *Clinical and genetic analysis of patients with vitamin D-dependent rickets type 1A*. *Clin Endocrinol (Oxf)*, 2012. **77**(3): p. 363-9.
56. Cheng, J.B., et al., *Genetic evidence that the human CYP2R1 enzyme is a key vitamin D 25-hydroxylase*. *Proc Natl Acad Sci U S A*, 2004. **101**(20): p. 7711-5.
57. Malloy, P.J., J.W. Pike, and D. Feldman, *The vitamin D receptor and the syndrome of hereditary 1,25-dihydroxyvitamin D-resistant rickets*. *Endocr Rev*, 1999. **20**(2): p. 156-88.
58. Dardenne, O., et al., *Targeted inactivation of the 25-hydroxyvitamin D(3)-1(alpha)-hydroxylase gene (CYP27B1) creates an animal model of pseudovitamin D-deficiency rickets*. *Endocrinology*, 2001. **142**(7): p. 3135-41.
59. Li, Y.C., et al., *Targeted ablation of the vitamin D receptor: an animal model of vitamin D-dependent rickets type II with alopecia*. *Proc Natl Acad Sci U S A*, 1997. **94**(18): p. 9831-5.
60. Panda, D.K., et al., *Targeted ablation of the 25-hydroxyvitamin D 1alpha-hydroxylase enzyme: evidence for skeletal, reproductive, and immune dysfunction*. *Proc Natl Acad Sci U S A*, 2001. **98**(13): p. 7498-503.
61. Erben, R.G., et al., *Deletion of deoxyribonucleic acid binding domain of the vitamin D receptor abrogates genomic and nongenomic functions of vitamin D*. *Mol Endocrinol*, 2002. **16**(7): p. 1524-37.

62. Balsan, S., et al., *Long-term nocturnal calcium infusions can cure rickets and promote normal mineralization in hereditary resistance to 1,25-dihydroxyvitamin D*. J Clin Invest, 1986. **77**(5): p. 1661-7.
63. Hochberg, Z., D. Tiosano, and L. Even, *Calcium therapy for calcitriol-resistant rickets*. J Pediatr, 1992. **121**(5 Pt 1): p. 803-8.
64. *A gene (PEX) with homologies to endopeptidases is mutated in patients with X-linked hypophosphatemic rickets. The HYP Consortium*. Nat Genet, 1995. **11**(2): p. 130-6.
65. Riminucci, M., et al., *FGF-23 in fibrous dysplasia of bone and its relationship to renal phosphate wasting*. J Clin Invest, 2003. **112**(5): p. 683-92.
66. Shimada, T., et al., *FGF-23 is a potent regulator of vitamin D metabolism and phosphate homeostasis*. J Bone Miner Res, 2004. **19**(3): p. 429-35.
67. Saito, H., et al., *Human fibroblast growth factor-23 mutants suppress Na⁺-dependent phosphate co-transport activity and 1 α ,25-dihydroxyvitamin D₃ production*. J Biol Chem, 2003. **278**(4): p. 2206-11.
68. Farrow, E.G. and K.E. White, *Recent advances in renal phosphate handling*. Nat Rev Nephrol, 2010. **6**(4): p. 207-17.
69. Sitara, D., et al., *Genetic evidence of serum phosphate-independent functions of FGF-23 on bone*. PLoS Genet, 2008. **4**(8): p. e1000154.
70. Yuan, Q., et al., *Increased osteopontin contributes to inhibition of bone mineralization in FGF23-deficient mice*. J Bone Miner Res, 2014. **29**(3): p. 693-704.
71. Barros, N.M., et al., *Proteolytic processing of osteopontin by PHEX and accumulation of osteopontin fragments in Hyp mouse bone, the murine model of X-linked hypophosphatemia*. J Bone Miner Res, 2013. **28**(3): p. 688-99.

72. Econs, M.J. and F. Francis, *Positional cloning of the PEX gene: new insights into the pathophysiology of X-linked hypophosphatemic rickets*. Am J Physiol, 1997. **273**(4 Pt 2): p. F489-98.
73. Tenenhouse, H.S., *X-linked hypophosphataemia: a homologous disorder in humans and mice*. Nephrol Dial Transplant, 1999. **14**(2): p. 333-41.
74. Owen, C., et al., *A novel Phex mutation in a new mouse model of hypophosphatemic rickets*. J Cell Biochem, 2012. **113**(7): p. 2432-41.
75. Lyon, M.F., et al., *The Gy mutation: another cause of X-linked hypophosphatemia in mouse*. Proc Natl Acad Sci U S A, 1986. **83**(13): p. 4899-903.
76. Shimada, T., et al., *FGF-23 transgenic mice demonstrate hypophosphatemic rickets with reduced expression of sodium phosphate cotransporter type IIa*. Biochem Biophys Res Commun, 2004. **314**(2): p. 409-14.
77. Rosenberg, T., et al., *A murine transgenic model for transcriptional regulation of the Na/Pi-IIa major renal phosphate cotransporter*. Am J Physiol Renal Physiol, 2007. **292**(5): p. F1617-25.
78. Ben Amor, M., et al., *Osteogenesis imperfecta*. Pediatr Endocrinol Rev, 2013. **10 Suppl 2**: p. 397-405.
79. Glorieux, F.H., *Osteogenesis imperfecta*. Best Pract Res Clin Rheumatol, 2008. **22**(1): p. 85-100.
80. Glorieux, F.H., et al., *Osteogenesis imperfecta type VI: a form of brittle bone disease with a mineralization defect*. J Bone Miner Res, 2002. **17**(1): p. 30-8.
81. Homan, E.P., et al., *Mutations in SERPINF1 cause osteogenesis imperfecta type VI*. J Bone Miner Res, 2011. **26**(12): p. 2798-803.

82. Becker, J., et al., *Exome sequencing identifies truncating mutations in human SERPINF1 in autosomal-recessive osteogenesis imperfecta*. Am J Hum Genet, 2011. **88**(3): p. 362-71.
83. Aubin, I., et al., *A deletion in the gene encoding sphingomyelin phosphodiesterase 3 (Smpd3) results in osteogenesis and dentinogenesis imperfecta in the mouse*. Nat Genet, 2005. **37**(8): p. 803-5.
84. Airola, M.V. and Y.A. Hannun, *Sphingolipid metabolism and neutral sphingomyelinases*. Handb Exp Pharmacol, 2013(215): p. 57-76.
85. Hannun, Y.A. and L.M. Obeid, *Many ceramides*. J Biol Chem, 2011. **286**(32): p. 27855-62.
86. Mullen, T.D., Y.A. Hannun, and L.M. Obeid, *Ceramide synthases at the centre of sphingolipid metabolism and biology*. Biochem J, 2012. **441**(3): p. 789-802.
87. Futerman, A.H. and H. Riezman, *The ins and outs of sphingolipid synthesis*. Trends Cell Biol, 2005. **15**(6): p. 312-8.
88. Merrill, A.H., Jr., *De novo sphingolipid biosynthesis: a necessary, but dangerous, pathway*. J Biol Chem, 2002. **277**(29): p. 25843-6.
89. Merrill, A.H., Jr., et al., *Sphingolipids--the enigmatic lipid class: biochemistry, physiology, and pathophysiology*. Toxicol Appl Pharmacol, 1997. **142**(1): p. 208-25.
90. Nilsson, A. and R.D. Duan, *Alkaline sphingomyelinases and ceramidases of the gastrointestinal tract*. Chem Phys Lipids, 1999. **102**(1-2): p. 97-105.
91. Stoffel, W., *Functional analysis of acid and neutral sphingomyelinases in vitro and in vivo*. Chem Phys Lipids, 1999. **102**(1-2): p. 107-21.
92. Kirschnek, S., et al., *CD95-mediated apoptosis in vivo involves acid sphingomyelinase*. J Biol Chem, 2000. **275**(35): p. 27316-23.

93. Duan, R.D., L. Nyberg, and A. Nilsson, *Alkaline sphingomyelinase activity in rat gastrointestinal tract: distribution and characteristics*. *Biochim Biophys Acta*, 1995. **1259**(1): p. 49-55.
94. Duan, R.D., *Alkaline sphingomyelinase: an old enzyme with novel implications*. *Biochim Biophys Acta*, 2006. **1761**(3): p. 281-91.
95. Khavandgar, Z., et al., *A cell-autonomous requirement for neutral sphingomyelinase 2 in bone mineralization*. *J Cell Biol*, 2011. **194**(2): p. 277-89.
96. Obeid, L.M., et al., *Programmed cell death induced by ceramide*. *Science*, 1993. **259**(5102): p. 1769-71.
97. Siskind, L.J., R.N. Kolesnick, and M. Colombini, *Ceramide forms channels in mitochondrial outer membranes at physiologically relevant concentrations*. *Mitochondrion*, 2006. **6**(3): p. 118-25.
98. Chipuk, J.E., et al., *Sphingolipid metabolism cooperates with BAK and BAX to promote the mitochondrial pathway of apoptosis*. *Cell*, 2012. **148**(5): p. 988-1000.
99. Olivier, S., et al., *Sodium nitroprusside-induced osteoblast apoptosis is mediated by long chain ceramide and is decreased by raloxifene*. *Biochem Pharmacol*, 2005. **69**(6): p. 891-901.
100. Snyder, C.M., et al., *Nitric oxide induces cell death by regulating anti-apoptotic BCL-2 family members*. *PLoS One*, 2009. **4**(9): p. e7059.
101. Kitajima, I., et al., *Ceramide-induced nuclear translocation of NF-kappa B is a potential mediator of the apoptotic response to TNF-alpha in murine clonal osteoblasts*. *Bone*, 1996. **19**(3): p. 263-70.

102. Chae, H.J., et al., *Dexamethasone suppresses tumor necrosis factor-alpha-induced apoptosis in osteoblasts: possible role for ceramide*. *Endocrinology*, 2000. **141**(8): p. 2904-13.
103. Hill, P.A. and A. Tumber, *Ceramide-induced cell death/survival in murine osteoblasts*. *J Endocrinol*, 2010. **206**(2): p. 225-33.
104. Sabatini, M., et al., *Effects of ceramide on apoptosis, proteoglycan degradation, and matrix metalloproteinase expression in rabbit articular cartilage*. *Biochem Biophys Res Commun*, 2000. **267**(1): p. 438-44.
105. MacRae, V.E., et al., *Ceramide inhibition of chondrocyte proliferation and bone growth is IGF-I independent*. *J Endocrinol*, 2006. **191**(2): p. 369-77.
106. Takeda, H., et al., *Sphingomyelinase and ceramide inhibit formation of F-actin ring in and bone resorption by rabbit mature osteoclasts*. *FEBS Lett*, 1998. **422**(2): p. 255-8.
107. Lee, S.E., et al., *Tumor necrosis factor-alpha supports the survival of osteoclasts through the activation of Akt and ERK*. *J Biol Chem*, 2001. **276**(52): p. 49343-9.
108. Iwamoto, T., et al., *Lactosylceramide is essential for the osteoclastogenesis mediated by macrophage-colony-stimulating factor and receptor activator of nuclear factor-kappa B ligand*. *J Biol Chem*, 2001. **276**(49): p. 46031-8.
109. Fukumoto, S., et al., *Current topics in pharmacological research on bone metabolism: osteoclast differentiation regulated by glycosphingolipids*. *J Pharmacol Sci*, 2006. **100**(3): p. 195-200.
110. Kakoi, H., et al., *Bone morphogenic protein (BMP) signaling up-regulates neutral sphingomyelinase 2 to suppress chondrocyte maturation via the Akt protein signaling pathway as a negative feedback mechanism*. *J Biol Chem*, 2014. **289**(12): p. 8135-50.

111. Kozawa, O., et al., *Sphingosine 1-phosphate induces he at shock protein 27 via p38 mitogen-activated protein kinas e activation in osteoblasts.* J Bone Miner Res, 1999. **14**(10): p. 1761-7.
112. Sato, C., et al., *Sphingosine 1-phosphate receptor acti vation enhances BMP-2-induced osteoblast differentiation.* Biochem Biophys Res Commun, 2012. **423**(1): p. 200-5.
113. Liu, R., M.C. Farach-Carson, and N.J. Karin, *Effects of sphingosin e derivatives on MC3T3-E1 pre-osteoblasts: psychosine elicit s relea se o f calc ium fr om intrace llualr stores.* Biochem Biophys Res Commun, 1995. **214**(2): p. 676-84.
114. Lyons, J.M. and N.J. Karin, *A role for G protein-coupled lysophospholipid receptors in sphingolipid-induced Ca²⁺ signaling in MC3T3-E1 osteoblastic cells.* J Bone Miner Res, 2001. **16**(11): p. 2035-42.
115. Grey, A., et al., *The phospholipids sphingosine-1-phos phate and lysophosphatidic acid prevent apo ptosis in os teoblastic cells via a signaling path way involving G(i) proteins and phosphatidylinositol-3 kinase.* Endocrinology, 2002. **143**(12): p. 4755-63.
116. Roelofsen, T., et al., *Sphingosine-1-phosphate acts as a developmental stag e sp ecific inhibitor of platelet-derived growth fa ctor-induced chemotaxis of osteoblasts.* J Cell Biochem, 2008. **105**(4): p. 1128-38.
117. Quint, P., et al., *Sphingosine 1-phosphate (S1P) receptors 1 and 2 coo rdinately induce mesenchymal cell migration through S1P activation of complementary kinase pathways.* J Biol Chem, 2013. **288**(8): p. 5398-406.
118. Kim, M.K., et al., *Sphingosine-1-phosphate stimulat es rat primary chondrocyte proliferation.* Biochem Biophys Res Commun, 2006. **345**(1): p. 67-73.

119. Masuko, K., et al., *Sphingosine-1-phosphate modulates expression of vascular endothelial growth factor in human articular chondrocytes: a possible new role in arthritis*. Int J Rheum Dis, 2012. **15**(4): p. 366-73.
120. Masuko, K., et al., *Sphingosine-1-phosphate attenuates proteoglycan aggrecan expression via production of prostaglandin E2 from human articular chondrocytes*. BMC Musculoskelet Disord, 2007. **8**: p. 29.
121. Ishii, M. and J. Kikuta, *Sphingosine-1-phosphate signaling controlling osteoclasts and bone homeostasis*. Biochim Biophys Acta, 2013. **1831**(1): p. 223-7.
122. Lotinun, S., et al., *Osteoclast-specific cathepsin K deletion stimulates SIP-dependent bone formation*. J Clin Invest, 2013.
123. Keller, B., et al., *Interaction of TGFbeta and BMP signaling pathways during chondrogenesis*. PLoS One, 2011. **6**(1): p. e16421.
124. Guenet, J.L., et al., *Fragilitas ossium: a new autosomal recessive mutation in the mouse*. J Hered, 1981. **72**(6): p. 440-1.
125. Stoffel, W., et al., *Neutral sphingomyelinase 2 (smpd3) in the control of postnatal growth and development*. Proc Natl Acad Sci U S A, 2005. **102**(12): p. 4554-9.
126. Stoffel, W., et al., *Neutral sphingomyelinase (SMPD3) deficiency causes a novel form of chondrodysplasia and dwarfism that is rescued by Col2A1-driven smpd3 transgene expression*. Am J Pathol, 2007. **171**(1): p. 153-61.
127. Marchesini, N. and Y.A. Hannun, *Acid and neutral sphingomyelinases: roles and mechanisms of regulation*. Biochem Cell Biol, 2004. **82**(1): p. 27-44.
128. Wittenberg, J. and A. Kornberg, *Choline phosphokinase*. J Biol Chem, 1953. **202**(1): p. 431-44.

129. Nakagami, K., et al., *Increased choline kinase activity and elevated phosphocholine levels in human colon cancer*. Jpn J Cancer Res, 1999. **90**(4): p. 419-24.
130. Babb, S.M., et al., *Oral choline increases choline metabolites in human brain*. Psychiatry Res, 2004. **130**(1): p. 1-9.
131. Millington, W.R. and R.J. Wurtman, *Choline administration elevates brain phosphorylcholine concentrations*. J Neurochem, 1982. **38**(6): p. 1748-52.
132. Houston, B., A.J. Stewart, and C. Farquharson, *PHOSPHO1-A novel phosphatase specifically expressed at sites of mineralisation in bone and cartilage*. Bone, 2004. **34**(4): p. 629-37.
133. Roberts, S., et al., *Functional involvement of PHOSPHO1 in matrix vesicle-mediated skeletal mineralization*. J Bone Miner Res, 2007. **22**(4): p. 617-27.
134. Stewart, A.J., et al., *The presence of PHOSPHO1 in matrix vesicles and its developmental expression prior to skeletal mineralization*. Bone, 2006. **39**(5): p. 1000-7.
135. Macrae, V.E., et al., *Inhibition of PHOSPHO1 activity results in impaired skeletal mineralization during limb development of the chick*. Bone, 2010. **46**(4): p. 1146-55.
136. Yadav, M.C., et al., *Loss of skeletal mineralization by the simultaneous ablation of PHOSPHO1 and alkaline phosphatase function: a unified model of the mechanisms of initiation of skeletal calcification*. J Bone Miner Res, 2011. **26**(2): p. 286-97.
137. Ali, S.Y., S.W. Sajdera, and H.C. Anderson, *Isolation and characterization of calcifying matrix vesicles from epiphyseal cartilage*. Proc Natl Acad Sci U S A, 1970. **67**(3): p. 1513-20.
138. Register, T.C., et al., *Roles of alkaline phosphatase and labile internal mineral in matrix vesicle-mediated calcification. Effect of selective release of membrane-bound alkaline*

- phosphatase and treatment with isosmotic pH 6 buffer.* J Biol Chem, 1986. **261**(20): p. 9354-60.
139. Anderson, H.C., et al., *Matrix vesicles in osteomalacic hypophosphatasia bone contain apatite-like mineral crystals.* Am J Pathol, 1997. **151**(6): p. 1555-61.
140. Anderson, H.C., *Molecular biology of matrix vesicles.* Clin Orthop Relat Res, 1995(314): p. 266-80.
141. Hale, J.E. and R.E. Wuthier, *The mechanism of matrix vesicle formation. Studies on the composition of chondrocyte microvilli and on the effects of microfilament-perturbing agents on cellular vesiculation.* J Biol Chem, 1987. **262**(4): p. 1916-25.
142. Wu, L.N., et al., *Changes in phospholipid extractability and composition accompany mineralization of chicken growth plate cartilage matrix vesicles.* J Biol Chem, 2002. **277**(7): p. 5126-33.
143. Goldberg, M., et al., *Sphingomyelin degradation is a key factor in dentin and bone mineralization: lessons from the fro/fro mouse. The chemistry and histochemistry of dentin lipids.* J Dent Res, 2008. **87**(1): p. 9-13.
144. Nesbitt, T., et al., *Coordinated maturational regulation of PHEX and renal phosphate transport inhibitory activity: evidence for the pathophysiological role of PHEX in X-linked hypophosphatemia.* J Bone Miner Res, 1999. **14**(12): p. 2027-35.
145. Luo, G., et al., *Spontaneous calcification of arteries and cartilage in mice lacking matrix GLA protein.* Nature, 1997. **386**(6620): p. 78-81.
146. Murshed, M., et al., *Extracellular matrix mineralization is regulated locally; different roles of two gla-containing proteins.* J Cell Biol, 2004. **165**(5): p. 625-30.

147. Milhas, D., et al., *Anterograde and retrograde transport of neutral sphingomyelinase-2 between the Golgi and the plasma membrane*. *Biochim Biophys Acta*, 2010. **1801**(12): p. 1361-74.
148. Wu, B.X., C.J. Clarke, and Y.A. Hannun, *Mammalian neutral sphingomyelinases: regulation and roles in cell signaling responses*. *Neuromolecular Med*, 2010. **12**(4): p. 320-30.
149. Richard, A., et al., *C2-ceramide primes specifically for the superoxide anion production induced by N-formylmethionylleucylphenylalanine (fMLP) in human neutrophils*. *Biochim Biophys Acta*, 1996. **1299**(2): p. 259-66.
150. Sanchez-Alavez, M., et al., *Ceramide mediates the rapid phase of febrile response to IL-1beta*. *Proc Natl Acad Sci U S A*, 2006. **103**(8): p. 2904-8.
151. Kolak, M., et al., *Adipose tissue inflammation and increased ceramide content characterize subjects with high liver fat content independent of obesity*. *Diabetes*, 2007. **56**(8): p. 1960-8.
152. Rutkute, K., R.H. Asmis, and M.N. Nikolova-Karakashian, *Regulation of neutral sphingomyelinase-2 by GSH: a new insight to the role of oxidative stress in aging-associated inflammation*. *J Lipid Res*, 2007. **48**(11): p. 2443-52.
153. Tellier, E., et al., *Role for furin in tumor necrosis factor alpha-induced activation of the matrix metalloproteinase/sphingolipid mitogenic pathway*. *Mol Cell Biol*, 2007. **27**(8): p. 2997-3007.
154. Marchesini, N., C. Luberto, and Y.A. Hannun, *Biochemical properties of mammalian neutral sphingomyelinase 2 and its role in sphingolipid metabolism*. *J Biol Chem*, 2003. **278**(16): p. 13775-83.

155. Rossert, J., H. Eberspaecher, and B. de Crombrughe, *Separate cis-acting DNA elements of the mouse pro-alpha 1(I) collagen promoter direct expression of reporter genes to different type I collagen-producing cells in transgenic mice.* J Cell Biol, 1995. **129**(5): p. 1421-32.
156. Li, J., et al., *Lithium chloride attenuates BMP-2 signaling and inhibits osteogenic differentiation through a novel WNT/GSK3- independent mechanism.* Bone, 2010. **48**(2): p. 321-31.
157. Bielawski, J., et al., *Sphingolipid analysis by high performance liquid chromatography-tandem mass spectrometry (HPLC-MS/MS).* Adv Exp Med Biol, 2010. **688**: p. 46-59.
158. Boukpepsi, T., et al., *Dentin alteration of deciduous teeth in human hypophosphatemic rickets.* Calcif Tissue Int, 2006. **79**(5): p. 294-300.
159. Majorana, A., et al., *Dentinogenesis imperfecta in children with osteogenesis imperfecta: a clinical and ultrastructural study.* Int J Paediatr Dent, 2010. **20**(2): p. 112-8.
160. Opsahl Vital, S., et al., *Tooth dentin defects reflect genetic disorders affecting bone mineralization.* Bone, 2012. **50**(4): p. 989-97.
161. Fleisch, H., et al., *Inhibition of aortic calcification by means of pyrophosphate and polyphosphates.* Nature, 1965. **207**(5003): p. 1300-1.
162. Muriel, M.P., et al., *Morphological and biochemical studies of a mouse mutant (fro/fro) with bone fragility.* Bone, 1991. **12**(4): p. 241-8.
163. Landin, M.A., et al., *Gene Expression Profiling during Murine Tooth Development.* Front Genet, 2012. **3**: p. 139.
164. Ronnholm, E., *The amelogenesis of human teeth as revealed by electron microscopy. II. The development of the enamel crystallites.* J Ultrastruct Res, 1962. **6**: p. 249-303.

165. Goldberg, M., et al., *Dentin: structure, composition and mineralization*. Front Biosci (Elite Ed), 2011. **3**: p. 711-35.
166. Eimar, H., et al., *Regulation of enamel hardness by its crystallographic dimensions*. Acta Biomater, 2012. **8**(9): p. 3400-10.
167. McKee, M.D., C.E. Pedraza, and M.T. Kaartinen, *Osteopontin and wound healing in bone*. Cells Tissues Organs, 2011. **194**(2-4): p. 313-9.
168. Anderson, H.C., *Matrix vesicles and calcification*. Curr Rheumatol Rep, 2003. **5**(3): p. 222-6.
169. Thouverey, C., et al., *Proteomic characterization of biogenesis and functions of matrix vesicles released from mineralizing human osteoblast-like cells*. J Proteomics, 2011. **74**(7): p. 1123-34.
170. Bose, R., et al., *Ceramide synthase mediates daunorubicin-induced apoptosis: an alternative mechanism for generating death signals*. Cell, 1995. **82**(3): p. 405-14.
171. Holland, W.L., et al., *Inhibition of ceramide synthesis ameliorates glucocorticoid-, saturated-fat-, and obesity-induced insulin resistance*. Cell Metab, 2007. **5**(3): p. 167-79.
172. Siddique, M.M., et al., *Ablation of dihydroceramide desaturase 1, a therapeutic target for the treatment of metabolic diseases, simultaneously stimulates anabolic and catabolic signaling*. Mol Cell Biol, 2013. **33**(11): p. 2353-69.
173. Gallego-Ortega, D., et al., *Differential role of human choline kinase alpha and beta enzymes in lipid metabolism: implications in cancer onset and treatment*. PLoS One, 2009. **4**(11): p. e7819.
174. William Li, H.C., V. Lopez, and T.L. Lee, *Effects of preoperative therapeutic play on outcomes of school-age children undergoing day surgery*. Res Nurs Health, 2007. **30**(3): p. 320-32.

175. Herr, I. and K.M. Debatin, *Cellular stress response and apoptosis in cancer therapy*. Blood, 2001. **98**(9): p. 2603-14.
176. Li, Z., et al., *Choline kinase beta is required for normal endochondral bone formation*. Biochim Biophys Acta, 2014. **1840**(7): p. 2112-22.
177. Tani, M. and Y.A. Hannun, *Analysis of membrane topology of neutral sphingomyelinase 2*. FEBS Lett, 2007. **581**(7): p. 1323-8.
178. Roberts, S.J., et al., *Probing the substrate specificities of human PHOSPHO1 and PHOSPHO2*. Biochim Biophys Acta, 2005. **1752**(1): p. 73-82.
179. Kirsch, T., *Biom mineralization--an active or passive process?* Connect Tissue Res, 2012. **53**(6): p. 438-45.
180. Dalgleish, R., *The Human Collagen Mutation Database 1998*. Nucleic Acids Res, 1998. **26**(1): p. 253-5.
181. Takai, S., et al., *Phosphatidylinositol 3-kinase/Akt plays a role in sphingosine 1-phosphate-stimulated HSP27 induction in osteoblasts*. J Cell Biochem, 2006. **98**(5): p. 1249-56.
182. Margolis, H.C., S.Y. Kwak, and H. Yamazaki, *Role of mineralization inhibitors in the regulation of hard tissue biomineralization: relevance to initial enamel formation and maturation*. Front Physiol, 2014. **5**: p. 339.
183. Lipina, C. and H.S. Hundal, *Sphingolipids: agents provocateurs in the pathogenesis of insulin resistance*. Diabetologia, 2011. **54**(7): p. 1596-607.
184. Yang, G., et al., *Central role of ceramide biosynthesis in body weight regulation, energy metabolism, and the metabolic syndrome*. Am J Physiol Endocrinol Metab, 2009. **297**(1): p. E211-24.